Space micropropulsion systems for Cubesats and small satellites: From proximate targets to furthermost frontiers

Igor Levchenko, Kateryna Bazaka, Yongjie Ding, Yevgeny Raitses, Stéphane Mazouffre, Torsten Henning, Peter J. Klar, Shunjiro Shinohara, Jochen Schein, Laurent Garrigues, Minkwan Kim, Dan Lev, Francesco Taccogna, Rod W. Boswell, Christine Charles, Hiroyuki Koizumi, Yan Shen, Carsten Scharlemann, Michael Keidar, and Shuyan Xu

Citation: Applied Physics Reviews **5**, 011104 (2018); doi: 10.1063/1.5007734

View online: https://doi.org/10.1063/1.5007734

View Table of Contents: http://aip.scitation.org/toc/are/5/1

Published by the American Institute of Physics

APPLIED PHYSICS REVIEWS—FOCUSED REVIEW

Space micropropulsion systems for Cubesats and small satellites: From proximate targets to furthermost frontiers

Igor Levchenko,[1,2,a)] Kateryna Bazaka,[2,a)] Yongjie Ding,[3] Yevgeny Raitses,[4] Stéphane Mazouffre,[5] Torsten Henning,[6] Peter J. Klar,[6] Shunjiro Shinohara,[7] Jochen Schein,[8] Laurent Garrigues,[9] Minkwan Kim,[10] Dan Lev,[11] Francesco Taccogna,[12] Rod W. Boswell,[13] Christine Charles,[13] Hiroyuki Koizumi,[14] Yan Shen,[15] Carsten Scharlemann,[16] Michael Keidar,[17,a)] and Shuyan Xu[1,a)]

[1]*Plasma Sources and Applications Centre/Space Propulsion Centre Singapore, NIE, Nanyang Technological University, Singapore 637616*
[2]*School of Chemistry, Physics, and Mechanical Engineering, Queensland University of Technology, Brisbane, Australia*
[3]*Plasma Propulsion Lab, Institute of Advanced Power, Harbin Institute of Technology, Harbin 150001, China*
[4]*Princeton Plasma Physics Laboratory, Princeton University, Princeton, New Jersey 08543, USA*
[5]*Institut de Combustion, Aérothermique, Réactivité et Environnement (ICARE), CNRS—University of Orléans, 1C avenue de la Recherche Scientifique, 45071 Orléans, France*
[6]*Institute of Experimental Physics I, Justus Liebig University, Heinrich-Buff-Ring 16, DE-35392 Giessen, Germany*
[7]*Division of Advanced Mechanical Systems Engineering, Institute of Engineering, Tokyo University of Agriculture and Technology, 2-24-16, Naka-cho, Koganei, Tokyo 184-8588, Japan*
[8]*Institut für Plasmatechnik und Mathematik, EIT, Universität der Bundeswehr München Werner-Heisenberg-Weg, D-85577 Neubiberg, Germany*
[9]*LAPLACE (Laboratoire Plasma et Conversion d'Energie), Université de Toulouse, CNRS, UPS, INPT Toulouse 118, route de Narbonne, F-31062 Toulouse cedex 9, France*
[10]*Astronautics Research Group, Faculty of Engineering and the Environment, University of Southampton, Southampton SO17 1BJ, United Kingdom*
[11]*Space Propulsion Systems Department, Rafael – Advanced Defense Systems Ltd., Haifa 3102102, Israel*
[12]*Consiglio Nazionale delle Ricerche (CNR-Nanotec), Bari 70126, Italy*
[13]*Space Plasma and Plasma Propulsion Laboratory (SP3), Research School of Physics and Engineering, The Australian National University, Canberra, Australian Capital Territory 2601, Australia*
[14]*Department of Advanced Energy, The University of Tokyo, Kashiwa, Chiba 277-8561, Japan*
[15]*Beijing Institute of Control Engineering, China Aerospace Science and Technology Corporation, Beijing 100090, China*
[16]*Aerospace Engineering Department, Fachhochschule Wiener Neustadt, Wiener Neustadt, Austria*
[17]*Mechanical and Aerospace Engineering, The George Washington University, Washington DC 20052, USA*

(Received 2 October 2017; accepted 4 December 2017; published online 22 February 2018)

Rapid evolution of miniaturized, automatic, robotized, function-centered devices has redefined space technology, bringing closer the realization of most ambitious interplanetary missions and intense near-Earth space exploration. Small unmanned satellites and probes are now being launched in hundreds at a time, resurrecting a dream of satellite constellations, i.e., wide, all-covering networks of small satellites capable of forming universal multifunctional, intelligent platforms for global communication, navigation, ubiquitous data mining, Earth observation, and many other functions, which was once doomed by the extraordinary cost of such systems. The ingression of novel nanostructured materials provided a solid base that enabled the advancement of these affordable systems in aspects of power, instrumentation, and communication. However, absence of efficient and reliable thrust systems with the capacity to support precise maneuvering of small satellites and CubeSats over long periods of deployment remains a real stumbling block both for the deployment of large satellite systems and for further exploration of deep space using a new generation of spacecraft. The last few years have seen tremendous global efforts to develop various miniaturized space thrusters, with great success stories. Yet, there are critical challenges that still face the space technology. These have been outlined at an inaugural International Workshop on Micropropulsion and Cubesats, MPCS-2017, a joint effort between Plasma Sources and Application Centre/Space Propulsion Centre (Singapore) and the Micropropulsion and Nanotechnology Lab, the G. Washington University (USA) devoted to miniaturized space

[a)]Authors to whom correspondence should be addressed: Levchenko.Igor@nie.edu.sg; Kateryna.Bazaka@qut.edu.au; Keidar@gwu.edu; and Shuyan.XU@nie.edu.sg

propulsion systems, and hosted by CNR-Nanotec—P.Las.M.I. lab in Bari, Italy. This focused review aims to highlight the most promising developments reported at MPCS-2017 by leading world-reputed experts in miniaturized space propulsion systems. Recent advances in several major types of small thrusters including Hall thrusters, ion engines, helicon, and vacuum arc devices are presented, and trends and perspectives are outlined. https://doi.org/10.1063/1.5007734

TABLE OF CONTENTS

I. INTRODUCTION

Micro- and nanosatellites emerged as a highly versatile and economical resource for the satellite community, becoming one of the major areas of development and growth. Enabled by advancements in miniaturized space robotics and microelectronics systems, space technologies that are lighter, smaller, and cheaper, yet equally or more functional in terms of the tasks they can perform have been developed. As such, these devices hold significant potential for the economical and efficient space exploration,[1,2] with Earth observation and remote sensing currently being the primary areas of use for nano- and microsatellites. Since 2011, the number of nano- and microsatellite launches have increased at the approximate annual rate of 40%, and it is projected that the demand for these spacecraft will continue to show strong growth, with estimated increase from 101 (in 2016) to 320 – 460 (in 2013) nano- and microsatellites launched globally per year [2017 Nano/Microsatellite Market Forecast by SpaceWorks].[3]

The increasing affordability of nano- and microsatellites and spacecraft redefined the major players in space exploration, with the commercial sector soon to be responsible for the majority of nano- and microsatellite spacecraft launches. This is a significant shift from the historical market distribution where only large commercial players and government organizations could afford to commit >$100M USD to develop, manufacture, insure, deploy, and operate spacecraft. In comparison, the total outlay for functional nano- and microsatellites and space assets start at $1M USD, with the starting cost of building a functional communications satellite estimated to be as low as $25 000 USD. As such, these assets provide a viable and economical solution for space exploration, environmental monitoring, and communication,[4] with immediate tangible benefits to the economic development, resource management, and connectivity of consumers globally. In addition to commercial uses as large and small surveillance platforms by companies such as Terra Bella and Planet and government organization such as NASA, and defense and intelligence missions, customization of on-orbit assets has also enabled their uptake by numerous universities and research institutions, e.g., Georgia Tech, contributing quantitatively and qualitatively to our understanding of Earth's systems. In addition to remote exploration,

satellites specifically dedicated to studying the effects of space environment on living organisms, e.g., GeneSat 1 by the NASA Ames Research Center and electronics, e.g., Cubesat ROBUSTA by Montpellier 2 University, have been developed and deployed. These endeavors will provide critical information for the design and development of technologies for interplanetary missions, e.g., exploration of planets such as Venus and Mars with small satellite and spacecraft systems. The general classification of small spacecraft is shown in Table I.

It is evident that the success of near- and deep-space microsatellite-enabled exploration relies firmly on the development of next-generation propulsion systems,[7] the design of which should be well-matched to the specific requirements of nano- and microsatellite technologies and provide effective and dependable means for controlling their motion in space. Among a multitude of currently pursued propulsion technologies, electric propulsion systems emerged as one of the most promising technologies, with Hall-type and gridded ion thrusters being the most well-known of these systems (Fig. 1).

Concomitant advancements in launch vehicles,[8] e.g., SpaceX Falcon and Arianespace Ariane rocket families that have seen their payload capacity significantly increased, and the introduction of dedicated small launch vehicles also expanded options for affordable space access for small satellites. Indeed, weighing as little as 1 kg for a 10 cm^2 "U"-class Cubesat nanosatellite and no more than 100 kg for a larger microsatellite, these devices take up a fraction of the weight of the conventional communication satellite, which can reach up to 5000 kg and thus can be delivered into space as part of secondary payload rides. To put this in perspective, a single launch of Falcon 9 rocket can accommodate the delivery of a hundred of 50 kg microsatellites onto orbit, at an approximate cost of $\$0.6 \times 10^6$ or less per Cubesat delivered onto orbit.

With strong market demand for affordable space assets, there is little doubt that the number of small satellites will continue to grow (Fig. 2). SpaceX alone has plans to deploy more than 4000 microsatellites into predefined orbits to create a global internet communication system. Similar large satellite networks for environmental monitoring, meteorology, global positioning systems, and tracking of small Solar System bodies, e.g., asteroids, and monitoring of near-Earth space environment are envisaged. Another example is the OneWeb constellation, the project aimed to deploy the first 10 satellites of 150 kg each equipped with low-power Hall thrusters, currently being built in France by Airbus.[9]

This, however, presents new challenges, particularly with respect to accurate management of satellite position on the desired orbit, autonomous operation, and the eventual decommissioning upon completion of its mission.[10,11] Furthermore, these assets need to be able to perform in the hostile environment rich in extreme temperature variations, trapped and transient radiation, and bombardment by high-velocity dust particles and space debris. Similarly, for Solar System and deep space exploration, e.g., of the Moon[12] and Mars[13,14] by robotic orbiters and landers, and of Saturn, comets, asteroids,[15] and deep space[16] by long-life probes, the development of sophisticated, multi-functional, and robust assets with the capacity to navigate towards outer space targets is necessary.

By using electrical energy to increase the velocity of the ionized propellant, electric propulsion systems combine high specific impulse and excellent efficiency at low thrust, which is essential for long-term control over relative position and orientation of orbiting nano- and microsatellites.[17] From this perspective, they compare favorably to solid and liquid

TABLE I. General classification of small spacecraft.[5]

Class	Mass (kg)
Minisatellite	100-180
Microsatellite	10-100
Nanosatellite	1-10
Picosatellite	0.01-1
Femtosatellite	0.001-0.01

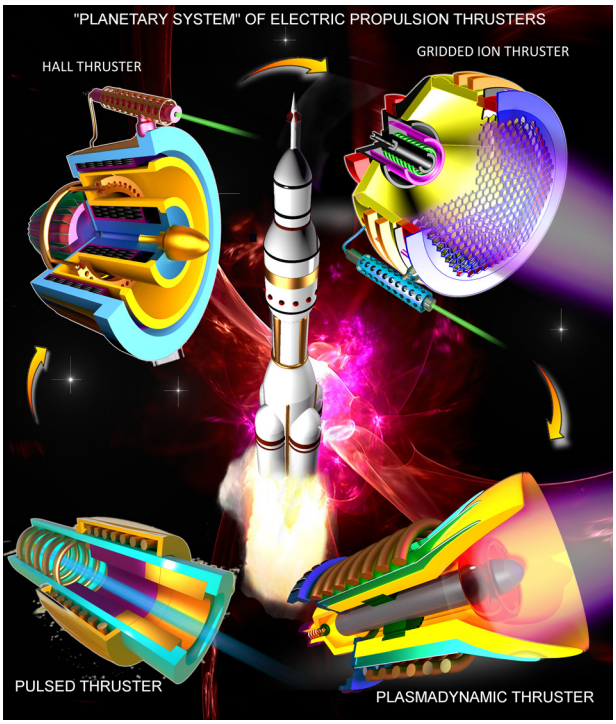

FIG. 1. A "Planetary system of electric propulsion thrusters"—four main types of electric propulsion systems currently tested and used on small satellites and Cubesats. The chemical propulsion systems, which include solid and liquid propellant rocket engines (in the center), feature very high thrust-to-weight ratio reaching 200, with the highest exhaust velocity of about 5000 $m \times s^{-1}$ for the best available chemical fuels (e.g., liquid hydrogen and liquid oxygen). Electric propulsion systems demonstrate much higher exhaust velocities reaching 10^4 $m \times s^{-1}$ (and importantly, there are no physical limitations for the further enhancement), but at significantly lower thrust levels and thrust-to-weight ratios not exceeding 0.01; hence, these systems are not capable of launching the vehicle from the Earth's surface. Plasmadynamic thrusters, pulsed plasmadynamic thrusters, gridded ion, and Hall thrusters form the primary set of electric propulsion platforms capable of powering small satellites. While the gridded ion and Hall thrusters feature the highest energy efficiency numbers reaching 75% (with a promise of even higher levels) at very high exhaust velocities, the continuously operated plasmadynamic systems are capable of producing much higher thrust-to-weight numbers; on the other hand, pulsed thrusters are the primary candidates for ultra-miniaturized systems, which could produce extremely low thrust pulses for precise maneuvering and positioning of small satellites.

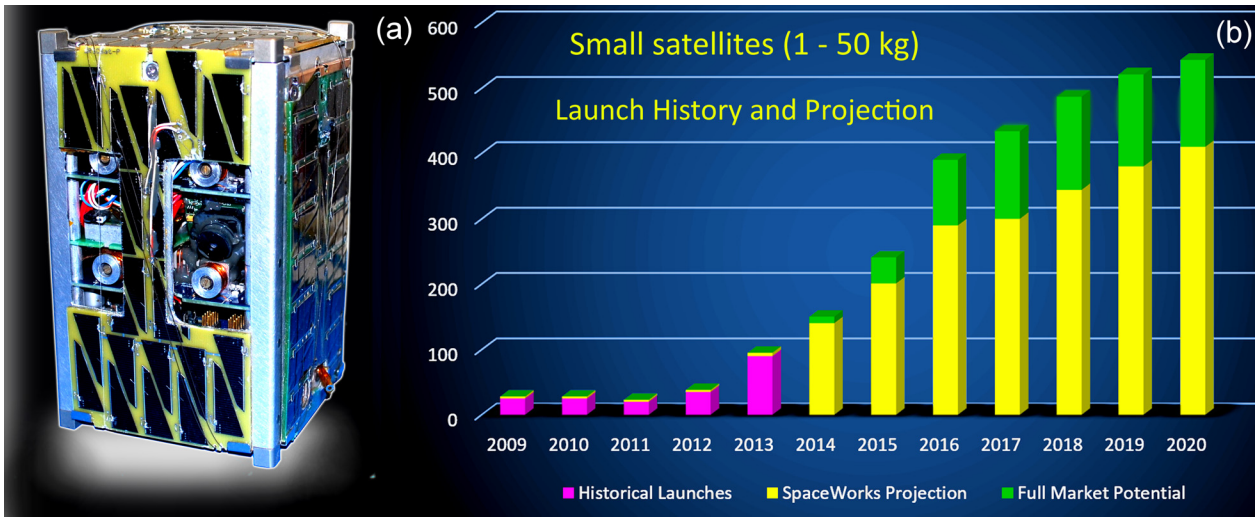

FIG. 2. Cubesats and their launch history. (a) A typical small satellite—BRICSat-P Cubesat of 2 U (2 dm^3, ≈2.5 kg) class equipped with electric propulsion thrusters, ready for the orbital flight.[6] Courtesy of Dr. Jin Kang. Being prime candidates for mega-constellations (large, coordinated groups of satellites capable of working synchronously and coordinately), Cubesats need efficient thrusters to enable efficient deployment, positioning, orbiting, and planned de-orbiting. (b) Nano/Microsatellite (1–50 kg) launch history and projection. Since 2012, launches have experienced a rapid increase, with nearly a tenfold jump between 2012 and 2017, with the trend expected to continue to 2020 and beyond. Data taken from "2014 Nano/Microsatellite Market Assessment," SpaceWorks Enterprises, Inc.[3]

propellant rockets and small chemical rockets, which both deliver a low specific impulse. Importantly, since the acceleration of the propellant relies on the action of electromagnetic or electrostatic forces, the performance of electric propulsion systems, namely, their exhaust velocity, is not physically limited below the speed of light, and thrust can be achieved at a low mass flow rate of the propellant. This means that for the same quantity of the propellant, electric propulsion can support longer missions.[18] Within this family of technologies, for Solar System exploration, devices that exploit electrostatic means of propellant acceleration, e.g., Hall- and gridded ion-type devices, offer better efficiency owing to relatively low energy lost on ionization and heating of the propellant. Another member of the family, the variable specific impulse magnetoplasma rocket also known as VASIMIR,[19] which employs radio waves for propellant ionization and heating and a magnetic field for its acceleration, promises to fill the niche for a system that can operate in high-thrust, low-specific impulse and low-trust, high-specific impulse modes. Other systems currently being developed include pulsed plasma thrusters,[20] magnetoplasma-dynamic thrusters, and numerous others. One of the critical challenges of electric propulsion systems lies in its dependence on the electric energy to increase the velocity of the ionized propellant, making the life-time and efficiency of the device power limited.

II. SPACE ELECTRIC PROPULSION: KEY TYPES AND PRINCIPLES OF OPERATION

Figure 1 depicts four main types of the electric propulsion devices, which could be subdivided into the two major classes: electrostatic thrusters (upper line, represented here with the gridded ion and Hall types) and plasmadynamic thrusters (lower line, illustrated by pulsed and continuously operating plasmadynamic devices). This classification does not cover the entire spectrum of the electric thrust systems, but encompasses a major fraction of these systems; several other types, which are less common yet still considered for Cubesat applications, will be also explored later in the article.

Nevertheless, the four above mentioned space thrust platforms form the majority of the presently-considered systems. Here, we will briefly outline their major advantages and shortcomings, as well as the key operational principles; interested readers are encouraged to explore the literature cited below and herein for further detail.

Gridded ion thrusters are the oldest system proposed for creating thrust in space by accelerating charged particles with the electrostatic field or expelling them while neutralizing the ionized beam with the flux of electrons ejected from a cathode. The main chamber of the modern thruster houses an anode into which propellant gas, most commonly Xenon, is supplied. Then, Xenon is ionized in the discharge and the biased internal mesh extracts ions from the plasma. The second mesh accelerates thus-extracted ions before they are ejected from the thruster. An external cathode is used to produce the electron flux, which compensates the electric charge of the ejected ion flux and ensures that the plasma that exits the thruster is neutral and does not impart a charge on the spacecraft. Importantly, modern ion thrusters also include a *magnetic system* which performs a similar function, i.e., it creates the conditions for maintaining closed drift of magnetized ions in the chamber and thus sustains efficient ionization of the neutral gas due to the electron bombardment.

However, the magnetized electrons cannot compensate the space charge of an accelerated flux near the accelerating grids. Thus, in gridded ion thrusters, the current density of the extracted ions is limited by a space charge created by the ion flux, and hence, the size (diameter) of the thruster shall be enlarged to ensure the required net current of the exhausted plasma. The highest density of ion current that can

be extracted from the quasi-neutral plasma is a function of accelerating voltage and the gap between the accelerating grids and is given by the Child Langmuir law

$$J_G = \sqrt{\frac{2e}{m}}\frac{U^{3/2}}{d^2}\frac{4}{9}\varepsilon_0, \tag{1}$$

where m is the ion mass, U is the voltage applied to the grids, ε_0 is the vacuum permittivity, e is the electron charge, and d is the effective acceleration distance.

In a *Hall thruster*, sometimes called stationary plasma thruster (SPT, Fig. 3), the propellant gas (typically Xe) is supplied to the coaxial accelerating channel through holes in the ring-shaped anode. Electric potential is applied to the external cathode (not shown in Fig. 3) relative to the anode. The geometry of this type of the thruster, specifically its axial symmetry, enables the production of a closed Hall current, and thus, a closed electron drift in the coaxial channel, which can be expressed as a function of the magnetic and electric field vectors B and E as

$$V_d = \frac{\mathbf{E}\times\mathbf{B}}{B^2}. \tag{2}$$

Electrons are magnetized by the radial magnetic field that intersects the axial electric field, which extends between the cathode and anode in the direction of the channel length, where the strength of the radial magnetic field is sufficient to selectively deflect lighter electrons to drift in azimuth as a Hall current, trapped in $\mathrm{E}\times\mathrm{B}$, but low enough as to not impede the motion of electric field-accelerated high-mass ions. Although the majority of the magnetized electrons are trapped within the $\mathrm{E}\times\mathrm{B}$ drift, collisions with accelerated ions, walls of the acceleration channel, and plasma instabilities enable a small fraction of these electrons to be released from the effect of the magnetic field, at which point they begin to drift to the anode.

It is worth noting that in the majority of Hall thrusters, the resulting flow of electrons, i.e., the electron leak current, does not typically go above 10%.[21] From this perspective, the radial magnetic field is an effective means for both electron magnetization within the channel, and concomitantly, *prevention of the electron drift between the electrodes*. Since the force lines of such a magnetic field are at the same electrical potential, it can be viewed as an arrangement of a large number of isopotential acceleration grids that are transparent to ions. Further details regarding the motion of electrons and ions and presently available means for the control of these fluxes can be found in Ref. 22 and other literature available.[23–25]

In the traditionally designed Hall thrusters, magnetic systems usually include a central coil and one or several external coils installed coaxially or around the thruster center. Permanent magnet-based[26] or hybrid magnetic systems (Fig. 3) are also possible. The permanent magnet-based thrusters do not require power supply for the magnetic system; however, the permanent magnets cannot be switched off.

III. MICROPROPULSION IN LABS

In this section, we will examine a state of the art of various micropropulsion systems, their parameters, and recent progress reported at the First Workshop on Micropropulsion and Cubesats (MPCS-2017). The results of flight tests will be addressed and described in Sec. V.

A. Hall thrusters

Traditionally, Hall thrusters attract a special attention of the electric propulsion community. Very high efficiency, simplicity, and potential durability make the Hall thruster one of the primary candidates for miniaturization and application in small satellites and Cubesats. Several types of miniaturized Hall thruster were presented at the MPCS-2017 meeting, including both traditional and cylindrical configurations.

1. Traditionally designed Hall thrusters

Traditional Hall thrusters inherit coaxial geometry with the central insert, which serves two main objectives, namely, as an inner wall confining the plasma and non-ionized propellant and a magnetic pole that helps to shape the magnetic field in the acceleration channel. The Singapore-based Plasma Sources and Application Centre/Space Propulsion

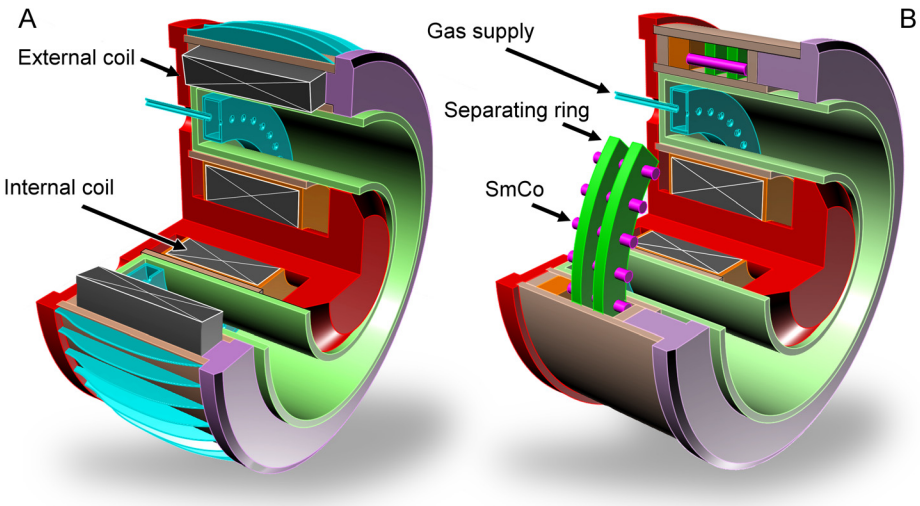

FIG. 3. Traditional (a) and hybrid (b) magnetic systems of the miniaturized (23 mm dia.) Hall thruster designed and tested at the Plasma Sources and Application Centre/Space Propulsion Centre, Singapore. Internal coil comprises around 1000 turns of 0.3 mm wire and can be connected in the straight and reverse direction. While a set of 24 to 50 Samarium-Cobalt permanent magnets ensure the principal magnetization, inner coil allows for a fast, flexible adjustment of the magnetic field configuration. Cathodes are not shown.

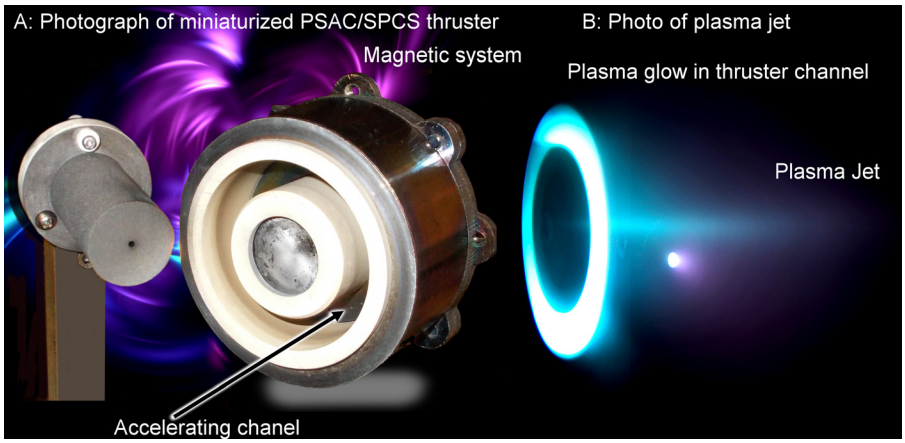

FIG. 4. Photographs of the miniaturized PSAC/SPCS thruster of the traditional coil-based design (A), and optical photograph of the plasma during a test in a chamber. Xenon supply rate is 1 mg s^{-1}, power is 100 W, and discharge voltage is 200 V. No overheating or excessive channel wall wear were detected. Several hundred switch pulses were fired without any failure. The magnetic field at the bottom of the channel is only fractions of μT, which can nevertheless help to guide slow electrons towards the anode. A well collimated jet is clearly visible.

Centre, Singapore (PSAC/SPCS) has developed, tested, and optimized two highly efficient versions of the miniaturized Hall thrusters: a version with electromagnetic coils and a hybrid version with external permanent magnets and an internal adjustment coil (Figs. 3 and 4). Both versions were tested and optimized, and similar results were obtained (see Table II, which lists the main parameters and characteristics of these thrusters). Specifically, these thrusters feature:

- *A highly efficient, light (80 g) thermionic cathode capable of working without external heating, consuming only 0.1 mg s^{-1} of Xenon;*
- *An optimized anode ensuring a very uniform supply of the working gas to the accelerating chamber, and a proper position relative to the magnetic field;*
- *An optimized configuration of the magnetic field for both the coil-based and permanent-magnet based design versions, with the inner coil used for a fine adjustment of the field configuration at the channel face;*
- *A very compact light-weight design, not exceeding 450 g for the coil-based version and 350 g for the permanent magnet-based version;*
- *A short ignition time (several seconds), including the time necessary for cathode heating.*

The thruster has demonstrated a relatively high efficiency (35%) with a very small integral plasma divergence angle of less than 28° (measured *in situ* during the thruster operation in a chamber using a robotised measurement system, described below), thus strongly confirming the chosen optimization approach.

TABLE II. Characteristics and parameters of the two PSAC/SPCS Hall thruster design versions.

Parameter	Basic	Hybrid
Mean channel radius, mm	10	10
Thruster diameter, mm	200	120
Mass, g	450	300
Thrust, mN	0–15	0–15
Power, W	50–200	50–200
Operating voltage, V	100–350	100–350
Operational current, A	0.2–0.7	0.2–0.7
Thrust at 50 W	3 mN	3 mN
Min. ignition voltage, V	50	50
Xe flow rate, mg s^{-1}	0.2–1.0	0.2–1.0
Specific impulse, s	1000–1500	1000–1500
Efficiency, %	30	35
Proven life, h	1000	Under test

No overheating or excessive channel wall wear were observed. A well-collimated, compact plasma jet can be observed in Fig. 4, which depicts an optical photograph of the traditionally designed (coil-based) thruster and a photograph of the generated plasma jet.

The magnetic core has a high Curie point, and the wall of the discharge channel is made of boron nitride (BN), which has a low sputtering yield and a relatively low secondary electron emission under Xenon ion bombardment, and thus is commonly used in Hall thruster channels. A compact magnetron-deposited low-sputtering boron nitride coating synthesized in PSAC/SPCS lab has demonstrated the total wear rate of several nm $\times$ h^{-1}, which corresponds to only 20 μm per 10 000 h of operation. To compare, the typical erosion numbers are: Al_2O_3—0.3 μm/h, diamond—0.7 μm/h, SiC—0.8 μm/h, and BN—1.1 μm/h, with 5000 h service time as a good benchmark for today's thrusters, such as a Snecma Safran Group device that completed a successful mission to the Moon.[29]

2. Coaxial Hall thrusters with permanent magnets

In recent years, Harbin Institute of Technology developed a way to obtain a focused magnetic field from a low power coaxial (i.e., traditionally designed) Hall thruster, using two permanent magnet rings, where the maximum strength of the magnetic field is outside of the channel ($Br_{exit}/Br_{max} = 0.75$ can be obtained) to increase the lifetime of the lower power Hall thruster.[30] Figure 5 illustrates the magnetic structure and configuration of these thrusters.

The approach of pushing down the maximum magnetic field to the plume zone and adjusting the channel length accordingly is proposed to achieve plasma discharge without wall losses. Through simulations, it is confirmed that ionization occurs in the channel and acceleration occurs outside of the channel when the maximum magnetic field outside of the channel is pushed down with two permanent magnetic rings. The wall will only receive bombardment from low-energy ions and electrons, so that the resulting power deposition is small and the wall temperature remains relatively low. This

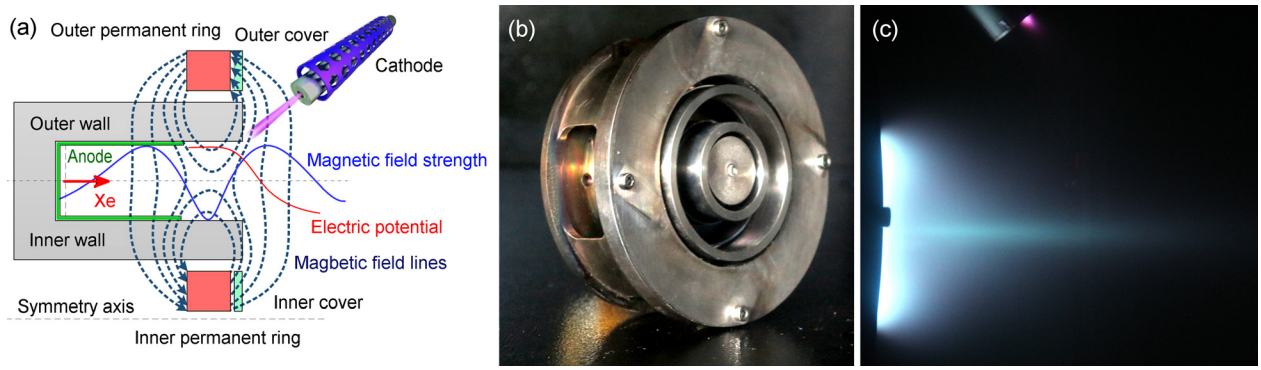

FIG. 5. (a) Magnetic structure and configuration of the thruster.[27] (b) and (c) A 200-W Hall thruster discharge with titanium as the wall material,[28] designed and tested at the Harbin Institute of Technology. The maximum anode efficiency of 34.2% was obtained.

effectively reduces the channel erosion, extending the operational lifetime of the thruster. Furthermore, there is no additional power consumption by the coils, which improves the efficiency of the entire system.

Further, Harbin Institute of Technology designed a 200-W Hall thruster with two permanent magnet rings to verify the technology. This thruster exhibits five interesting features. First, the magnetic field is only generated by the inner and outer permanent magnetic rings. Second, nonmagnetic stainless steel is employed in the gas distributor and anode, and the material for the entire thruster and other metal structures is titanium. There are no other magnetic conductors and no magnetic screen is used. Third, the anode is hollow, and its front face is at the internal magnetic separatrix position. The distance from the zero-magnetic region to the channel outlet is shorter than that of other Hall thrusters, which means the magnetic field gradient is larger than that in the traditional Hall thruster. Fourth, the length of the channel can easily be modified, while the mean diameter and width are unchanged, by using various sets of ceramic rings. Finally, the thruster shell surface is 50% hollow; thus, ceramics in the discharge chamber are directly exposed to effectively reduce their temperature. References 31 and 32 validate preliminary visual observations, i.e., the feasibility of the proposed thruster, which can realize a discharge without wall energy loss or erosion when discharge is through straight and oblique channels ($Br_{exit}/Br_{max} = 0.75$). The maximum anode efficiency is 29.1% (a straight channel) and 34.2% (an oblique channel) with a discharge power level of 200 W. When the channel length is increased to $Br_{exit}/Br_{max} = 0.9$, the anode efficiency can reach 42%.[27]

With the aim of improving the performance and lifetime of lower power Hall thrusters, Harbin Institute of Technology has done some research work on the channel wall material[28] and on anode design.[33–35]

As the ionization occurs in the channel and acceleration occurs in the plume, the simulation and experimental results indicate that maximum electron temperature can be found in the plume zone, while the electron temperature in the channel is relatively low. The secondary electron emission yield of the channel material will have a small but measurable effect on the performance of the thruster, which was verified experimentally. While discharging through a channel with walls of titanium[28] and graphite, it was confirmed that the material with a low sputtering yield can be used to further increase the lifetime of the lower power thruster. Figures 5(b) and 5(c) are the photographs of the prototype of the 200-W hall thruster and the plume discharge, respectively, with the wall material of titanium. While adopting the design with two permanent magnet rings with no other magnetic conductor, a double-peak magnetic field can be formed with a large gradient, with the result that the anode location and shape will affect the performance of the thruster. The simulation and experimental results indicate the indented U-shape hollow anode can further improve the thrust, specific impulse, and efficiency.[33–35] Moreover, two lower-power Hall thrusters designed by the Harbin Institute of Technology with power levels of 10–20 W and 50–100 W, using two permanent magnet rings, yielded also quite high anode efficiency at preliminary tests. In addition, 1.35 kW and 5 kW larger-power Hall thrusters using a permanent magnet have been designed and tested at Harbin Institute of Technology, providing a maximum efficiency of up to 65%. Thus, the hybrid thrusters with permanent magnet could be efficient in a wide range of power levels.

3. Miniaturized cylindrical Hall thrusters

Attempts to miniaturize the Hall-type devices in the framework of the traditional coaxial scheme were not successful enough, and thus the idea appeared to eliminate the inner pole and thus to diminish the mean radius of the channel. The Hall thrusters without the inner insert are called *cylindrical thrusters*. This geometry was first proposed and studied in the Princeton Plasma Propulsion Lab (PPPL).[37]

The cylindrical Hall thruster (CHT) features high ionization efficiency, quiet operation, ion acceleration in a small surface-to-volume ratio channel, and the performance comparable with that of the state-of-the-art Hall thrusters.[38,39] The principle of operation of the CHT is based on a closed $E \times B$ electron drift and electrostatic acceleration of nonmagnetized ions in quasineutral plasma formed in a hybrid magneto-electrostatic trap (Fig. 6). A smaller surface-to-volume ratio in comparison to a typical annular Hall thruster (the so-called Stationary Plasma Thruster or SPT[40]) makes it less subject to channel wall erosion by ion sputtering and more suitable for miniaturization and operation at low power

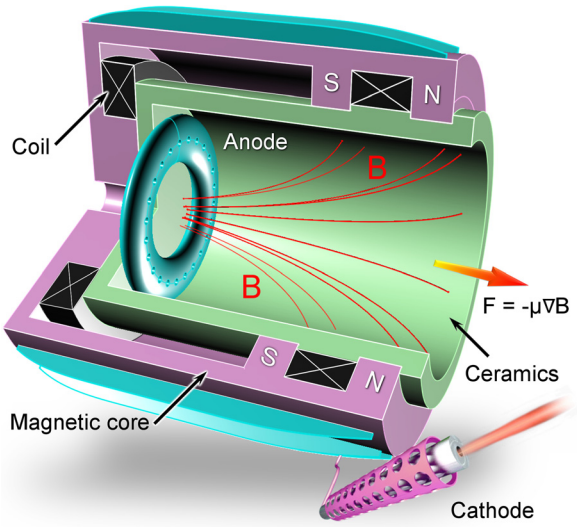

FIG. 6. Schematic of a cylindrical Hall thruster (CHT).[36] A smaller surface-to-volume ratio in comparison to a typical annular Hall thruster makes it more suitable for miniaturization and operation at low power levels. Magnetic field of cusp-type or magnetic mirror-type configurations is typically used in CHT.

levels (< 200 W) which are characteristic for micro propulsion regimes. A more detailed comparison of the CHT with other types of Hall thrusters is given elsewhere.[39,41]

The magnetic circuit of a typical CHT (Fig. 6) includes at least two sources of magnetization (electromagnet coils or permanent magnets) and the magnetic core made of a magnetic material such as a low carbon steel. The magnetic field configuration produced by this circuit can be cusp-type or magnetic mirror-type (Fig. 6).[36] The best performance parameters of the small (2.6 cm diameter) 200 W-class CHT were achieved for the mirror-type configuration produced by the co-direct currents in both electromagnet coils.[42] Even stronger effect on the acceleration region was obtained with the enhancement of the available electron supply from the cathode.[39] The latter was achieved with the increase of the current between the cathode emitter and the cathode keeper of the hollow cathode-neutralizer, or with the increase of the hot-wire current of the filament cathode.[43]

For the CHT operation with the hollow cathode or the filament cathode, the thruster efficiency increased with the increase in the keeper current or the filament current, respectively. For example, for the 2.6 cm CHT, the thruster anode efficiency increased from about 25% to about 40% as the keeper current increased from 0 to 2.5 A.[44] In these regimes, the anode thruster power was 75–200 W. In these regimes, the maximum magnetic field at the mirror was ∼1.5 kG.[45] To produce this magnetic field, the electromagnet coils consumed 50–100 W. Because of this additional power consumption, the overall efficiency of these low power CHTs reduce drastically.

For implementation of the smallest possible CHT scaled down to operate at the lowest power, the magnetic circuit with permanent magnets is needed. The use of permanent magnets instead of electromagnet coils offers a significant reduction of both the total electric power consumption and the thruster mass. A number of permanent magnet versions of the miniaturized CHT (CHTpm) of different overall dimensions were developed and characterized in the power range of 50–300 W (Fig. 7).[47]

The discharge and plasma plume measurements revealed that the CHT with permanent magnets and electromagnet coils operate rather differently.[47] In particular, the angular ion current density distribution from the permanent magnet thrusters has a halo shape, with the majority of high energy ions flowing at large angles with respect to the thruster centerline [Fig. 7(c)]. It was suggested that a strong magnetic field outside the permanent magnet CHT causes these unusual characteristics of the plasma plume. Note that this halo shape of the plasma plume is also common for other types of Hall thrusters with permanents magnets and cusped magnetic field topology, including high efficiency multistage plasma thruster (HEMP),[48] and its miniaturized derivative, diverging cusped field thruster (DCFT).[49,50]

In recent experiments, the magnetic shield attached to the magnetic circuit of the CHTpm was used to reduce the outside magnetic field [Fig. 7(b)]. This modified CHTpm produced a significantly narrower plasma plume of a typical conic shape (Fig. 3). Plasma potential measurements

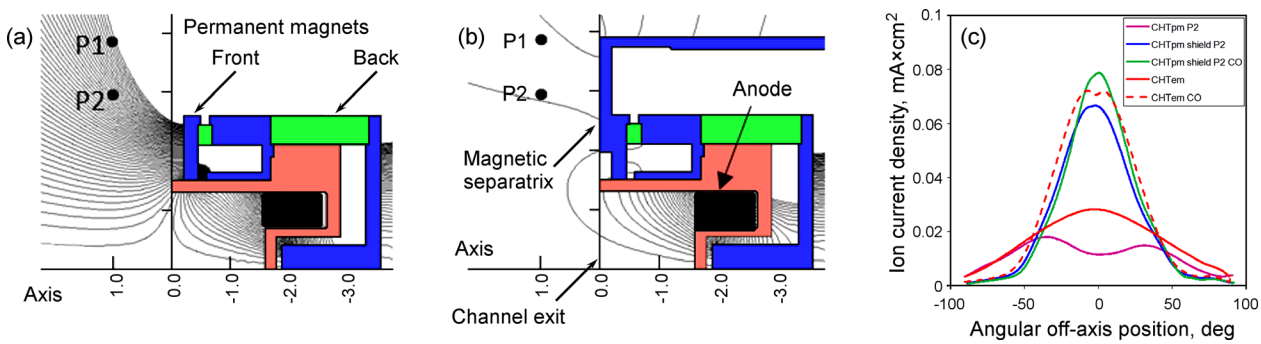

FIG. 7. A 2.6 cm diameter CHT with permanent magnets: (a) without the magnetic shield, $B_{zmax} \approx 2.5$ kGauss at the magnetic mirror and (b) with the magnetic shield, $B_{zmax} \approx 1.8$ kGauss. Magnetic iron parts made from a low carbon steel are marked in blue. Samarium-cobalt permanent magnets are marked in green. Two cathode placements, P1 and P2 used in CHTpm experiments are also shown. Reprinted with permission from J. Appl. Phys. **108**, 093307 (2010). Copyright 2010 AIP Publishing LLC. (c) Effect of the magnetic shield on the plasma plume of the CHTpm thruster. The results of the plume measurements for the CHTpm and CHTpm thrusters with the auxiliary keeper discharge [so-called current overrun (CO) regime with the keeper current of 2.5 A] are also shown. All thrusters were operated at the discharge voltage of 250 V and Xenon gas flow rate of 0.35 mg/s. For the CHTpm thrusters, the cathode placement P2 is shown in (a) and (b). For the CHTpm thruster, the cathode placement was different: the cathode outlet orifice was located approximately 5.4 cm away radially and 2 cm downstream from the center of the channel exit. All dimensions are in cm. Reprinted with permission from Raitses *et al.*, Paper IEPC-2011–175.[46] Copyright 2011 ERPS.

revealed that for the CHTpm without the magnetic shield, a significant portion of the acceleration region (~50%) is placed outside the permanent magnet thruster. In this outside region, the magnetic field is 100–300 Gauss with a stronger axial component than the radial component. It was suggested that this outside electric field causes the increase of the plasma plume divergence leading to the reduction of the thrust. The magnitude of the outside magnetic field can be greatly reduced when the magnetic shield is added to the magnetic circuit [Fig. 7(b)]. The electric field outside the CHTpm also reduces with the addition of the magnetic shield. These results are consistent with recent plume measurements using flux probes and LIF which demonstrated a significant plume narrowing for the CHTpm with magnetic shield, as compared to the plume from the CHTpm without the shield [Fig. 7(c)].[51] Performance measurements of the magnetically shielded CHTpm showed that this thruster can operate more efficient with the anode efficiency of about 27%–29%,[51] than the CHTpm without the magnetic shield ~20%.[52] Moreover, the overall efficiency of the magnetically shielded CHTpm was higher than the overall efficiency of the electromagnet CHT when the power consumed by electromagnet coils is taken into account.

Thus, the experiments have demonstrated the feasibility of high performance CHT with permanent magnets when the magnetic shield is added to the magnetic circuit of this thruster. A key effect of the magnetic shield is on the reduction of the defocusing magnetic field outside the thruster channel and, as a result, the reduction of the ion accelerating electric field in this region. This allows a better focusing of the plasma plume that explains a larger thrust measured for the CHTpm, with the magnetic shield.

Recently, Harbin Institute of Technology designed a cylindrical permanent-magnet Hall thruster with a low power of 50–100 W.[53] The magnetic field distribution in the channel is guided by the magnetically insulated anode, altering the intersection status of the magnetic field line passing through the anode and the wall.

Experimental and simulation results show that a high potential is formed near the wall by the magnetically insulated anode. As the ionization moves towards the outlet, the energy and flux of the ions bombarding the channel wall can be reduced effectively. Due to the reduction in the bombardment of the wall by high-energy ions, the thrust and specific impulse significantly increase, compared with those of the non-magnetically insulated anode. When the discharge voltage is 200 V, the anode mass flow rate is 0.30 mg/s, and the magnetically insulated anode is adopted; thrust increases from 2.81 mN to 3.82 mN, which accounts for a 36.0% increase, the specific impulse increases from 956 s to 1,301 s, which indicates a 36.0% increase, and the efficiency increases from 15.3% to 24.9%, which represents a 9.6% increase. Meanwhile, the length of the sputtering area is clearly reduced, as shown in Fig. 8. The starting position of the sputtering area is in front of the magnetic pole, which can effectively prolong the service life of the thruster.

Neutral flow dynamics is a basic physical process that has a very important effect on the ionization and plasma

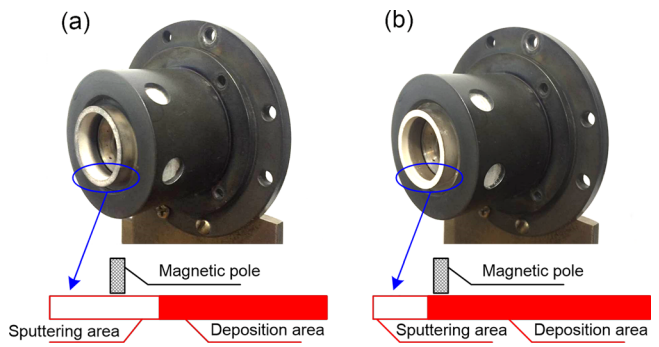

FIG. 8. Photographs of a thruster after a discharge. (a) A non-magnetically insulated anode and (b) magnetically insulated anode. The length of the sputtering area is clearly reduced. The thrust increased to 3.82 mN from 2.81 mN (36.0%); the specific impulse increased to 1,301 s from 956 s (36.0%), and the efficiency increases to 24.9% from 15.3% (i.e., by 9.6%). The starting position of the sputtered area is at the front of the magnetic pole, and this could be considered as a factor which can effectively prolong the service life of the thruster.

motion of a cylindrical Hall thruster. A new Hall thruster design employing a circumferential vortex inlet mode is proposed by Lab of Plasma Propulsion, Harbin Institute of Technology.[54] This new mode makes propellant gas diffuse in the form of a circumferential vortex in the discharge channel of the thruster. Simulation and experimental results show that the neutral gas density in the discharge channel rises upon application of the vortex inlet mode, effectively extending the dwell time of the propellant gas in the channel. According to the experimental results obtained over a range of anode mass flow rates, the vortex inlet increases the propellant utilization by 3.1%–8.8%, thrust by 1.1%–53.5%, specific impulse by 1.1%–53.5%, thrust-to-power ratio by 10%–63%, and anode efficiency by 1.6%–7.3%, considerably improving the cylindrical Hall thruster performance.

4. Miniaturized Hall thrusters with magnetic shielding and wall-less configurations

In conventional Hall thrusters, the material of the annular chamber walls determines to a large extent the plasma discharge properties, and consequently, the propulsion performances as well as the operational lifetime.[55] Plasma-surface interactions are responsible for power losses,[56] structure component thermal stress,[57] and erosion of the dielectric walls due to the bombardment by high-energy ions.[58] The large charged particle flux towards the walls is a direct consequence of the magnetic field topology. In a Hall thruster, the accelerating electric field originates from the sharp decrease of the electron mobility in the channel outlet region, wherein the magnetic field strength peaks. An efficient barrier to slow down electrons in their way towards the anode requires a radial magnetic field, the lines of which intersect the walls. Such a configuration creates a radial electric field that accelerates ions towards the walls with energies above the material sputtering threshold.

The magnetic shielding (MS) is a recent concept, where the aim is to significantly reduce the charged-particle flux to the channel walls, which has been shown to greatly lower wall erosion over a broad range of input powers.[59,60] The

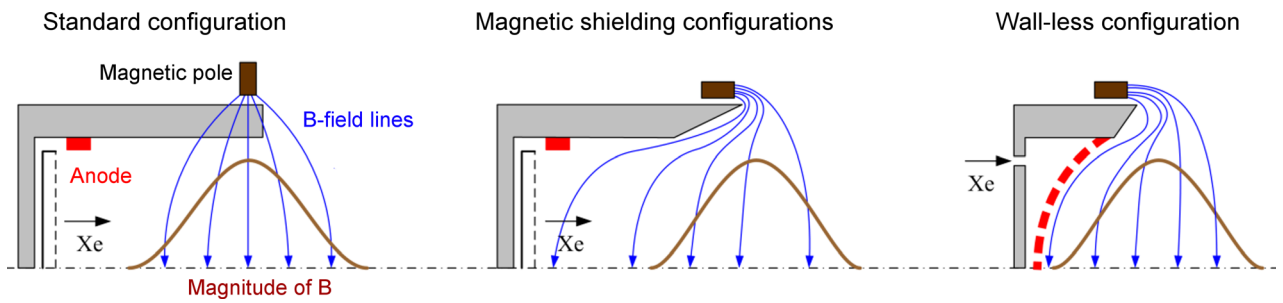

FIG. 9. Typical configuration and magnetic field topology for a classical (left), a magnetically shielded (middle), and a wall-less Hall thruster (right). In the magnetically shielded (MS) configuration, unique field topography is obtained, where so-called grazing lines, which are parallel lines in the proximity of the walls, effectively reduce the strength of the radial component of the electric field. These lines reach the anode region, where the temperature of electrons is low. Along these grazing lines, the mobility of the electrons is high, which facilitates a large plasma potential in the proximity of the wall.

thruster service life is therefore significantly extended while conserving the performance level. Briefly, MS relies on preventing the magnetic field lines from crossing the walls in the acceleration region. The unique MS field topology is formed by these parallel lines near the walls, also termed "grazing lines," which extend to the anode region where electrons are cold. The high electron mobility along the magnetic lines allows for the maintenance of a high plasma potential in front of the walls. Such a topology strongly reduces the magnitude of the radial electric field component. Another relevant characteristic of the MS approach is the shift of the magnetic field peak slightly beyond the channel exit plane. As magnetic and electric fields are closely linked in a Hall thruster, the ion energy is in this way limited inside the channel. Finally, the concave field lines also help directing the ions away from the wall. Figure 9 portrays the magnetic field topology for a standard (unshielded) and a magnetically shielded Hall thruster.[61–63]

The utility of the MS configuration has first been realized and demonstrated in high power devices. However, more recently, studies have also been performed at a low power with the 200 W-class ISCT200-MS and the 300 W-class MaSMi-60 Hall thrusters.[64,65] The two thrusters have chambers of about the same size and the wall material is BN-SiO_2 and BN, respectively. The ISCT200-MS uses permanent magnets, whereas the MaSMi-60 uses magnetizing coils to generate the magnetic field. These works demonstrate that efficient MS can be achieved at a low power, with a drastic reduction in the wall erosion rate and substantial improvement in the thruster lifetime despite wear of the magnetic pole pieces. While the plasma plume divergence angle is not notably affected in MS, the thrust-to-power ratio, specific impulse, and efficiency are lower compared to the results from high-power devices. These works indicate that the drop in performance may originate from a poor propellant utilization, as the increase in the amount of multiply-charged ions due to high electron temperature in MS consumes a small fraction of the power.[64] A plausible explanation is the reduction in the plasma production volume that is imaged by the near wall dark zone typical of an efficient shielding [see Figs. 10(a) and 10(b)]. This effect diminishes when the thruster size is increased, hence the observed negligible impact at high input powers.

Another advantage of the MS configuration is the possibility to use conducting channel walls without negatively affecting the device performance. Experiments with the ISCT200-MS thruster equipped with carbon walls reveal stable operation with unchanged parameters compared to ceramic walls,[66] which paves the way to cheaper and simpler Hall thrusters.

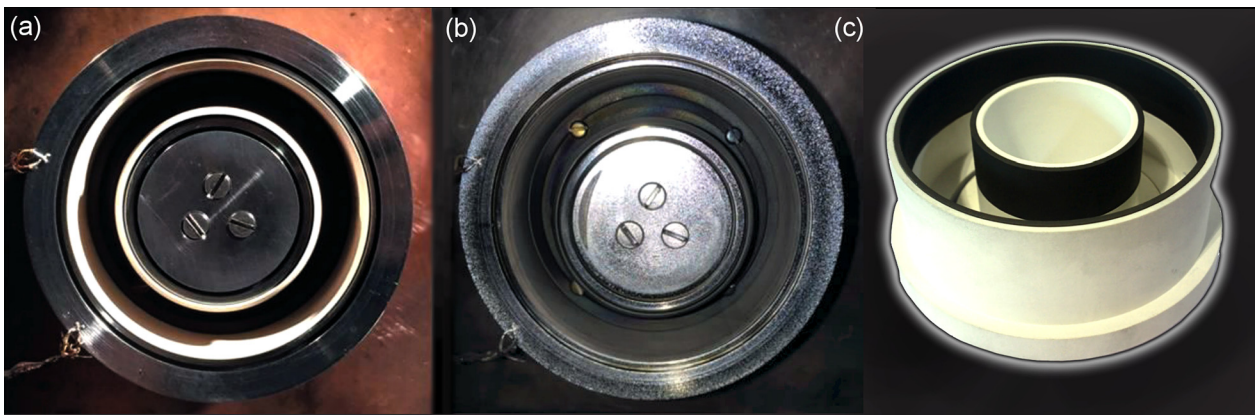

FIG. 10. A comparison of the MaSMi-60's discharge channel and pole faces before (a) and after ~20 h of operation (b). Note the uniform layer of carbon deposited on the inner and outer cannel walls, suggesting the presence of magnetic shielding, and the level of front inner and outer pole face erosion. Reprinted with permission from Conversano *et al.*, Paper IEPC-2015-100. Copyright 2015 EPRS.[63] (c) Conducting discharge channel walls with the graphite inserts for testing the magnetic shielding operational regimes. Reprinted with permission from J. Appl. Phys. **122**, 033305 (2017). Copyright 2017 AIP Publishing LLC.[70]

There is another alternative to limit interactions between the plasma and the surface in Hall thrusters, hence prolonging the lifetime of the device. The basic principle is to shift the ionization and acceleration regions outside of the discharge chamber. This unconventional design was named a Wall-Less (WL) Hall Thruster.[67] In a WL thruster, the anode is moved to the exit plane of the dielectric channel keeping the architecture unchanged. As a consequence, the electric field is shifted entirely outside of the channel, in a region where the magnetic field gradient is negative. The performance level of a WL ion accelerator strongly depends upon the anode geometry. In order to prevent large electron losses at the anode, a magnetic barrier must be created by making the magnetic field lines parallel to the anode surface,[68] as illustrated in Fig. 9. Such a topology is achieved by injecting the magnetic flux in the axial direction. In addition, the anode is curved to avoid any interaction with the magnetic field lines. An optimized WL configuration resembles the MS configuration, nevertheless no lines extend deep into the channel. This difference makes the generation of a WL topology easier compared to a MS topology. There are various possible designs for WL Hall thrusters, all of them sharing optimized propellant gas injection to favor ionization within a narrow region ahead of the anode. As the anode acts as a gas distributor, the channel can be eliminated, which reduces the mass, volume, and complexity of the device compared to conventional Hall thrusters. It has been recently demonstrated that moving the magnetized discharge in the vacuum does not compromise the ion production and acceleration. First experimental efforts show that WL thrusters can deliver several mN of thrust with a specific impulse above 1000 s and an efficiency in excess of 20% for input power below 400 W.[69] Currently, the large ion beam divergence angle remains a weak point of this design. Nonetheless, possible solutions do exist, such as the use of screens or novel anode architectures.

A high-efficiency low power Wall-Less Hall thruster would offer significant benefits for micro-spacecraft propulsion in terms of device integration, the operating envelope, lifetime, fuel options and cost. From a more fundamental standpoint, a wall-less ion source is an ideal platform for the study of cross-field discharge configurations with sophisticated laser-aided diagnostics. It provides an easy access to key regions of the plasma and it allows for the study of the physical phenomenon without the influence of wall processes.

Finally, it is worth introducing a very recent new Hall thruster architecture developed to offer a low cost, erosion-free solution for microsatellite propulsion. The design relies upon a two-peak magnetic field topology obtained with permanent magnets only and an extended anode.[27,33] This unconventional design can be seen as a hybrid approach between the MS and WL concepts, as the discharge is largely outside of the chamber and walls are magnetically protected from the charged-particle flux. Numerous works reveal a high thrust level and efficiency around 30% at low power. Furthermore, this design is able to operate with conducting walls,[28] which indicates MS-like behavior [Fig. 10(c)]. Although the concept has still to demonstrate a stable operation over a long time period with a significant increase in the lifetime, it must be considered at this stage as a potential option for electric micropropulsion.

B. Other types of miniaturized thrusters

Even though Hall thrusters occupy a large niche among existing electric propulsion devices, there are many other types of electric propulsors which are subject to extensive research and design efforts. In this section, we will consider several of these miniaturized devices that have attracted attention at MPCS2017.

1. Micro-cathode arc thrusters for Cubesat propulsion

Since 2009, the George Washington University's Micropropulsion and Nanotechnology Laboratory (MpNL) has developed several successful configurations of micro-thrusters, including a Ring Electrode, a Coaxial Electrode, and an Alternating Electrode, which exhibit distinct performance and operational characteristics with respect to thrust, operational lifetime, EM/RF emission, etc. Evaluation of the requirements for additional sub-systems that are needed for integration with any small satellite platform including enclosures, power converters, plasma power units/pulsed power units, high current and low current printed circuit boards, telemetry sensors, command processors, is currently underway at the MpNL and Electromagnetic Compatibility (EMC), where an investigation plan has been chalked out with the assembly of an EM/RF test and measurement equipment stack covering HF (1–30 MHz) to SHF (~10 GHz), with automated control.

Recently, a novel thruster design, namely, the micro-cathode arc thruster (μCAT), was developed and investigated.[71,72] This thruster improves on the vacuum arc discharge thruster by applying a specially designed external magnetic field.[73] The unique magnetic field conditions achieved in a vacuum arc offer several potential advantages in these devices.[74]

The μCAT micropropulsion subsystem, which is being developed for use in space Attitude and Orbit Correction applications, is presently a very active research program at MpNL. In December 2012, the basic GWU microthruster technology was selected by NASA Ames Research Center, via a Center Innovation Fund 2013 research grant, "Micro-Cathode Arc Thruster Phonesat Experiment," as a potential in-space propulsion system for LEO operations of a Phonesat, a Cubesat-format spacecraft. Elsewhere, the μCAT family of technologies is also being investigated for in-space propulsion needs of a range of spacecraft, from Nanosatellite (1–10 kg) to bigger than Microsatellite (~100 kg) in a variety of mission scenarios. Under the auspices of the ongoing Phonesat Experiment, experimental hardware and software components are being designed and tested. The goal of the project is to integrate multiple μCAT sub-systems, with the Phonesat bus avionics, to demonstrate commanding of the thrusters for Attitude control and orbit maneuvers. To test control systems, an Android App compatible with the PhoneSat bus will be developed to control 4 thrusters to enable the tests in a vacuum chamber.

The μCAT is a simple electric propulsion device that combined with a magnetic coil and an inductive energy storage power processing unit (PPU) results in a low mass (<100 g) system. A picture of the μCAT system and two types of the thrusters are shown in Fig. 11. Figure 11(a) shows the schematic design of the ring electrode μCAT (RE-μCAT), which consist of an annular titanium cathode and an annular copper anode of the same diameter and 1 mm width. The annular ceramic insulator tube having same inner and outer diameters and a width of about 1 mm was used as a separator between the arc electrodes. Figure 11(b) shows the schematic design of the coaxial μCAT. Instead of the ring electrodes, this design employs cylindrically-shaped cathode and anode.

The μCAT operates by producing a fully ionized plasma on the inner surface of the electrode. The plasma is formed at the cathode spots[73,74] and expands into the vacuum zone under the applied magnetic field gradient.

Optical visualization showed that the cathode spot consists of either a homogeneous bright region or of cells and fragments with a typical total size of about 10–100 μm.[74] The μCAT is equipped with a coil that provides magnetic field strength in the range of 0–300 mT. It is known that the presence of a transverse magnetic field at the cathode surface produces arc rotation in the J × B direction.[74]

The observed vacuum arc cathode spot rotation has important implications for propulsion since the cathode spot rotation leads to the uniform cathode erosion, which is critical for assuring long thruster lifetime. In previous work,[75] the μCAT cathode spot rotation has been measured under different magnetic field strength utilizing a 4-probe assembly of Langmuir probes. Four single probes were located along the azimuth direction inside the thruster channel to measure the ion current along the plasma stream. The rotation speed was calculated using a quarter of circumference of the thruster inner surface divided by the delay time between each two adjacent peaks. It was found that the spot rotation speed increased about 5 times (from 20 to 100 $m \times s^{-1}$) as the magnet field strength increased from 0 to 300 mT.

The ion velocities in the plasma jet generated by the micro-cathode arc thruster were measured by means of the time-of-flight method equipped with an enhanced ion detection system (EIDS).[72] Two characteristic regions in the ion velocity distributions were identified when measured as a function of the distance from the cathode, with the magnetic field strength as a parameter. The first region (approximately up to 80 mm from the cathode) is the inter-electrode zone in which plasma is being produced and accelerated by the pressure gradient due to electron-ion coupling, i.e., by a gas dynamic mechanism.[76] The second region (80–150 mm) is the plasma expansion inside and outside of the thruster where ion acceleration was observed. The average ion velocities increase with the strength of the magnetic field and with distance from the plasma source.

Typically, the micro-cathode thrusters are designed to produce thrusts at μN to tens of μN level. Thus, accurately resolved thrust bit measurements have to be conducted to estimate this force. To this end, a specialized measurement system known as the thrust stand mass balance (TSMB) has been used to measure forces in the μN to mN range. The thrust measurement with a different strength of the magnetic field has been described and discussed elsewhere.[71] The average impulse bit increases from about 0.1 μN-s at zero magnetic field to up to about 1.15 μN-s in the case of 0.3 T magnetic field. Thus, it can be concluded that the impulse bit increases tenfold when the magnetic field is applied.

A comparison was made to assess the thruster performance without any magnetic field and with a magnetic field of B = 0.3 T. It was found that the magnetic field leads to an increase in velocity and thus the specific impulse by a factor of 1.5. Also, most importantly for propulsion applications, the magnetic field could lead to an impulse bit increase by a factor of 10.

An analysis of the possible thruster contamination due to the backflux was also performed. It was found that due to the fully ionized plasma state, the plasma jet leaving the thruster has a divergent cone of about 45° half-angle. No ion current was detected on 0° probe, suggesting that there is no backflux from the plasma plume.

Overall, μCAT has a thrust-to-power ratio of about 20 μN/W, with the efficiency of up to 15%.[74] One of the major inefficiencies of the system is associated with the fact that only about 10% of the discharge current is the ion current, which contributes to the thrust.[20] 90% of the discharge current is conducted by electrons contributing to the anode heating. By utilizing the ablative anode material (or modifying the anode geometry) so that anode ablation becomes significant, a twofold result is expected: the anode temperature

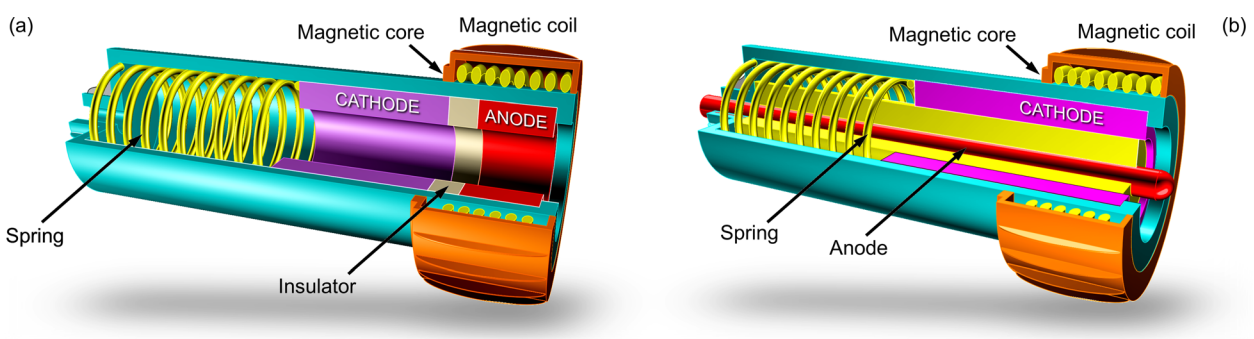

FIG. 11. (a) Schematic design of a ring electrode μCAT and (b) schematic design of a coaxial electrode μCAT. Designed and tested at the Washington University's Micropropulsion and Nanotechnology Laboratory (MpNL).

will be decreased due to ablative cooling, and the anode material will be injecting, thus increasing the flow rate. Flow rate directly contributes to the thrust increase if flow velocity can be maintained. The main idea is that anode material must be injected in the acceleration region. As such, ion-neutral collisions will lead to neutral acceleration and formation of the ion-neutral flow. Since under these conditions, the ion acceleration and the momentum-transfer collisions from ions to neutrals occur in the same region simultaneously, momentum is not only transferred to the neutral-gas but also the total momentum delivered by the electric force to the ion-neutral flow is greatly increased.[20] Schematically the concept is shown in Fig. 12.

Thus, μCAT system has been developed. It has been found that the magnetic field strongly affects thruster characteristics, increasing the specific impulse and the impulse bit. The cathode spot motion was observed and results indicated that the magnetic field leads to cathode spot rotation that is critical for uniform cathode erosion. The plasma plume distribution outside of the thruster channel has been presented to analyze the effect of the magnetic field on the plasma plume. μCAT equipped with a magnetic field operates efficiently and gives great flexibility in producing specific impulse and impulse bit by simply varying the magnetic field strength.

2. Electrospray thrusters

In electrospray emitters or colloid emitters, an electrostatic voltage is applied between a liquid propellant, exiting from a small diameter capillary, and an extraction electrode. At the capillary's facet, the electric field deforms the surface of the liquid into a sharp tip, i.e., the Taylor cone. The liquid needs to be electrically conducting for a Taylor cone to form. Field enhancement at the tip leads to high local electric field strengths, causing droplets of the propellant or, ideally, pure ions to be emitted. The term electrospray emitter is usually understood in a narrower sense to include only emitters using an ionic liquid as propellant and to exclude liquid metal ion sources (LMIS), which are considered to fall into a category of their own. The term field emission electric propulsion (FEEP) should cover all the types of thrusters mentioned in this paragraph so far, but is mainly used in the LMIS community. We understand colloid emitters to be synonymous with electrospray emitters, with the former term being more popular in Europe.

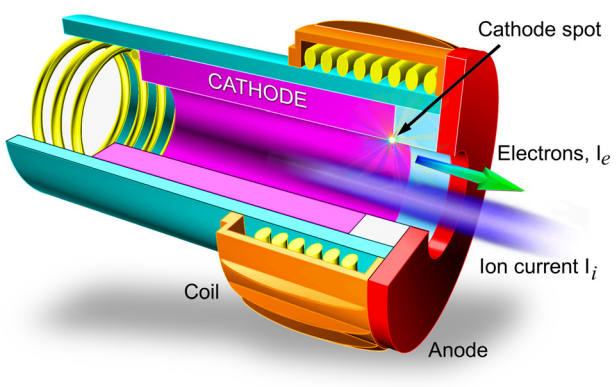

FIG. 12. Schematics of the proposed concept of micro-cathode arc thruster with high thrust (μCAT-HT).

An important advantage of electrospray emitters (using ionic liquids as propellant, which we will assume from now on) is that they can operate in an ambipolar mode. With a suitable choice of the ionic liquid, this has the potential of eliminating the need for an external neutralizer. Another advantage quoted frequently, particularly in comparison with liquid metal ion sources, is that the risk of contamination of the spacecraft should be lower. Whether this is indeed the case is still a matter under investigation.

Conventionally manufactured thrusters, that is thrusters made using the precision mechanics methods available in a mechanical workshop, are too large for very small satellites, such as Cubesats.[77] From this potential application alone, the need for miniaturization of (electric) thrusters is obvious. Miniaturization of electric propulsion has been pursued over the past decade at least, and there appears to be a general consensus that successful miniaturization of thrusters will be an enabling technology for new space applications. Electrospray thrusters are quite promising in this context because they scale favorably upon miniaturization, which means that their performance per unit volume or mass becomes better as the geometric dimensions are shrunk. This is contrary to, for example, thrusters based on a stationary plasma, which suffer from the increased surface-to-volume ratio as the geometric dimensions of the device are reduced.

Electrospray emitters with flight heritage or at least at a high TRL have been covered in a recent review by Lemmer.[77] Electrospray thrusters are available commercially from Busek, Inc., in the United States.[78] These devices appear to be manufactured using high precision conventional machining.

Further miniaturization, however, will most likely require the use of techniques from the engineering of microelectromechnical systems (MEMS). The field of MEMS has evolved from the planar microfabrication technologies developed for microelectronics, with photolithography and thin film deposition and etching processes as the most essential technologies. These have been complemented by technologies like surface micromachining and bulk micromachining of silicon that allow the microfabrication of (almost) three-dimensional structures. Prominent examples of MEMS devices are the acceleration sensors that are ubiquitous in consumer electronic products. In spite of all progress in MEMS, the number of manufacturing processes available to the designing engineer is considerably lower than in conventional mechanical machining. In MEMS technology, for example, there exist no processes based on the plastic deformation of materials, and no metal cutting processes like turning, to name just two examples.

Miniaturization via MEMS technologies, i.e., by approximately two orders of magnitude compared to conventional precision engineering, brings with it the paradigm of massive parallelization of microthrusters. No longer will individual thrusters have to be tailored to the impulse bit and thrust ranges demanded by a specific mission. Instead, analog to the developments in display technology, thrusters of the desired thrust will be created by operating a large or very

large number of identical single microthrusters, like the individual pixels comprising displays of very different sizes. This concept of multiplexing or scaling-up-by-numbering-up is expected to preserve the advantageous properties of the individual thruster, like a high specific impulse,[79] while at the same time providing a pathway to rather short development cycles and to reduced cost, given a proper economy of scaling. Other consequences of massive parallelization might be the relaxation of lifetime requirements, since a suitably designed array of microthrusters can be expected to degrade gradually, as opposed to a conventional thruster whose failure will usually cause the entire mission to fail unless backup (for which there will hardly be space in Cubesats) is available. Again this is similar to display technology where the failure of individual pixels usually does not render a display completely useless.

A positive side effect of successful microthruster development may be that individual microthrusters or small arrays of such microthrusters could be used for the very high precision attitude and orbit control maneuvers required by scientific deep space missions, for example, LISA-like missions.[82]

For the past decades, microelectromechanical systems engineering has relied predominantly on silicon technology,[83] profiting not least from the tremendous technological progress in the microelectronics industry, as demonstrated by Moore's Law. Consequently, microfabricated electrospray thrusters reported in the literature have been based on silicon technology at least for the fabrication of the most critical layer, i.e., the one containing the capillaries. The extraction electrodes or acceleration electrodes may be fabricated using conventional precision engineering, and either be aligned externally in a test fixture, or integrated with the silicon die to form hybrid devices. Electrospray emitters with both extraction and acceleration electrodes made in a completely integrated planar process silicon technology sequence were demonstrated by the European MicroThrust consortium.[84] Their fabrication process, based on various deep etching steps and on wafer-level assembly by low temperature glue bonding, owes its complexity not least to the limited number of planar microfabrication technologies available. This demonstrates that the design rules imposed by current MEMS technologies are a limiting factor to the rapidness of development cycles.

Porous tungsten emitters, so-called impregnated LMIS, combine the advantages of both needle and capillary systems. An example of such system is shown in Fig. 13(a).[80]

Nevertheless, silicon technology is the current state of the art in microfabricated electrospray thruster research.[84] Externally wetted microfabricated emitter tips have recently been reported.[85] However, the vast majority of MEMS emitters uses capillary type emitters as described above, called internally wetted emitters in this context. The hydraulic resistance of the capillaries has been identified as a key parameter for stable operation. By adding a layer with microchannels, the hydraulic resistance can be adjusted using genuine MEMS technologies,[86] possibly replacing previous approaches like adding orifices along the capillary or filling the capillaries with microspheres.[87]

Measuring the very small thrusts delivered by electrospray devices can be achieved on force balances based on modified measurement electronics from high precision scales.[88] Unlike other (larger) electric propulsion devices, electrospray thrusters, when operated by battery power and controlled by radio, can be placed on a test rig without any electric or fluidic connections that would be prone to introducing external torque. Different designs of test rigs have been reported, most recently a magnetically levitated test bed that allowed to demonstrate the ability of electrospray thrusters to serve as precise actuators in small satellite attitude control.[89]

The operation of multiplexed electrospray microthrusters has to the best of our knowledge not been shown with individually addressed emitters. Since in all work reported so far, several emitters share a common extraction electrode, the question arises whether the emission is synchronous and homogeneous over the array of emitters. For an array of 480 porous emitters, measurements of the spatial uniformity and estimations of the fraction of tips emitting have been reported by MIT.[90] The propellant in this device was supplied passively,[91] and the thruster was operated in an ambipolar mode with a change in polarity every thirty seconds. Whether the alternating ambipolar operation of an entire microthruster array is preferable to the parallel operation of two microthruster arrays of opposite polarity, possibly also operated alternatingly,[92] is a topic currently under investigation.

Figure 13(b) shows a flight assembly consisting of four thruster cluster assemblies, each containing 9 LMIS units and assembled in a truncated pyramid shape structure. This platform was intended for Laser Interferometer Space Antenna (LISA Pathfinder) project, a precursor co-operative mission between ESA and NASA to detect gravitational waves.[81]

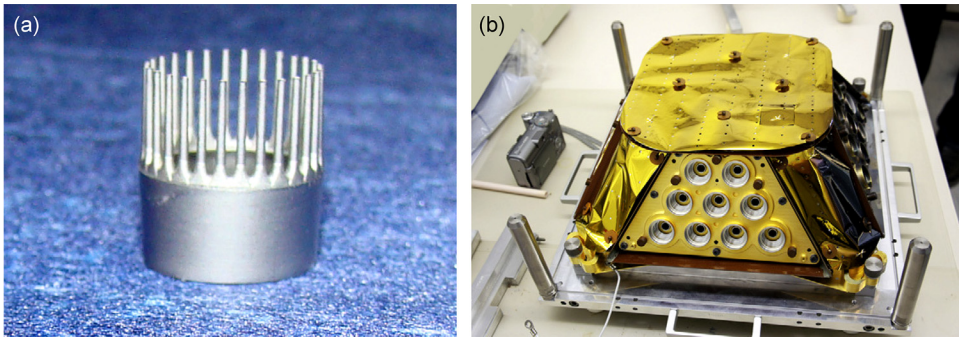

FIG. 13. (a) Porous tungsten emitters (impregnated LMIS) in the form of crown with 28 needles. Reprinted with permission from M. Tajmar *et al.*, Ultramicroscopy **111**, 1–4 (2010).[80] Copyright 2010 Elsevier. (b) Flight assembly consisting of four thruster cluster assemblies, each containing 9 LMIS units and assembled in a truncated pyramid shape structure. Reprinted with permission from C. Scharlemann *et al.*, Acta Astronaut. **69**, 822–832 (2011).[81] Copyright 2011 Elsevier.

As an alternative to silicon based MEMS technology, photostructurable epoxy polymers like SU-8 are being considered as the materials of choice.[93,94] Employing a sequence of several photolithography steps, this technique allows the integration of both capillaries and extraction grid support, separated by a spacer layer, using the same lithography apparatus, thus providing an alignment precision in the range of less than two micrometers. Using angled evaporation of a start-seed-layer onto the extraction electrode support and subsequent galvanic coating, two other genuine MEMS technology processes, the extraction electrode itself can be integrated.[93]

A fairly recent all-photolithography approach to the miniaturization of electrospray thrusters makes use of the novel technology of 3D microlithography, also known as microstereolithography or two photon-lithography.[94,95] In 3D microlithography equipment such as the Nanoscribe series of instruments,[96] a laser beam whose photon energy is not high enough to cause photoresist exposure is passed through microscope optics. Around the focus of the optics, the intensity is so high that two photon processes may occur. The volume in which this happens, and in which the photoresist is exposed by two photon absorption, will usually be smaller than the wavelength of light at least in the horizontal directions. By scanning this focus through the photoresist in three dimensions, almost arbitrary structures can be created. Figure 14 is a scanning electron microscope image of a demonstrator structure made by two photon microlithography. Stereolithographically produced electrospray emitters monolithically integrated with extraction electrodes have also been reported at a micrometer sized voxel resolution.[97] The obvious advantage of 3D microlithography is that the design rules are quite relaxed compared to both silicon technology or stacked multilayer 2D lithography of photostructurable polymers. The latter, for example, cannot provide undercut geometries that will certainly be required by any extraction electrode design optimized for its ion optical properties. Also, the high resolution that allows the creation of openings with a diameter of a few micrometers will allow for an optimized design of the propellant feed system, regarding both the hydraulic properties of the channel and the shape of the emitter at the end of the capillaries. Here, a tapered design ("volcano emitters") is preferable to mitigate the problem of undesired wetting of the photopolymer by the ionic liquid.[98] Tapered emitter structures with a diameter of less than two micrometers have been made in photostructurable polymer, aligned to the capillaries contained in a pre-fabricated photopolymer membrane, using Nanoscribe 3D technology.[95]

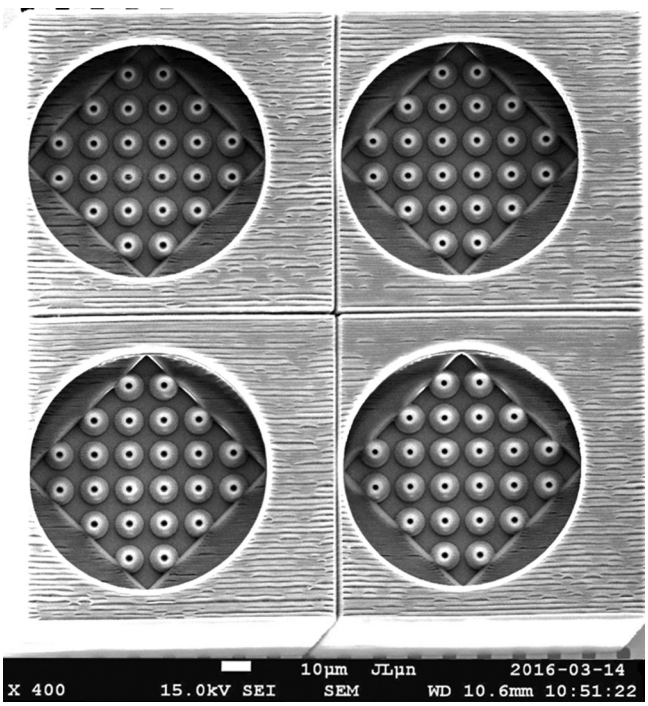

FIG. 14. SEM image of a structure comprising tapered emitters, and an integrated spacer and extraction electrode support layer, produced with a Nanoscribe instrument at the Karlsruhe Nano Micro Facility, Germany. The emitters are aligned to holes in a porous silicon substrate.

Electrospray emitters made with various MEMS technologies appear to be viable candidates for future Micropropulsion systems, and no clear favorite among the competing technologies has emerged so far.

3. Miniaturized high-density helicon thrusters

Helicon plasma[99] sources are very promising, since they can produce a high-density RF plasma of up to $\sim 10^{13}\,\mathrm{cm}^{-3}$ over a wide range of external parameters, in the presence of an axial magnetic field. There are many various helicon sources already developed for plasma propulsion as well as for fundamental studies of plasma phenomena. These sources have an advantage of an electrodeless design, i.e., no direct contact between the plasma and electrodes because electrodes/antennas are wound around a discharge insulation tube, leading to a longer operation time without wear of electrodes and contamination of the plasma. At Tokyo University of Agriculture and Technology, plasmas with a very broad range of discharge diameters of 0.3–74 cm and of an axial lengths of 4.7–486 cm were produced[100,101] (these are world records).

High-density, but small diameter plasma sources with a good efficiency and controllability are important for space propulsion, since they can be utilized as, e.g., an attitude control and clustered-compact thruster in space. However, there have been few experiments to produce small helicon plasmas less than a few cm inner diameter (i.d.). For example, a device with a 2.5 cm i.d.[102] was demonstrated by our group (the smallest diameter at that time of operation), producing an electron density n_e greater than $10^{13}\,\mathrm{cm}^{-3}$ with an input RF power $P_{rf} = 400\,\mathrm{W}$. Later, a device with an i.d. of 2 cm was reported by Batishev[103] (n_e data not shown), where these can be operated under a low pressure condition on the order of Pa range with the axial magnetic field.

Here, recent experimental results on the RF plasma production from helicon sources of a very small diameter will be reviewed, where the plasma diameter is further reeduced to less than 2 cm by the use of the Small Helicon Device (SHD),[104] as shown in Fig. 15. Here, plasma production in Inductively Coupled Plasma (ICP) and helicon modes, as well as plasma acceleration in this electrodeless condition where the acceleration antenna is also located outside of a

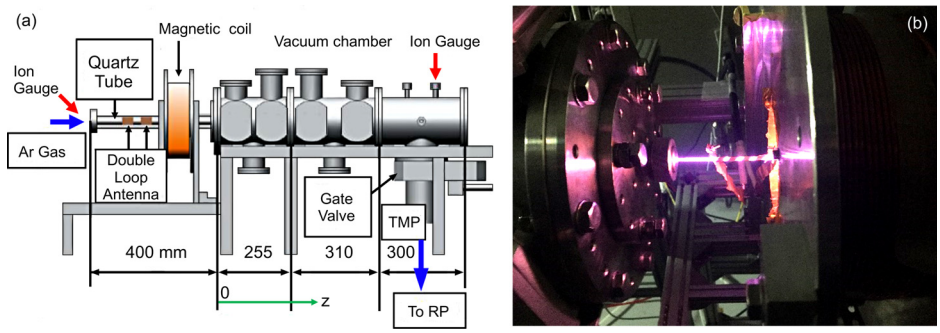

FIG. 15. (a) Small Helicon Device (SHD) and (b) photo of 1 mm diameter rf plasma. These sources have an advantage of electrodeless condition (no direct contact between a plasma and electrodes because electrodes/antennas are wound around a discharge insulation tube), leading to a longer operation time without wear of electrodes and impurity contamination into a plasma. Here, plasmas with a very broad range of discharge diameter of 0.3–74 cm and of an axial length of 5–490 cm, approximately, were produced by various helicon sources.

quartz discharge tube, will be discussed. This device can accept various sizes of small-diameter quartz tubes with the use of permanent magnets and/or electromagnets, as well as to accept various types of production and acceleration antennas. Working gas is introduced from the left-hand side in Fig. 15, and on the right-hand side, the discharge quartz tube is connected to the vacuum chamber, 16.5 cm in i.d. and 86.5 cm in an axial direction, which works as a buffer tank of the discharge tube.

In this device, we have produced high-density plasma of up to $\sim 10^{13}\,\mathrm{cm}^{-3}$ with a very small diameter of 0.1–2 cm with and without the magnetic field, applying the RF frequency across a broad range of 7 – 435 MHz.[105,106] It should be noted that these small size sources operating under a low pressure have not been tried before, except for our work discussed here.

A fill argon pressure P_0 could be lowered down to less than Pa range. Attempts have also been made to accelerate the plasma with a scheme of an azimuthal mode number $m=0$ half cycle acceleration,[100,101,107] using an $m=0$ antenna wrapped around the quartz tube. Note that both plasma generation and its acceleration are advantages of the electrodeless device configuration.

In characterizing the plasma, a range of diagnostics were used, including a Langmuir/Mach probe for deriving n_e and electron temperature T_e as well as the plasma flow velocity v_i. However, such probing is restricted to the downstream region and relatively large areas due to its size. In addition, Laser Induced Fluorescence (LIF) method[108,109] was used to derive argon ion and its neutral velocity distribution functions. Furthermore, spectroscopic measurements were conducted to use a collisional radiative (CR) model to estimate n_e and T_e by a visible monochromator.[110,111] The latter two optical methods are powerful means for the measurement of small sized plasmas. This is because the optical measurements are not restricted by the plasma size, whereas it is difficult to insert conventional electrostatic probes into a small diameter plasma due to a geometrical restriction and a strong perturbation of the plasma.

In experiments on rf plasma production, devices with an i.d. from 2 cm down to 0.1 cm were tested, namely, using diameters of 2, 1, 0.5, 0.3, and 0.1 cm. As an example of the smallest i.d. of 0.1 cm, a photo of the RF plasma without a magnetic field is shown in Fig. 15(b). Here, rf frequency of $f=435$ MHz with $P_{rf}=200$ W was injected with the use of a pre-ionization by the 12 MHz rf power supply in the 2 cm i.d. tube, connected to a 0.1 cm i.d. tube, with P_0 of a few Pa to 100 Pa. From optical measurements based on the CR model, shown above, n_e in a high pressure region was estimated to exceed $10^{11}\,\mathrm{cm}^{-3}$.

In producing small diameter rf plasmas, the use of the higher frequency region (above typical 13.56 MHz) showed a better plasma performance in the low P_{rf} region at the power of less than a few tens of W.[105] From the helicon wave dispersion relation, a higher frequency is more conducive to a small diameter plasma to keep other parameters, such as the magnetic field and parallel wavelength, with fixed n_e. The electron excursion length in one RF period is inversely proportional to f^2 (for simplicity, in the case where no magnetic field is used), which is also useful for a small diameter plasma with higher rf frequency.

In the case of the 2 cm diameter tube, the electron densities of $n_e \sim 10^{10}\,\mathrm{cm}^{-3}$ were obtained at $f=50$ or 70 MHz compared to no plasma production at a lower rf frequency (at P_{rf} less than 10 W). Note that in the high P_{rf} range of more than several 100 W, lower f, such as 7 MHz, provided a better alternative due to the fact that this low f showed a clear density jump to enter $n_e \sim 10^{13}\,\mathrm{cm}^{-3}$,[105] while the jump was not observed in the high f range with $P_{rf}<1$ kW. In the n_e measurement, in addition to electrostatic probes, an Ar II line intensity $I_{\mathrm{Ar\ II}}$ from a monochromator could also be used to estimate n_e from nearly constant value of the square root of $I_{\mathrm{Ar\ II}}$ divided by n_e (if T_e does not change significantly), considering a solid angle in the measurement. It should be noted that a mirror magnetic field configuration showed a similar behavior as the divergent field one, and the Electron Cyclotron Frequency (ECR) plasma production in a low frequency region of less than 500 MHz was successful.

With respect to the plasma production efficiency,[112,113] denoted as N_e/P_{rf}, where N_e is the total number of electrons in the entire plasma volume, small diameter cases (i.d. <2 cm) showed nearly the same dependence as the larger diameter counterparts. Here, the scaling is proportional to a^2, where a is the plasma radius. This production efficiency is attractive, being close to the classical diffusion estimation by a factor of ~ 3.

Now, we will discuss v_i exhausted from the plasma source. First, in the case where no acceleration was used, i.e., a simple rf source without an additional scheme, will be discussed. When changing the gas species from argon to hydrogen through helium gases, i.e., the use of lighter ions, higher v_i was found in the case of i.d. of 2 cm.[106] This was attributed to the fact that v_i increases inversely proportional to the square root of ion mass if other parameters are not changed. In the highest velocity case, using hydrogen gas, velocities v_i of ~40 km/s were observed.

As the second case, a small-diameter RF plasma with additional acceleration, i.e., $m = 0$ half cycle acceleration method, was tried.[100,101,107]

In a single first half cycle, axial Lorentz force which can accelerate and exhaust the plasma can be expected from the product of the induced azimuthal current and the radial component of the external divergent magnetic field. On the other hand, the second half cycle has a back Lorentz force; however, this force does not affect the plasma source (spacecraft) substantially due to the fact the plasma produced in the source hitting the inner wall of the front side (or staying within the vessel region) of the source has no total net force onto the entire spacecraft system itself. Experimentally, in the low coil current I (15 A peak to peak) case of $m = 0$ coil with a winding number of 20 turns, an increase of v_i by less than several tens of percent near this coil region was found as expected. Further increases of I, e.g., to a few hundred A peak to peak, resulted in a substantial threefold increase in n_e and v_i.

Thus, a very small but high-density, of up to 10^{13} cm^{-3}, rf plasma has been successfully produced with i.d. less than 2 cm (down to 0.1 cm), by increasing the frequency above 7 MHz. Attractive plasma production efficiency was obtained with an electrodeless condition, and an additional acceleration scheme was also tried. These results are very useful for the development of propulsion systems for long-term operation in the near earth region, as well as they provide fundamental knowledge for the advancement of deep space propulsion.

4. Scalability and reliability of vacuum arc thrusters for Cubesat missions

In this section, we will discuss the challenges for the design of a vacuum arc thruster (VAT) propulsion system for a 1U Cubesat. While the VAT is a fairly robust and simple device, this chapter aims to demonstrate the issues associated with designing a propulsion device for reliable operation under the conditions that are intrinsic to a severely power-, space-, and mass-limited device.

Vacuum arc thrusters are very simple propulsion devices. In a vacuum arc, the discharge is initiated on the cathode surface. The generation of the plasma is dependent on the material and surface structure and takes place in so-called arc spots. These arc spots consist of a highly ionized cathode material which is accelerated due to pressure-driven and electromagnetic forces, the details of which have been described elsewhere.[114] A quasi-neutral plasma leaves the cathode surface with velocities of $v = 10^4$ m/s, thus producing the thrust

$$T = \dot{m}_{arc} \times v, \tag{3}$$

where $\dot{m}_{arc} = rI_{arc}m/Z$.

Based on these calculations, the performance of the VAT can be determined from the arc current I_{arc}, the ion mass m, charge state Z, the streaming velocity v, and the arc-to-ion-current ratio r. Hence, performance of VAT is largely influenced by the type of the material used for the cathode. As an example, measurements are presented that have been performed at Comat Aerospace, France in a dedicated vacuum facility (pressure 10^{-5}–10^{-7} mbar, 0.6 m in diameter, 1 m long). The VAT used has a coaxial geometry[115] with an annular anode and a cathode made with different materials placed on an axis. The gap between the anode and cathode is 10 mm. The arc pulse duration is on the order of 10 μs, repeated at a frequency of 20 Hz. Measurements of impulse bit have been performed with a torsional thrust stand. The thruster is installed on the arm of the thrust stand, and the impulse bit is measured from the response by the reaction force.[116] Different cathode materials have been tested and thrust measurements are reported in Table III. The averaged thrust $\overline{T}$ is calculated as the product of the measured impulse bit and the frequency.

In order for the VAT to be able to be employed in a CubeSat, apart from selecting the adequate material, the VAT has to be scaled down and simplified. For the CubeSat, the VAT is designed and built based on a design with an inductive energy storage (IES) circuit PPU and a simple coaxial thruster head geometry.[117] In the PPU, an inductor is charged through a semiconductor switch. When the switch is opened, a voltage peak $L_{di/dt}$ is produced, which breaks down the thin metal film coated anode-cathode insulator surface at relatively low—CubeSat compatible—voltage levels (≈200 V).[118] The typical resistance of this metal film coated insulator surface is ~100 Ω.

Porosity of this surface and/or small gaps in the metal film generates micro-plasmas by high electric field breakdown. These micro-plasmas expand into the vacuum and allow a current to flow directly from the cathode to the anode along a lower resistance plasma discharge path (~10's of mΩ) than the initial, thin film, surface discharge path. The current that was flowing in the solid-state switch is fully switched to the vacuum arc load in less than 1 μs. Typical currents of up to 100 A (for ~100–500 μs) can be conducted with supply voltages of ~25–30 V. Consequently, most of the magnetic energy stored in the inductor is deposited into the plasma pulse. The efficiency of the PPU may thus be >90%.

The repetition rate of the individual pulse as well as the energy can be changed easily by varying the frequency and duration of the input signal to the IES circuit, which may be

TABLE III. Influence of a cathode material on VAT performance. Courtesy of Antoine Blanchet and Luc Herrero, Comat Aaerospace company, France.

Cathode material	Energy capacitor (mJ)	Impulse bit (μNs)	T (μN)
Titanium	972	2.04	40.8
Aluminium	972	2.58	51.6
Tungsten	972	3.27	65.4

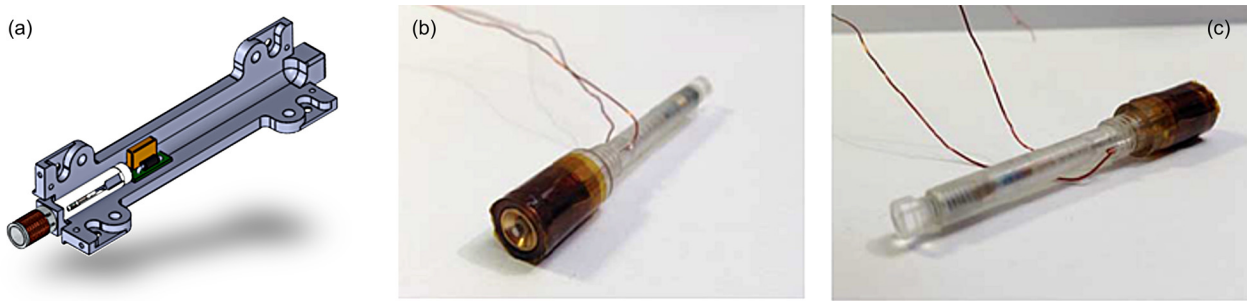

FIG. 16. A schematic of the thruster head mounted in a CubeSat Rail (a), and pictures of a thruster head [(b) and (c). In a vacuum arc, the discharge is initiated on the cathode surface. Plasma is generated depending on the material and surface structure in so-called arc spots. These micro-plasmas expand into the vacuum and allow current to flow directly from the cathode to the anode along a lower resistance plasma discharge path.

controlled using TTL electronics. Repetition rates of up to 1 kHz can be obtained. The impulse bits can be varied in 1 μNs steps, limited by the input power, taking into account an average thrust efficiency of $\sim$3 μN/W.

For Cubesat propulsion, numerous mission requirements have to be fulfilled. The Cubesat requirements for a typical LEO mission demonstrating the feasibility of a Cubesat constellation limit the total mass of the system to $\sim$250 g, including the PPU and 4 thrusters to be controlled by this PPU. The total power provided for propulsion is $\sim$2 W, the bus voltage is limited to 3.7 V. The mission ΔV has been calculated to 7.5 m/s, which would be obtained by $\sim$7 00 000 pulses, assuming Ti as a cathode material.

Once the power supply has been designed, the thruster heads need to be configured. Four thruster heads are required for position control of the CubeSat. The mass budget amounts to approximately 25 g each. This mass includes propellant (cathode material) plus a support structure, insulator and an anode. As no external cooling can be provided, the layout is based on radiation cooling. In addition, the outside geometry of the CubeSat is not to be altered due to the launcher requirements. The propellant for the ΔV, assuming Ti as a cathode material, amounts to 0.8 g per thruster head. The thrusters were installed into the frame of the CubeSat using a coaxial design, thereby limiting the cathode diameter to 1.5 mm (Fig. 16; the board of four thrusters for Cubesat and schematic of the control circuit are shown in Fig. 17). However, as the cathode material is used, plasma production is moving away from the outside plane of the satellite towards a more recessed location, which reduces performance. Hence a feed mechanism needs to be devised which fulfills the mass and space requirements imposed be the mission.

Another issue is lifetime. As mentioned in each embodiment, a thin film coating of metal (typically the material of the cathode) is applied onto the insulator surface, forming a conducting path from the cathode to the anode. This thin film enables the so-called "self-triggered" or "triggerless" mode of operation as described above. A key facet of this mode of operation of the discharge is the re-deposition of the metal vapor onto the insulator surface. In the steady-state, it is important that after each pulse, a sufficient flux of ions flows back to re-deposit onto the insulator surface during or after the pulse, to replenish conducting material that has been ablated during the breakdown and subsequent conduction of the discharge. Our empirical data show that a given coating on an insulator seems to last for a long time ($>10^7$ pulses), when optimum conditions are given. The main issue with this kind of thruster operation is that each ignition erodes a fixed amount of the thin film material. If the amount that is replenished is less than what is eroded, initial breakdown becomes increasingly difficult to achieve, demanding higher and higher voltages until finally the vacuum breakdown voltage is reached, which cannot be delivered by the PPU anymore. On the other side, if more material is redeposited than what is eroded, the thin film becomes a very low impedance connection between the anode and cathode, leading to a leakage current and subsequent failure of the IES ignition mechanism. Hence, an optimum point of operation needs to be found. The amount that is re-deposited depends to a large amount on the pulse length and pulse current, which in turn can be adjusted only to a very limited amount due to the power constraints given by the CubeSat layout. Thus, for the selected propellant/I-Bit combination, a fixed geometry (insulator thickness, cathode size) has to be selected to ensure reliable operation of a low-voltage ignition vacuum arc thruster.

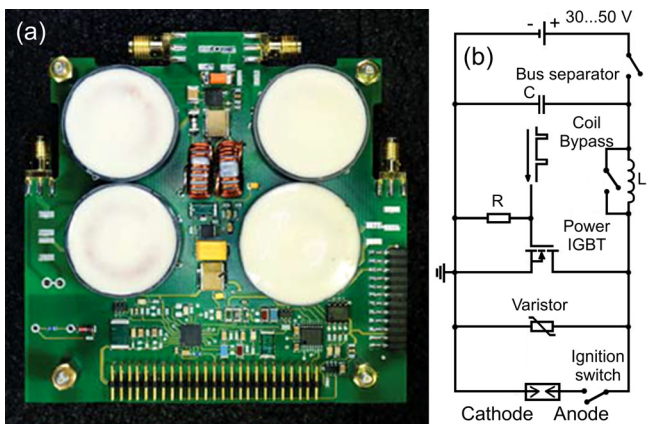

FIG. 17. The board of four thrusters for Cubesat (a) and schematic of the control circuit (b). Starting from the S/C bus, the 3.7 V, 0.5 A DC input should be converted into controllable pulses of 200–300 V with adjustable duration using the PPU (b). An additional step-up converter is used to charge a capacitor. After charging, the capacitor is separated from the bus to reduce EMI effect and acts as a sole source for the further pulse production through the IES circuit. Using this circuit, pulse energies up to 3 J could be produced in 7 ms pulses. The unit has $9 \times 9 \times 15$ mm with a total mass of 150 g. Pulse repetition of 0.1–1 Hz can be achieved with ignition voltages up to 1 kV. Plasma burning voltages of 25 V with plasma currents of up to 50 A are produced.

The final issue for extended operation of a VAT is contamination. The metal plasma is leaving the cathode surface in a cosine distribution, which unfortunately leads to contamination of the solar panels due to metal deposition. While on short missions, this is not an issue as the amount of material expelled is very small, for longer missions this may have to be taken into account.

A potential solution is the use of an axial magnetic field, which not only confines the thruster plume but also adds mass due to the additional hardware needed. Thus, designing a vacuum arc thruster system for a 1U Cubesat poses a challenge in many respects and requires careful design to be able to achieve a successful mission.

5. Rotamak-like system for the miniaturized propulsion

Spherical plasma sources and related Rotamak configurations have been studied extensively since the late 1970s as a potential candidate for realizing nuclear fusion as a source of long-term energy security. A spherical discharge vessel, through manipulation of the configurations of the external sources enables one to operate in a "field reversed configuration" and other current drive schemes. The far reaching implications of earlier theoretical and experimental studies of the spherical plasma source laid the groundwork for the development of a gradually expanded Rotamak (GER) device as an up and coming contender for electric propulsion. The Space and Propulsion Centre (SPC) in Singapore at the National Institute of Education, Nanyang Technological University has concluded preliminary studies on the utilization of a spherical plasma source for propulsion-based applications.

The spherical plasma device investigated in this work shows encouraging prospects for the realization of a pure electromagnetic thruster capable of sustaining high density, non-inductive plasmas. The GER thruster would eventually feature the generation of azimuthal plasma currents which would cause indiscriminate acceleration of plasma species (electrons, ions, and neutrals) through an axial body force. Highlights of the GER also would include the non-requirement of pre-ionization stages, neutralizers and high voltage grids as commonly seen in conventional electric propulsion devices such as ion thrusters and Hall thrusters. Most notably, the potential for scalable operational power regimes, reduced wall bombardment and removal of moving components currently points to a solution for extended space flight for long haul missions in low Earth and geostationary orbits as well as for deep space exploration depending on operational configuration.

Preliminary studies done at the SPCS have shown the ability for the generation of dense plasmas in a spherical vessel that can be sustained with a pair of parallel RF coils mounted outside the confinement vessel. Another pair of coils placed orthogonal to the RF coils enables the provision of a poloidal magnetic field through the application of a DC pulse which confines the plasma and increases the plasma density in the center of the spherical discharge vessel. With the modification of the configuration and geometry of the discharge vessel, the spherical plasma source has the potential for realizing a fully electromagnetic thruster which provides acceleration/thrust by an axial body force and does not require neutralizes or high voltage grids which are commonly present on conventional electric propulsion engines. Most notably, such a propulsion device would allow for larger thrust values per unit propellant that enables sustained space flight for longer haul missions.

The schematic diagram of the experimental setup of the discharge vessel is shown in Fig. 18. The spherical discharge vessel was constructed out of Pyrex and measures 28 cm in its internal diameter. The discharge vessel is also outfitted with connections to a vacuum pump-out suite as well as gas inlets for the introduction of discharge gases. The vacuum suite used in this work comprises of a two-stage rotary and turbo-molecular pump system which enables a pumping capacity of 450 l/s and a base pumping pressure of $\sim 1 \times 10^{-4}$ Pa. The working gas used in this work is high-purity argon which is introduced into the vessel through a glass tube connecter through a KYKY mass flow controller which accurately controls the flow rate. The overall discharge pressure can then be manipulated with a manual gate valve leading to the vacuum

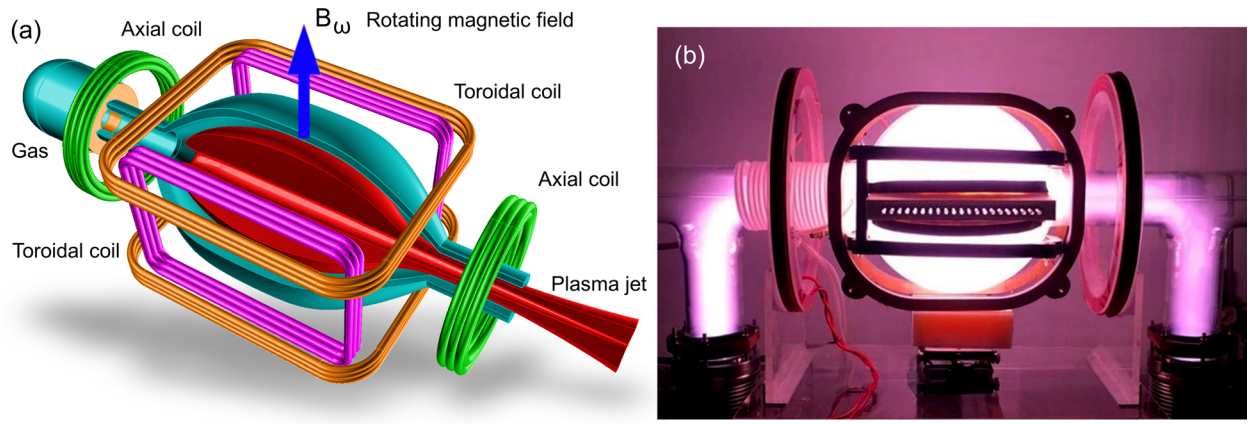

FIG. 18. Rotamak-like mini-thrust platform being developed in PASC/SPC, Singapore. (a) Schematics and (b) photo of Rotamak-like discharge in the model system. The GER thruster would eventually feature the generation of azimuthal plasma currents which would cause indiscriminate acceleration of plasma species (electrons, ions and neutrals) through an axial body force. Preliminary studies done at the SPCS have shown the ability for the generation of dense plasmas in a spherical vessel that can be sustained with a pair of parallel RF coils mounted outside the confinement vessel.

suite. The discharge vessel is also equipped with an adjourning plasma diagnostic array. This array was constructed out of a machined ceramic block which was cemented over a slot in the poloidal plane of the discharge vessel. The array comprises of 21 symmetrically drilled holes (10 mm apart) for the radial insertion of magnetic and electric probes for diagnostic of discharge parameters. The probes are sealed in place when pumping down to base pressure with the aid of temperature resistant Viton O-rings seated in between the ceramic block and probes.

The transverse oscillating magnetic fields (OMF) are generated by a pair of parallel Helmholtz coils measuring 34 cm in diameter and are separated by a distance of 15.5 cm. The plasma is generated by a 5 kW/2 MHz RF generator through an RF matching network. An additional external steady vertical magnetic field (VMF) is produced by a pair of parallel circular coils measuring 34 cm in diameter, separated by 55 cm on the axis of the discharge vessel. The coils are connected to an adjustable pulsed DC power supply for the provision of a pulsed current through the coils when triggered externally. A series of miniature hand-wound magnetic pickup coils are placed internally to the discharge vessel through hollow quartz guide tubes sealed in the ceramic diagnostic ports that are used to measure the internal oscillating magnetic fields. An artistic representation of the Rotamak-based space propulsion thruster is shown in Fig. 19.

6. Printable cathode arc thrusters

Arc thrusters are gaining increased attention as a nanosatellite propulsion system because of its simple, scalable, and robust operation capabilities. An arc thruster typically consists of two electrodes separated by an insulator which is covered by a thin conducting layer. The thin conducting layer acts as a trigger to start the erosion of the cathode, which enables the use of a low mass power processing unit.[119] During the operation, erosion of the cathode leads to a change in a cathode-insulator-anode interface geometry, which can limit the operational lifetime of the thruster and affect the produced thrust. Therefore, a cathode feeding mechanism is an important component to keep the arc thruster geometry constant during long duration operations.

Active and passive cathode feeding systems have been previously implemented on arc thrusters.[115,120,121] A passive feeding system uses a compression spring to feed the cathode to the discharge chamber, where a cathode feeding rate is completely dependent on the erosion profile of the electrode. Compared to a passive system, an active feeding system, which uses a piezoelectric actuator with a spiral spring, can accurately control the feeding rate to achieve uniform erosion of the cathode.[121] Although an inline active feeding system can improve the efficiency of a VAT, it requires the use of an additional power spring and a computer controlled piezoelectric actuator. Moreover, the increased complexity of the entire VAT system makes it difficult to use in a low-cost nanosatellite and the clusters of a VAT.

The novel concept of a VAT using material printing can be an alternative of conventional VATs. Recent progress in the printed electronics enables fabrication of complex-shaped electrodes on flexible dielectric substrates using metal-based conductive ink. Printing technologies, such as inkjet and screen printing offer to produce low-cost electrodes with high resolution in the range of $10 \sim 40\ \mu$m.[122] Instead of rigid metal electrodes, a printed electrode on a thin dielectric film can be used in a VAT, which is called a printed Cathode Arc Thruster (pCAT). Compared to conventional VATs, a pCAT does not require a feeding mechanism, which can significantly simplify the complexity of a thruster system. Although a single printed electrode contains limited amounts of propellant, the lifetime of a thruster can be improved by a cluster of pCAT, an example of which is shown in Fig. 20. The cluster form of pCAT contains multiple thrusters and each one capable of being fired independently. A clustered pCAT, therefore, can provide the capability to control the level and direction of thrust by

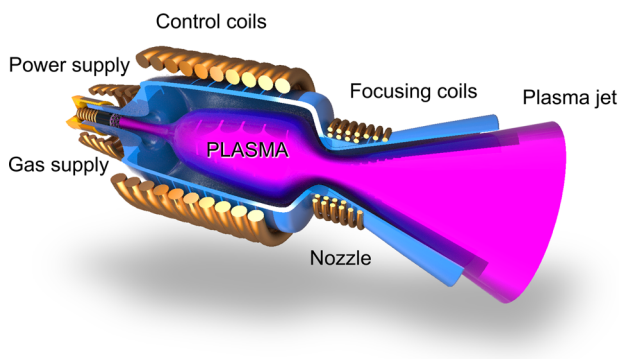

FIG. 19. Artistic representation of the Rotamak-based space propulsion thruster. Such a thruster could be capable of producing relatively high (reaching several N) thrust levels, provided the sufficient power supply levels.

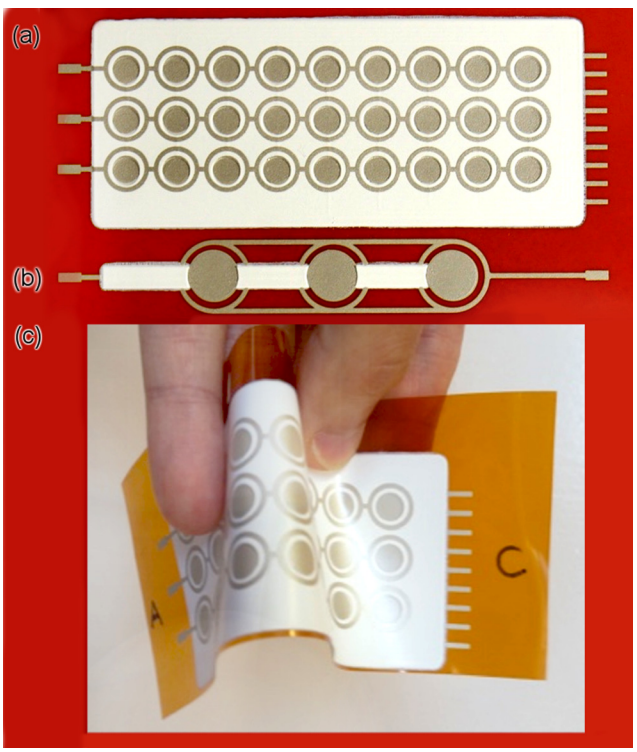

FIG. 20. Photographs of a printed cathode arc thruster (pCAT) in various forms. (a) Clustered pCAT; (b) pCAT in the form of a tape; and (c) testing flexibility of a pCAT.

independent variation of each thruster operations. As pCATs can be fabricated in the form of a thin film or roll, it can be easily integrated on the surface of a nanosatellite or be deployed as solar arrays.

C. Hollow cathode neutralizers for micropropulsion

Cathode neutralizers are an integral component of several types of electric thrusters, namely, Hall thrusters (HT) and ion thrusters.[123] The function of the cathode neutralizer is threefold: (1) it serves as the negative terminal of the thruster circuit, thus responsible for the generation of the thruster's accelerating electric field; (2) it produces sufficient electrons to neutralize the ion beam ejected from the thruster; and (3) it generates the primary electrons for the thruster unit ignition process. To couple with Hall and ion micro-thrusters, the cathode must be able to generate discharge current levels below 1 A. The need for such low discharge current capability stems from the operational discharge voltages of these thrusters, of several hundred volts.[124]

1. Overview of cathode techniques for μ-propulsion

Four cathode technologies that may generate the required discharge currents exist: (1) hollow cathodes, (2) RF cathodes, (3) carbon nanotube cathodes, and (4) simple heated filaments. Hollow cathode technology is well matured and hollow cathodes have been extensively used for Hall and ion thrusters. These cathodes require propellant flow rates of about 10%–20% of the thruster flow rate[125] in order to suppress space charge limitation near the emitter surface, thus allowing the required current density of electrons to be emitted.[126]

At their nominal current levels, hollow cathodes can operate in a self-sustained mode in which no external power is needed to maintain sufficient emitter temperatures; therefore, making these cathodes energy-efficient. On the other hand, these cathodes require meticulous thermal design to prevent heat loss from the emitter.[127] Historically, almost all hollow cathodes generate discharge current levels from several to tens of amperes.

RF cathodes are used mainly for ion thrusters and are able to generate discharge current level of hundreds of milliamperes to several ampere.[128] In RF cathodes, the energy source, i.e., the antenna, does not come into contact with plasma, which can avoid potential issues with the discharge cathode life.[129] However, these cathodes are characterized by an electron-extraction-cost of over 100 W/A, making them energy-costly.[130] Additionally, RF cathodes are operated using RF power supplies thus must account for DC-RF losses and reflected power.

Carbon nanotube (CNT) cathodes are a relatively new technology,[131] yet these cathodes attract some interest in the electric propulsion community and are even offered as available high-TRL product.[132] These cathodes do not require propellant and consume power of several watts. Still, CNT cathodes are current limited to tens of milli-ampere and require relatively high voltage, of several hundred volts, to sustain operation.

Finally, it is possible to heat a Coiled Tungsten Filament Cathode (CTFC) to generate the required electron currents. Although a simple solution, heated wires have short life spans of tens to hundreds of hours under ion bombardment coming from the thruster. In addition, the high work function (>4 eV) of the filament material leads to low current generation and high heating power requirement due to high material temperatures and radiative heat losses.[43]

All four types, along with their advantages and disadvantages, are listed in Table IV.

2. Currently existing and future cathodes for μ-propulsion

To assess the current state of low discharge current operation techniques of cathode neutralizer technologies, we look at a thruster-cathode coupled operation for the cases of very low power thrusters. Table V presents several types of cathode neutralizers used in coupled operation with micro Hall and ion thrusters. In addition, the cathode operational techniques, and ensuing additional requirements for heating power and mass flow rate, are specified. It may be deduced from the table that the preferable low current neutralizer type is the hollow cathode. However, in all cases presented here, the cathode was not operated in a self-sustained mode as an additional heater and/or keeper power were needed to maintain sufficient electron emitter temperatures.

Therefore, it is concluded that micro Hall and ion thrusters do not currently have dedicated low-current hollow cathode solutions. These thrusters are compelled to operate with hollow cathodes designed for larger current thrusters, the operation of which is adjusted by adding supplemental heater and/or keeper power; a factor that reduces overall thruster unit efficiency.

By virtue of its extensive in-space heritage, a low energetic cost during thruster operation, relatively simple design and operation flexibility, hollow cathode technology is a natural candidate for Hall and ion micro-thrusters. Nonetheless, due to a historical lack of interest in very low power thrusters, and design or operation adjustments required to enable sub-ampere operation, only few low current hollow cathodes were designed to date. This review lays out contemporary low current cathode development efforts and their applicability to micro electro-propulsion. List of low current hollow

TABLE IV. Advantages and disadvantages of the types of cathode neutralizers.

Technology	Advantages	Disadvantages
Hollow cathode	Matured technology Energy-efficient	Discharge currents >1 A
RF cathode	Matured technology Long lifetime	Energy-costly Sophisticated power supply
Carbon Nanotube (CNT) cathode	Propellant-less Energy-efficient	Discharge currents <0.1 A High operation voltages
Coiled Tungsten Filament Cathode (CTFC)	Propellant-less Simple design	Discharge currents <0.1 A Short lifetime Energy-costly Radiative heating of thruster

TABLE V. Cathode neutralizer types and operation conditions used to operate micro Hall and ion thrusters.

Thruster	Facility	Discharge current (A)	Neutralizer type	Neutralizer power	Neutralizer mass flow rate (mg/s)
SPT-20[133] (HT)	Pivoine (CNRS)	0.2-1	CTFC	?	0
SPT-50[134] (HT)	NASA Lewis (currently NASA Glenn)	0.8-2	Hollow cathode	Heater - 80 W	0.25
BHT-200 (HT)[135]	Busek Inc. Co.	0.5-1.5	Hollow cathode	Heater - 3 A Keeper - 0.5 A	0.098
MHT-9 (HT)[136]	MIT	0.5-1.5	Hollow cathode	Heater - 4 A Keeper - 0.5 A	0.098
Micro Hall Thruster[137] (HT)	Stanford University	0.12-0.15	Hollow cathode	Heater - 4 A Keeper - 0.25 A	0.16
CHT[138] (HT)	PPPL	0.49-0.54	Hollow cathode	Heater -? A	0.2
MiXI[139] (GIE)	UCLA	0.07-0.5	CTFC	88 W	0

cathodes, developed at present, is presented in Table VI. Five significant development endeavors are being presently conducted, both in academia and in industry. It can be seen from the table that Ba-O is the most common type of emitter incorporated, mainly due to its low work function relative to the popular LaB6 emitter used in most medium and high power thrusters.

Not surprisingly, even lower work function materials, such as C12A7 (electride), are being experimented with, as in TU Dresden. It can be seen from the table that all cathodes under development were operated against low power thrusters, as it is an important validation milestone as part of a cathode development plan. From a technological point of view, Rafael's RHHC cathode is at the most advanced phase following a lifetime and ignition cycles experiments. To demonstrate the state of the art of low current hollow cathodes, we hereby present the low current characterization experiment of the RHHC cathode.

3. Rafael's heaterless hollow cathode for micropropulsion

Rafael's Heaterless Hollow Cathode (RHHC) [Fig. 21(a)] is a hollow cathode designed to operate at discharge current levels of 0.5–1.1 A with mass flow rate values of 0.1–0.25 mg/s. To assure fast ignition, within 10 s, and to minimize ignition power consumption, the RHHC employs heaterless ignition in which the plasma discharge is generated via an initial voltage breakdown pulse under cold cathode conditions.[146] The RHHC includes a meticulous thermal design to assure sufficient emitter temperatures, minimize its power consumption, and allow for self-sustained operation even at the lower end of its discharge current operational envelope.[144]

To date, the RHHC passed a set of qualification tests; namely, full characterization test,[147] initial breakdown voltage test, manufacturability consistency test, 5000 h long steady state operation test and a 3500 cold ignitions test. In addition, the cathode was coupled with the CAM200[148] low power HT in several dozen experiments as well as with the HT-100D HT. As a part of its qualification campaign, the RHHC's capability to deliver discharge current levels down to 0.2 A was examined. Moreover, the particular conditions under which the cathode might not be able to operate in self-sustained mode were explored. The experiment took place at Rafael in the cathode test facility[149] dedicated for the experimentation of cathodes in diode mode configuration; that is, against a cylindrical anode to emulate the thruster's electrical configuration.

For the experiment, the cathode was fed with 0.2–0.25 mg/s of Xenon gas. A dedicated keeper power supply was used for cathode ignition, after which an anode discharge was initiated. Within 5 s after initiation, the keeper power supply was turned off and the anode power supply sustained cathode operation. The anode discharge current was adjusted to values of 0.2–0.5 A and left to operate for a minimum of 1 h at each operational point to examine the cathode's capability to operate stably in self-sustained mode. Since the energetic cost

TABLE VI. List of low current hollow cathodes under development at present.

Cathode name	Designer	I_d (A)	$\dot{m}_c$ (mg/s)	Emitter type	TRL	Record
Low current hollow cathode[140]	TU Dresden	0.35-2	0.15-0.25 (Ar)	C12A7 (Electride)	3	Operated with HT—unstable operation
KH-3[141]	Fakel EDB	0.5-1	0.15-0.2	Ba-O	3-4	Operated with HT (PlaS-40) for 150 h
HC-1[142]	Sitael S.p.A.	0.3-1	0.08-0.5	LaB6	4-5	Characterization
SHC-1A[143]	KhAI	0.2-0.5	0.2-0.3	Ba-O	5-6	Operated with HT (HT-100D) Full characterization Operated with HT (SPT-20M) 1510 ignition cycles test
RHHC[144,145]	Rafael Ltd.	0.2-1.2	0.1-0.35	Ba-O	6	Full characterization Operated with HT (HT-100D, CAM200) 5000 h steady state test 3500 cold ignition cycles test

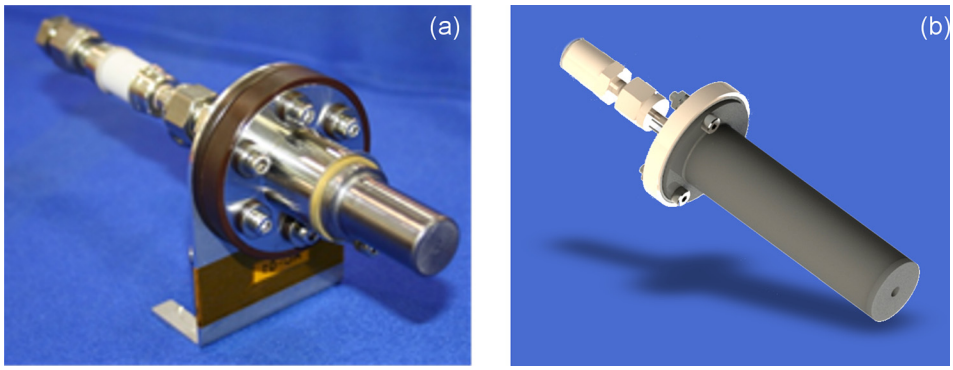

FIG. 21. (a) Rafael's Heaterless Hollow Cathode. (b) Hollow cathode designed and tested in PSAC, Singapore.

of a hollow cathode can be evaluated as the potential fall from the cathode plume to the cathode emitter potential,[150] it was necessary to measure this voltage drop. To do so, two common practices of experimental cathode research were used—(1) measurement of the voltage drop from the floating keeper to cathode potential, while correcting for the floating keeper sheath voltage drop, and (2) emissive probe measurement in the cathode plume using the inflection point method.[151]

All measured voltages decrease with an increase in the discharge current. This typical cathode behavior is a result of the cathode emitter heating mechanism that relies on ion bombardment for maintaining sufficient emitter temperatures.[152] Simply put, as the discharge current is reduced cathode sheath voltage must increase to raise the impinging ion velocity, thus providing the required heating ion flux into the emitter.

An important observation is the ability of the cathode to operate in self-sustained mode at discharge current levels below 0.35 A. At even lower discharge current levels, an addition of keeper current of 0.05 A is needed to maintain cathode operation, resulting in an acceptable "power penalty" of approximately 1.5 W.

Finally, it is interesting to note that the emissive probe measurements indicate on overall cathode voltage drop between 20 and 40 V. These values are in accord with similar measurements of higher power thruster-cathode coupling tests and prove adequate cathode operation.

Additional cathode qualification activities should include thruster-cathode coupling tests and ultimately a joint thruster-cathode lifetime test.

4. Efficient cathode techniques at PCAS/SPCS, Singapore

Similar high efficient systems were designed and tested in the Plasma Sources and Application Center/Space Propulsion Centre, Singapore. The main distinguishing features of the small efficient cathodes designed specifically for small (about 20–40 mm diameter) Hall-type thrusts are low operational temperature and weight. The PSAC cathode consists of a lanthanum hexboride thermionic emitter, a cathode tube, and a choke cathode orifice that is made of rhenium/tantalum/carbon. The heater is made of a serpentine type tungsten-rhenium alloy resistive wire over a boron nitride cylindrical templet. The cathode tube is a superposition of a thin tantalum tube with a graphite shunt. The keeper is made of either pyrolytic carbon or titanium alloy. The cathode is capable of operating in a fully self-sustained mode (Fig. 22). Table VII shows the typical cathode performance in krypton discharges. In the typical experiment, the anode flow was kept at 0.4 mg/s whereas the cathode was fed with Xenon at varying flow rates. The self-sustained operation can be maintained down to as little as 0.028 m/s of Xenon (or 30 microgram), with the anode current of 0.75 A [Fig. 21(b)].

D. Virtual thrusters: Modeling miniaturized systems

In this section, we look briefly into some general approaches to modeling the miniaturized thrusters, and specifically, Hall thrusters which offer quite a large efficiency and specific impulse,[137,153] as compared to other types of electric propulsors.

It is evident that the process of miniaturization of Hall Thrusters to mass, volume and power consumptions relevant to CubeSats and small spacecraft applications should rely heavily on the progress made in modelling and simulation of small thrust systems, with a view to make the process of miniaturization faster and cheaper.[154] Specifically, in this section, we discuss numerical methods used to model gas- and plasma-dynamics with plasma-surface interaction in HT discharge channel and plume.

In fact, with the scale reduction, measurements become more and more difficult and invasive. In addition, with the

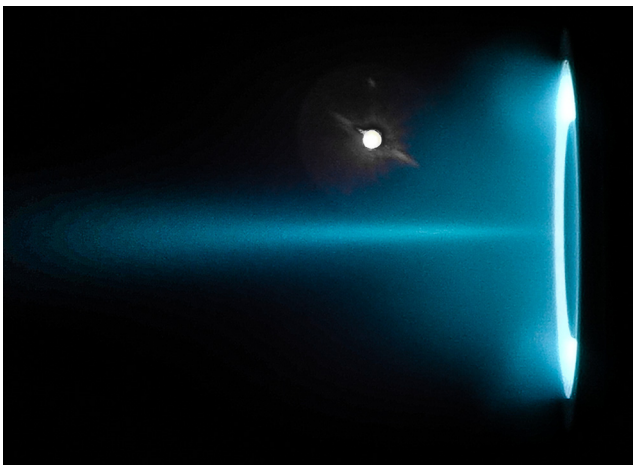

FIG. 22. Photograph of PSAC/SPCS miniaturized Hall thruster firing at 0.5 mg s^{-1} of Xe supply. The typical characteristics of the cathode with krypton discharge are listed in Table VII.

TABLE VII. Characteristics of the PSAC developed cathode.

Cathode (Xe: mg/s)	Anode (Kr: mg/s)	P (Pa)	V keeper (V)	*I_anode* (A)
0.028	0.4	5.9×10^{-3}	50.2	0.75
0.035	0.4	5.9×10^{-3}	44.2	0.75
0.042	0.4	6.0×10^{-3}	47.4	0.73
0.056	0.4	6.1×10^{-3}	52.7	0.65
0.056	0.4	6.1×10^{-3}	53.5	0.60

progress made in the high-performance computer (HPC) technology, the high fidelity of reproduction and fast execution time of numerical models are rapidly improving. Due to the small size of micro-HTs, the questionable scaling schemes[155,156] and frequently used implicit algorithms[157] are no longer necessary. Finally, EP experiments in vacuum chambers are also very expensive and do not allow to reproduce typical Space environments like numerical models do.

There are two fundamentals types of numerical approaches: fluid and kinetic. Due to the fact that electron thermalization and isotropization rates are quite low in HTs, kinetic approaches are more suitable to represent the important deviations of electron distribution functions from Maxwellian one. In particular, among the different kinetic schemes, the particle-based methodology[158,159] is a very promising tool due to its versatility, ease of implementation, high quality in reproducing detailed mechanisms, and good scalability with the number of processors used.

1. Particle-in-cell—Monte Carlo collision approach

Particle-in-Cell—Monte Carlo Collision (PIC-MCC) model in the electrostatic approximation consists of the mixed Eulerian-Lagrangian (particle-mesh) solution of coupled Boltzmann and Poisson equations. By means of a Klimontovich-Dupree representation of distribution functions, electron and ion Boltzmann equations reduce to the solution of equations of motion for macro-particles (clouds of real particles representing small regions of the phase space). The charge density is deposited on a spatial mesh (whose size is on the order of the Debye length) where the electric potential is solved and from where the electric field is interpolated back to the macro-particle locations. Before pushing the virtual particle and restarting the PIC cycle again, a MCC module is called to process volumetric (electron-neutral, ion-neutral,[160] and Coulomb collisions[161]) or surface events (secondary electron emission,[162] ion sputtering,[163] etc.).

The most important features of PIC-MCC models of small-scale HTs are

- *A solution of Poisson equation for the self-consistent electric field. It allows resolving the deviation from the quasi-neutrality hypothesis; this aspect is very important for a micro-HT whose length scale is only few orders of magnitude larger than Debye length ($L/\lambda_D \approx 100$) and the lateral sheaths can have a strong influence on the bulk plasma physics. Nowadays, different dedicated free software packages are available for the numerical solution of Poisson equation;*[164–166]
- *A detailed description of the electron-wall interaction. With a high surface-to-volume ratio, plasma-wall interaction plays an important role, not only as loss but also as an active source of particle and energy terms. In fact, innovative material solutions have never been as important as in the micro-HT case. In particular, the secondary electron emission module can be implemented in a PIC-MCC code including the dependence from the electron impact energy and angle, and the ability to reproduce the strong non-equilibrium character of secondary electron distribution function composed from low energy true secondary, middle-energy inelastic and high-energy backscattered electrons*,[162] *and*
- *An ability to reveal micro-instabilities typical of ExB low temperature plasma devices*,[167] *such as ion acoustic, electron cyclotron drift, spoke, resistive, sheath, and beam-plasma instabilities.*

2. Kinetic models

Among the different fully kinetic models developed for HTs discharges (more often for the magnetic layer than for the anode layer version) that deserve a mention are the 1D-radial models of Sidorenko[168] and Taccogna,[169] who have found the importance of the secondary electron emission triggering no classical sheath behavior and beam-plasma instability, and 1D-azimuthal models of Boeuf[167] and Lafleur,[170] who have shown the importance of an electron-cyclotron drift instability. Different two-dimensional (azimuthal-axial,[156,157] radial-axial,[171] and radial-azimuthal[172,173]) models have also been developed that highlight the importance of the correlations between the different components.

Finally, a particular mention must be made for efforts to create a database[174] of cross section processes in relation to the possibility of using alternative propellants (e.g., iodine, carbon dioxide, methane, etc.) and air-breathing (i.e., nitrogen and oxygen) electric propulsion in low-earth orbit (LEO).

As a characteristic example of a numerical approach, the results from 3D fully kinetic simulation of SPT-20 HT[175] may be examined. In particular, Fig. 23 shows the electric potential (a) and electron density (b) distribution in the discharge channel (one quarter of the azimuthal sector is reported), where the anode is at $z = 0$ and the exit plane is at $z = 28$ mm. The acceleration region is evident in the last 3 mm, while a radial asymmetry between inner and outer wall is detected from the electron density.

IV. TEST EQUIPMENT AND SYSTEMS

Convenient, precise test and measurement systems are important components vitally needed for the fast, efficient development, and optimization of micropropulsion platforms. The Automated Integrated Robotic Systems for Diagnostics and Test of Electric and μ-Propulsion Thrusters (AIRS-DTEμP) designed and built at PSAC, Singapore, is an example of a modern, integrated microcontroller-based data acquisition and robotic actuation suite comprising digital electronics, microcontrollers, custom-made hardware, and

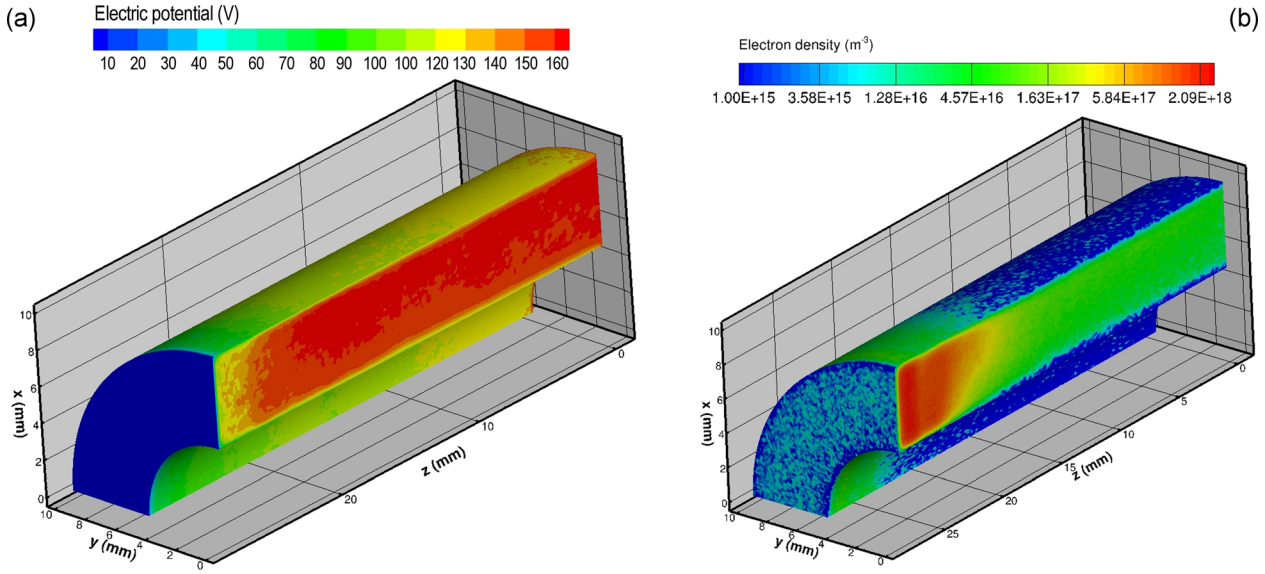

FIG. 23. Three-dimensional maps of (a) electric potential (V) and (b) electron density (m^{-3}) as results of 3 D PIC-MCC simulation of an SPT-20. See the description in the text and literature cited therein.

accessorial software for diagnostics and characterization of electric propulsion thrusters in a large vacuum space environment simulator (Fig. 24). The components of the characterization suite have been aggregated into modular add-on units for rapid re-arrangement and easy customization to suit various applications. The modules include a force calibration system for accurate thrust measurements in various thrust stands, and spatially resolved measurements in a multi-probe array comprising Langmuir and Faraday probes for plume diagnostics of plasma thrusters.

Plume and thrust characteristics of a miniaturized Hall thruster were successfully measured *in situ*, enabling users to vary process controls and efficiently optimize the thruster performance. The system revealed a further potential for real-time flight mission diagnostics and control.

The developed system has been deployed in a large space simulation facility at the Plasma Sources and Applications Centre/Space Propulsion Centre, Singapore (PSAC/SPCS), and the systems were tested with an operational Hall thruster developed by the same Centre. Results of the measurements have shown that the experimental data obtained from the acquisitions suite are reliable and the profiles and trends for the thruster performance under parametric investigations agree well with work done by other groups.

It should be noted that similar systems could be very useful for *in situ* diagnostics of plasma-based technological processes, especially those requiring precise control of parameters for, e.g., self-assembly of complex metamaterials[176,177] and controllable growth of the surface-based nanostructures.[178,179] Moreover, scalability aspects of the industry-oriented processes[180] could also benefit from similar systems.[181–183]

V. FLIGHT TESTS: MICROPROPULSION IN SPACE

A. Micro-pulsing and FEEP thrusters on Cubesats

Although EP has proven a cost effective, more robust and efficient alternative to chemical propulsion for large

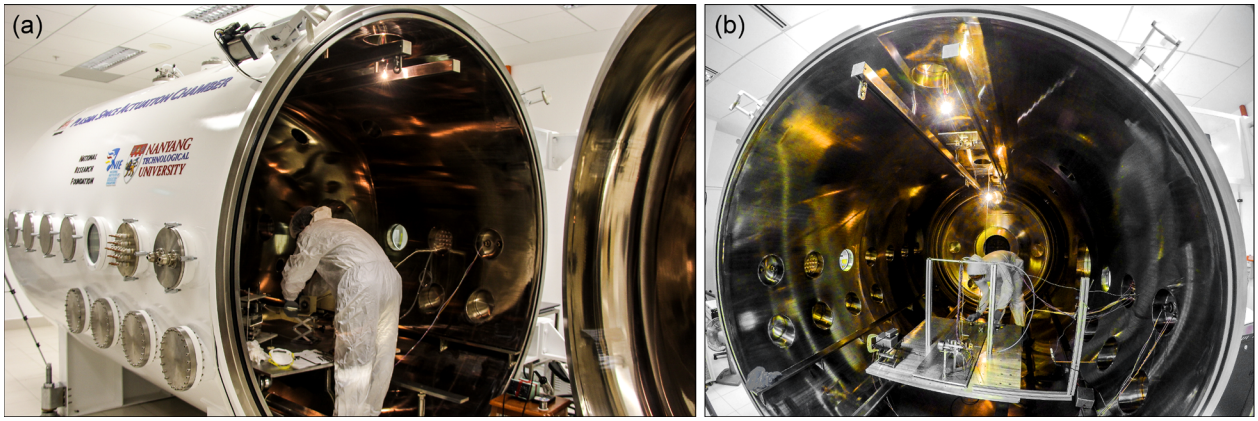

FIG. 24. Test chamber (a) and the automated integrated robotic systems for diagnostics and test of electric and μ-propulsion thrusters (b) designed and tested at PSAC, Singapore. The system incorporates a force calibration system for presize thrust measurement, and spatially resolved measurement system with Langmuir and Faraday multi-probe arrays for plume diagnostics of plasma thrusters. Reprinted with permission from J. Lim *et al.*, IEEE Trans. Plasma Sci. **46**, 338–344 (2018) and J. Lim *et al.*, IEEE Trans. Plasma Sci. **46**, 345–353 (2018). Copyright 2018 IEEE.

spacecraft, its effectiveness when employed in small satellites needs further investigation. The economies of scale favor the large satellites, with a lower limit of 50 kg being discussed openly at recent conferences in 2017. In fact, some groups are proposing 27U Cubesats for scientific missions that would probably be better served using bar fridge sized mini-satellites, of which there have been a number launched.

So quo vadis EP for Cubesats?

The whole Cubesat concept is based on the premise of using commercial off the shelf (COTS) components in satellites based on a 10 cm cube having a weight of 1 kg. As an example of what is possible, an AU03 is an Australian Cubesat that is part of the European conceived QB50 project that launched 40 satellites in low earth orbits (LEOs) comprising 2 Cubesat units (2 U) built by university staff and students from around the world.[184] In August 2015, the Space Plasma Power and Propulsion Group at the Australian National University decided to fund AU03 which was in hiatus. A consortium of the University of Sydney, the University of New South Wales (Kensington), and the ANU was formed, with the UNSW charged with assembly, system integration and testing following their experience with AU02. The cost of COTS components was approximately $US60 000, to which has to be added the cost of a tracking ground station that the ANU developed for $US15 000. The whole project was completed in 9 months, including space simulation tests at the ANU, and then delivered to ISIS for integration into the NanoRacks launching system. Many man years of work by very dedicated scientists and engineers went into this project, which have not been costed.[185] On 25 May 2017, AU03 was inserted into orbit from the International Space Station at an altitude of 400 km and is expected to decay in 1 to 2 years.

What role can EP play given the constraints alluded to above: 2 U or 3 U, cost of $US100 000 and COTS components?

The following discussion will be based on gas propellants[186] rather than the solid erosion based thrusters such as cathodic arc, the Pulsed Plasma Thruster that erodes PTFE and others that propose to use iodine.

First, the average power per orbit of a 2U covered with solar cells is between 1 and 2 W, so a propulsion module would have to have its own energy storage and power handling independent of the satellite power rails. Those imagining immense beams or ravening energy will be sorely disappointed as the EP must be pulsed and consequently the gas supply must be pulsed and as closely coupled to the thruster as possible. Assuming the EP to be a completely self-contained system fitting into a 1U, then it is difficult to imagine the propellant system being more than 0.5U and weighing around 500 grammes, including the containment pressure vessels, regulators, valves, etc.

This is not sufficient for orbit maintenance although missions involving constellations of satellites could profit from station keeping, relative to others in the swarm, and this, perhaps, is where microthrusters can play a role.

At the ANU, the SP3 group is well advanced with the design, development, and vacuum testing of a radio frequency (RF) excited plasma electrothermal thruster called Pocket Rocket [Fig. 25(a)].[188] The advantages of using rf rather than DC heaters is that the plasma created heats the gas directly rather than the walls, or nozzle, of the thruster, thus allowing a very rapid switch-on of some milliseconds rather than many minutes for more traditional electrothermal systems. The drawback is that RF systems that operate in vacuum have to be developed and tested. This has been successfully achieved in collaboration with the Power Systems group at Stanford University resulting in an integrated class E2, 13.56 MHz 30 W generator with integrated impedance match to the plasma antenna that is $10 \times 10 \times 0.7$ cm and weighs 150 g.[189] A prototype of a mini Pocket Rocket attached to the RF system has been tested in vacuum, successfully producing a plasma in the discharge channel and not around the RF components.[190] The latter posed considerable problems but was finally solved after many design/fabrication/test iterations between California and the Australian Capital Territory.

A lightweight gas system using small gas cylinders commercially available for bottled wine preservation has also been developed and successfully tested in vacuum.[191] The gas system is pulsed along with the RF to make best use of the available energy and to conserve the propellant. Work is ongoing on the power unit, its integration within a 1 U and possible mission scenarios.[192] Initial tests with an external RF generator and an external Xenon gas supply showed a thrust of about 2 mM for 70 W of rf and 50 sccm of gas flow.[193] The cold gas thrust was about 0.7 mN. The newly developed systems described above should reduce the rf power to about 30 W and the gas flow to 10 sccm, which would allow for about 400 min of continuous thruster operation. An advanced design using four canisters would allow for a full day's operation. Fluid simulations are being run to optimize the cold gas nozzle design allowing a fall-back operation condition.[194]

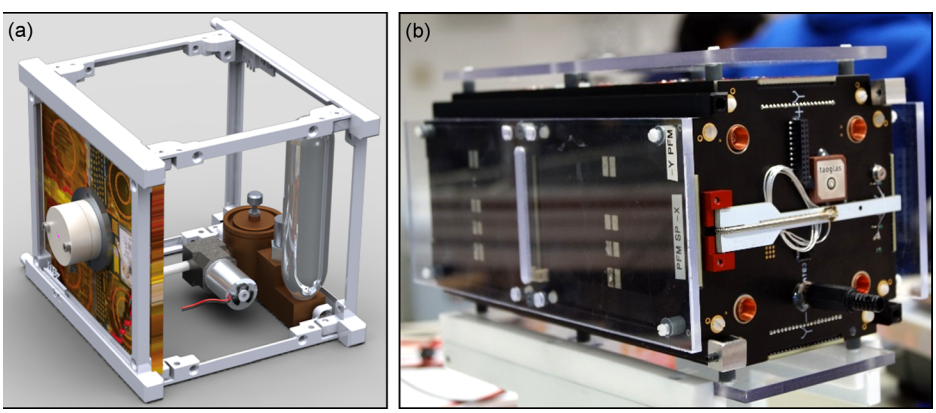

FIG. 25. Integration of various thruster types within the CubeSat platform. (a) Radiofrequency power unit and Pocket Rocket electrothermal thruster fed by the Argon gas propellant subsystem are installed in the 1U Cubesat. Image credit to A. Stuchbery.[187] Initial tests with an external RF generator and an external Xenon gas supply showed a thrust of about 2 mM for 70 Watts of RF and 50 sccm gas flow. (b) Four PPTs integrated in the CubeSat PEGASUS, launched in June 2017.

TABLE VIII. Characteristics and performance values for PPTs in comparison with the IFM (FEEP) technology.

Property	4×μPPT module[197]	IFM[198]
Technology	Electromagnetic	Electrostatic
Specific impulse, s	700–1500	2000-4000
Power/thrust ratio, W/mN	240–950	100
Thrust range, mN	0–0.012	0.001-0.5
Total impulse, Ns	≈ 5.7	>5000
Δv for 2 kg spacecraft, m/s	8.6	2800
Number of axes	2	1
System weight, kg	0.3	870
System volume, dm^3	0.3	0.8

Another example of the space flight tested thrust system is the μ-propulsion platform—a thruster subsystem developed for the United States Naval Academy's (USNA) Ballistically Reinforced Communication Satellite (BRICSat-P). These thrusters are integrated into the USNA's 1.5U BRICSat-P, to perform three maneuvers and prove their ability to propel a CubeSat.[195] BRICSat-P was launched in May 2015. It is currently in orbit, but due to power issues, a consistent communication has not yet been established. Some preliminary data have been downloaded from the satellite, and it shows that the satellite has successfully operated the propulsion system. Communication received from the CubeSat thus far has also verified the thruster's ability to detumble. The preliminary data show that the propulsion system was able to reduce initial tumbling from an estimated 30°/s to within 1.5°/s after 48 h. This was accomplished without any additional passive or active attitude control mechanism, such as magnetic torque, permanent magnets, or hysteresis rods. Analyses showed that with an absence of these attitude control systems, the satellite will continue to tumble at an average of 5°/s continuously due to the disturbance torques, if the thrusters were to not function. However, the data showed that the two axes that are controlled directly by the propulsion system have reached the target rotation rate of 1.0°/s at a much earlier time, and the intermediate axis is the only axis still above 1.0°/s at the 48 h mark. After another 48 h, all three axes were stabilized to below 1.0°/s.

The cold gas thrust system was installed on the 8U CADRE 1 Chaser spacecraft. The cold gas thrusters featuring 70 s specific impulse and 50 μN × s impulse bits (ensured a 3 D orientation capabilities for this relatively small satellite.

Not always the efforts on powering small satellites with pulsed thrusters were successful. In 2013, the CubeSat STRaND-1 was launched with a PPT developed by the Surrey Space Center (SSC). However, communication with the satellite was never achieved. In January 2017, the CubeSat Aoba-VELOX-3, a cooperation between the Nanyang Technological University, Singapore and the Kyushu Institute of Technology, Japan, was launched. However, no information about the performance of this satellite or its propulsion system was published up to this point. The Aoba-VELOX-4, which will also carry a PPT, is under preparation and shall explore the surface of the Moon.[199] Another PPT-powered CubeSat mission, the Austrian CubeSat PEGASUS from the University of Applied Sciences Wiener Neustadt (FHWN), was launched in June 2017. The PPT is a coaxial type and the system consists of four single units driven by a common power electronics[200] [Fig. 25(b)]. These PPT were mainly considered as a technology demonstration but will also support the ADCS tasks of the satellite. The performance of this system is provided in Table VIII. However, since the PPT will be commissioned only in December 2017, no data about function and performance are available at this time.

Figures 26(a) and 26(b) show the 2 U Actively Controlled CubeSat (TOM) with μCAT thrusters installed, and NASA Delivered Hardware—μCAT (George Washington University/NASA), successfully launched to orbit on Falcon-9 in 2016.

The FEEP technology was used for spacecraft potential control devices for many missions such as the recent US mission MMS.[201] Initial efforts to develop this technology also for propulsive means in the framework of the European Space Mission, specifically for GOCE (Gravity field and steady-state Ocean Circulation Explorer) and LISA (Laser Interferometer Space Antenna)[202] missions, were unsuccessful mainly due to a very complicated manufacturing technique. Further development of the technology itself and the utilized manufacturing methods, in combination with the development of highly miniaturized power electronics,[203] has led to a break-through. The present system, called Indium FEEP Multineedle Emitter (IFM) (shown in Fig. 27), has a much broader thrust range and produces higher maximum thrust at the same high specific impulse (>4000 s) than the system originally developed for LISA.[204] Detailed characteristics and performances are listed in Table VII. This new technology uses a multi-emitter of 28 adjacent emission sites, connected to one single propellant tank and power electronics,[205] and suites as propulsion system for micro- and nano-satellites. Wide thrust range (1 μN – 0.5 mN) and a

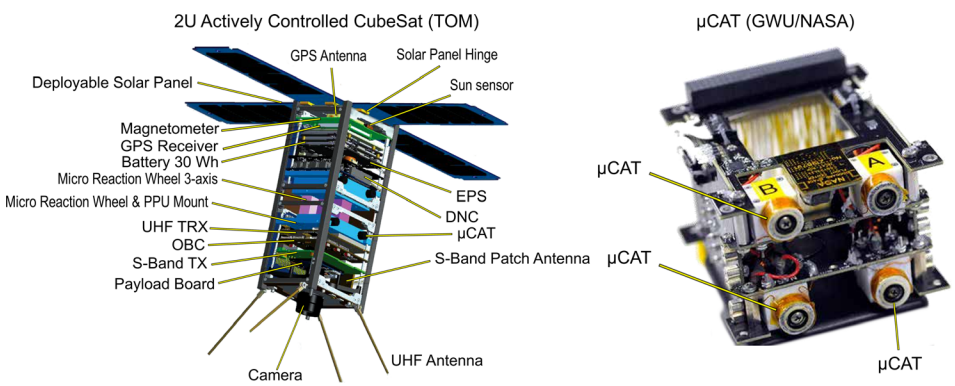

FIG. 26. (a) 2U Actively Controlled CubeSat (TOM) with μCAT thsusters installed and (b) NASA delivered hardware—μCAT (George Washington University/NASA). Courtesy: NASA.[196]

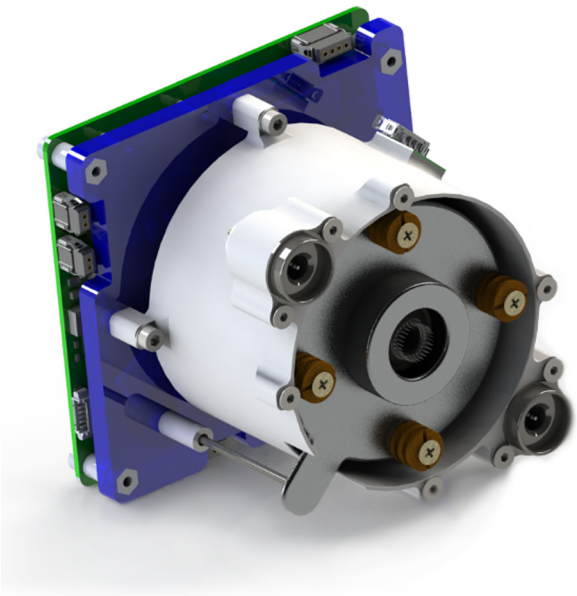

FIG. 27. The IMF nano thruster. The first in-orbit demonstration is planned for late 2017 on satellite from ICEYE in a clustered configuration of seven units.[213]

high specific impulse (2000–5000 s) allow significant increase in the mission range for small satellites, offering the possibility of high delta-v manoeuvres (several kilometres per second). The first in-orbit demonstration is planned for late 2017 on satellite from ICEYE in a clustered configuration of seven units.

B. Miniaturized ion thrusters on microsatellites

The University of Tokyo has operated two miniature ion thrusters in space on two microsatellites during 2014–2015. One miniature ion thruster was equipped on Hodoyoshi-4, 50-kg-class LEO satellite.[206,207] The ion thruster and all of the sub-components were developed using COTS-based components and the system was assembled as a single module including Xenon tank. The propulsion system was named MIPS for a Miniature Ion Propulsion System.[208] It is the world-first miniature ion thruster operating on a microsatellite having a mass of less than 100 kg.[209] The other ion thruster was equipped on PROCYON, a 50-kg-class micro-space probe orbiting around the sun.[210] The ion thruster was unified with eight cold-gas thrusters into one propulsion system, named as I-COUPS (Ion thruster and Cold gas thruster Unified Propulsion System, Fig. 28).[211,212] A single Xenon tank supplied the gas to both the ion thruster and the cold-gas thrusters to reduce the total mass of the propulsion system. It is the world-first microsatellite equipped with a full-set propulsion: a main-engine for delta-V and multiple thrusters for RCS and also the world-first micropropulsion usage on an interplanetary orbit.

The ion thrusters described here utilize microwave discharge plasmas for both the ion source and neutralizer.[214] Electron cyclotron resonance heating plasmas were produced by a 4.25 GHz microwave and 0.15 T magnetic field of samarium-cobalt magnets. The ion source and the neutralizer have an identical design of a discharge chamber whose inner diameters were 20 mm. They consume 1.0–1.5 W microwave inputs each. The difference was a downstream part: a two-grids system for the ion beam or a 4- or 6-holed orifice plate for the electron emission. Typical values of required mass flow rates were different, at 20 μg/s and 10 μg/s, respectively. The ion thruster produces a 3.5–6.0 mA ion beam depending on the microwave power and mass flowrate, corresponding to the thrust of 212–363 μN.

The MIPS was the first ion propulsion system that used the ion thruster described above and it was equipped on Hodoyoshi-4. The main purpose of this propulsion system is the verification of the miniature ion propulsion system in space. The development began in September 2011 at The University of Tokyo in collaboration with the Next Generation Space Technology Research Association (NESTRA). It included all subcomponents required to operate the ion thruster and its unification into a single module. The MIPS consists of four units: an ion-thruster unit, a power-processing unit, a gas management unit, and a MIPS-control unit. All units are placed on a double-deck frame to handle the MIPS as a modular component in a satellite. The engineering model of MIPS was completed in March 2013 and the flight model in February 2014. The flight model had the total weight of 8.1 kg and volume of $34\,\text{cm} \times 26\,\text{cm} \times 16\,\text{cm}$ and it provided $220 \pm 6\,\mu$N of thrust at a system power consumption of 28.1 ± 0.5 W.[209]

The Hodoyoshi-4 equipped with the MIPS was launched on 20 June 2014. The initial flight operation of the ion propulsion system was conducted on 28 October 2014. It showed successful ion thruster operations in space. Every communication of the satellite and ground station was

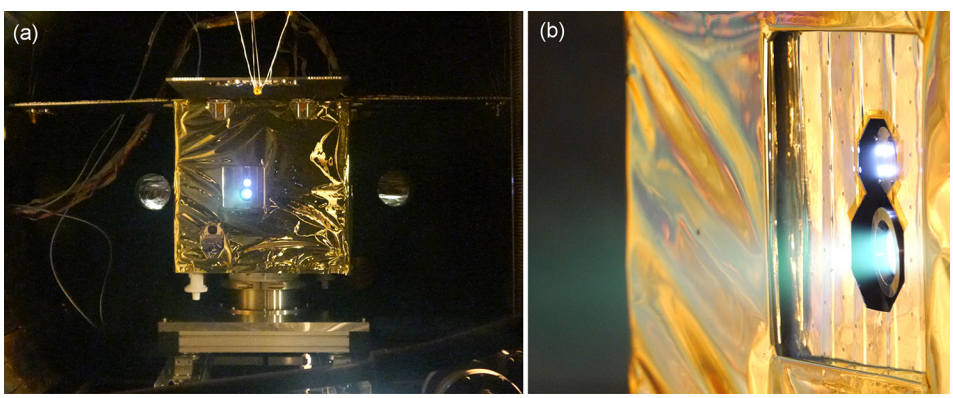

FIG. 28. A ground test of the I-COUPS flight model equipped on the PROCYON; (a) PROCYON flight model was placed in a vacuum chamber deploying the solar array panels and operating the ion thruster; (b) magnified view of the operating ion thruster.

limited within 10 min since it was sun-synchronous orbit satellite. Operation of the ion thruster was conducted only within that communication time, and each operation of the thruster was as short as 5 min. The ion thruster of MIPS experienced 4 times of operations in space showing the same performance confirmed by the ground tests.

In parallel to the MIPS, the development of the I-COUPS began in 2013 for the application in a micro-space probe, PROCYON (PRoximate Object Close flYby with Optical Navigation) developed by the University of Tokyo and Japan Aerospace Exploration Agency.[210] The nominal mission was the verification and demonstration of bus technologies for a deep space exploration using a 50 kg-class space probe. The advanced mission was the demonstration of a fly-by observation of a near-Earth asteroid after the orbit transfer using an ion thruster. That micro-probe required three different propulsion capabilities: (1) a reaction control, (2) a short-time and high thrust, and (3) a high delta-V. To satisfy those requirements, it was necessary to combine chemical propulsion and electrical propulsion, and I-COUPS was proposed that shared Xenon gas for cold-gas thrusters and an ion thruster. The I-COUPS was different from the MIPS with respect to an additional cold-gas thruster unit and assembly integrated in the satellite for the weight saving. The total mass of the I-COUPS was 9.96 kg, including 2.57 kg of Xenon. The power consumption was 7.3 W at its standby condition, 11.5 W at two cold-gas thrusters operation, and 40.0 W at an ion thruster operation.[210,212]

The PROCYON was launched on 3 December 2014 as a small secondary payload along with the main payload Hayabusa-2 and inserted into the intended orbit around the sun.[215] After the completion of the initial checkout of the satellite, the propulsion system was turned on and cold-gas thrusters started the attitude control maneuver. The measured gas pressure and generated torques agreed well with the expected values from the ground tests. Thereafter, the cold-gas thrusters were successfully operated during one year, including several tests of translational thrusts as long as 600 s. The ion thruster was first fired on 28 December 2014 and 30 min successful thrust generation was confirmed using Doppler shift data of the commutation wave. Nevertheless, several unexpected phenomena and malfunctions were found in the initial operations, and the project team spent two months (Jan–Feb in 2015) to settle those problems. Thereafter, the ion thruster started the continuous firing and accumulated the total operating time up to 223 h. The averaged ion beam current was 5.62 mA corresponding to the thrust of 340 μN (thrust coefficient of 0.943 was used as the averaged value of three Doppler data in the initial operations). After the 223 h, the ion thruster suddenly stopped the operation due to high voltage anomaly. The project team regarded that this anomaly was caused by the short between the screen grid and accelerator grid due to metal flakes generated by the grid sputtering (the ion thruster had been operated at two times higher mass flow rate than the ground test for its stable operation). The operations after that event were focused to clear the grid short.

C. Miniaturized Hall thrusters in space

Since the first flight of Hall thrust on a Meteor satellite at the end of 1971,[216] many in space experiments of Hall thrusters have been performed by Russia, Europe, and the United States. Fully referencing the previous experiences of in-space verification and application, two in-space tests of Hall thrusters were performed in China, namely, the Integrated EP system on SJ-9A satellite in 2012,[217] and the magnetic field focused type thruster named HEP-100MF on Shijian-17 satellite in 2016.

1. Integrated EP system on SJ-9A satellite

The integrated EP system on SJ-9A satellite is the first in-space verification of electrical propulsion system in China, and as such it attracted significant attention. In fact, the integrated EP system includes both a Hall thruster and a Xenon ion thruster (Fig. 29). The objectives of the verification include

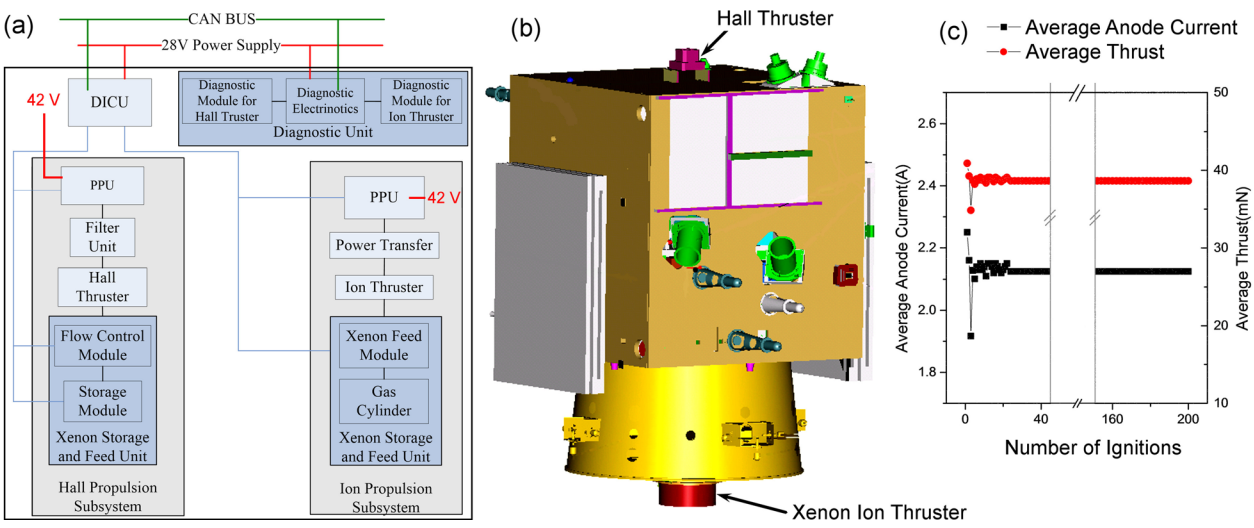

FIG. 29. Test flight of miniatursed Hall-type and ion thrusters. (a) Configuration of integrated electric propulsion system on satellite SJ-9A; (b) installation of integrated electric propulsion system on satellite SJ-9A; (c) typical in-space cyclogram of the Hall thruster operation on satellite SJ-9A.

- *The Integrated EP system should accomplish the desired circle of operation to verify its reliability. And obviously, its thrust and specific impulse should also be measured in space, and compared with the result of ground tests to evaluate the impact of the vacuum environment on thruster performance.*
- *The Integrated EP system should be able to verify its adaptability to typical aerospace instruments and the space synthesis environment;*
- *Monitoring the impact of the electrical thruster operation on the satellite, including the plume plasma parameters near the satellite, and the pollutants caused by the plasma plume.*

To sum up the above objectives, the integrated EP system on SJ-9A satellite needs to focus on solving the following issues:

Safety of the satellite: It is well known that electric propulsion system is typically equipped with high voltage, high power components, and has complicated interaction mechanism with the satellite. As it is the first on-orbit validation of this system, major security issues, such as high voltage breakdown, electromagnetic compatibility, and plume shielding of communication signals, are all considered in the analysis, and precaution methods are designed and ground tested.

Thrust measure scheme design: Because of ground test limitations, including the limited vacuum chamber size, the residual gas in the chamber, accuracy limitations of the thrust stand, vibration of the ground, the uncertainty of thrust measurements always exist. The measurement of the thrust and specific impulse by means of in-space verification is, of course, a very valuable opportunity.

Plume diagnostic: Many concerns regarding the security risk of an electrical propulsion system are caused by the complexity of the interaction mechanism of its plasma plume. Indeed, a large number of analytical results are not commonly accepted for the lack of a creditable parameter for the plume plasma. Therefore, the plume parameter should be an in-space diagnostic to solve the constraints of ground test conditions.

According to the objectives of verification, BICE defined and designed the integrated electrical propulsion system, as shown in Fig. 29(a), which consists of the following components:

- *A Hall propulsion subsystem, including a Hall thruster, its corresponding Xenon storage and feeding unit, and a Power processing unit;*
- *A Xenon ion propulsion subsystem, including a Xenon ion thruster, its corresponding Xenon storage and feeding unit, and a power processing unit;*
- *A plume diagnostic unit, including two EP plume diagnostic modules, each includes a Langmuir probe, a RPA and a quartz crystal microbalance, which are quite similar with the configuration of EPDP on SMART-1*[218] *and LISA Path Finder;*[219]
- *A DICU (Digital Integration and Control Unit), responsible for the overall system control logic, security policy implementation, and data analysis and processing.*

The ion thruster is installed in the positive Z axis of the satellite, and the Hall thruster is installed in the negative Z axis. Thus, one thruster lifts the orbit of the satellite, and the other reduces it; the thrust could be precisely calculated through the accurate measurements of the satellite orbit. As impulsion of the two thrusters could offset each other, there is no need to use chemical propulsion for impulsion compensation. In order to increase measurement accuracy, the track change is measured after four consecutive firing cycles, and each firing lasts 10 min.

Both the Xenon ion and Hall thrusters were first ignited on 7 November 2012. Each of them was switched on and off for 208 times until 30 December 2013. Typical test data for the Hall thruster are shown in Fig. 29(c). It can be seen that with the increase in firing time and time exposed to space, the thruster performance stabilized. After twenty times of ignition, the anode current and thrust of the Hall thruster remains virtually stable. The test results show that both the Hall and Xenon ion thrusters meet the design requirements, with the consistency of each ignition being quite good. After completing the target number of in-space ignition, the integrated electric propulsion system was working on the SJ-9A as an application system for 4 years.

In-space test of SJ-9A has dispelled many doubts about the application of electric propulsion to small satellites and provided a good basis for system design, particular with regard to security schemes of following applications of electric propulsion system.

2. HEP-100MF thruster on XY-2 satellite

After the successful verification of the SJ-9A, several satellite platforms in China began to consider the application of electric propulsion technology, and many works have been carried out with that aim. The HEP-100MF, which is a magnetic focused Hall thruster, is verified on the XY-2 GEO satellite, which is another characteristic in-space test. The consideration of plume diagnostic and system security are similar to those for SJ-9A, and therefore there is no need for extensive preliminary rehearsals.

Unlike SJ-9A, however, XY-2 is working on the geostationary orbit, which means that thrust measurements cannot be performed using orbit track changes. Therefore, different from the typical electrical thruster installing scheme whose thrust vector always passes through the satellite centroid, thrust vector of the HEP-100MF thruster is set at an angle away from the centroid of the XY-2 satellite. Therefore, every operation of the HEP-100MF thruster will produce a disturbance torque. Under the specially designed control mode for thrust measurement, only momentum wheels are used to absorb the disturbance torque produced by the electric thruster. By calculating the change of momentum wheel speed before and after the HEP-100MF thruster firing, the momentum produced by the operation of the electric thruster can be accurately obtained, and its thrust and specific impulse can be thus calculated.

VI. OUTLOOK AND PERSPECTIVES

There is little doubt that micro- and nanosatellites, and their massive constellations are poised to revolutionize the way in which we explore space, providing an affordable and

highly-adaptable means for near Earth large data collection and universal connectivity, as well as advancing our deep space exploration capability.

However, practical realization of miniaturized, automated systems that can actively respond to their environment and ultimately self-repair to ensure durable and efficient performance remains a technological challenge. It relies on concomitant and complimentary advances in micro- and nano-fabrication, materials engineering, electronics and robotics, as well as novel paradigms for the integration of these advances into conceptually novel, robust, multifunctional, and reliable space assets, as articulated by the Nanotechnology Roadmap initiative released by NASA in 2015.

Of equal importance is the development of compatible miniaturized thrust systems for maneuvering for small space assets to support their near Earth and deep space missions. As highlighted by this review, these thruster systems need to possess several critical characteristics. These include long service life, which covers both high-efficiency of operation and minimal degradation, and, eventually, self-healing capacity, reliability and precision, and compatibility with other satellite systems. The attainment of these characteristics is not trivial, and despite tremendous progress over the last decade, many road blocks that still remain. Indeed, for every success story presented at the inaugural International Workshop on Micropropulsion and Cubesats, MPCS-2017, Bari, Italy (Fig. 30), an equal or greater number of present and future challenges in miniaturized space propulsion systems were outlined.

One of the key practical challenges on the path of miniature thruster development is associated with the difficulty in assessing space performance on the ground. Indeed, despite a wealth of testing methods available, promising ground performance does not always correlate with the behavior of the asset in space, which hinders rapid thruster optimization and advancement. Thus, the development of modelling and experimental testing facilities that more adequately reflect the performance of thruster technologies in space are needed. A related issue is that of integration of the developed thruster capabilities with the critical systems of the actual satellite.

FIG. 30. Prepare for take-off! The group of participants of the International Workshop on Micropropulsion and Cubesats at a 13th century Castel del Monte on a hill in Andria, southeast Italy (UNESCO World Heritage Site). Like the Castel crowning a hill, electric propulsion technology crowns the whole pyramid of rocket technology which is based on powerful chemical rocket engines but requires quite tiny, extremely sophisticated, knowledge-intensive, science-consumptive plasma thrusters to drive our spaceships to planets and stars.

Another area where significant advancement is necessary is the development of microfabrication techniques suitable for fabrication of thruster technologies, whose operation relies on micro- and nano-scale effects, such as electrospray thrusters and printed cathode arc thrusters. This is the area where significant gains with regard to the development of robust, efficient, and affordable thruster systems suitable for micro- and nano-satellite assets can be attained.

While not discussed in much detail in this review, the concept of self-healing and multifunctional thruster architectures that can self-repair by switching their mode of operation is one that can revolutionize the thruster technology, particularly with respect to Hall, ion, helicon, and vacuum arc devices, and significantly expand its capacity in supporting long-term missions.[2,220] Such architectures will emerge on the back of the fundamental advancements in plasma-enabled material synthesis and thruster engineering.

It is important to emphasize that as the number of microsatellite assets continues to grow, the significance of their timely decommissioning and removal from orbit will become a pressing issue. Indeed, with some proposed constellations reaching hundreds of assets in number, the capability for end-of-life permanent removal of such assets will become one of the key design requirements.

Based on a highly representative international survey of the current effort on micropropulsion systems outlined at the MPCS-2017 meeting, we can state that the consolidated effort of many teams involved in development of various types of micropropulsion platforms is vitally needed to maintain at a state-of-the-art level of the field. This nontrivial task requires planned, proactive activities, but eventually, it will pave the way to the really active small satellites and their constellations, as well as many emerging applications.

Among others, the following high priority tasks of paramount importance could be formulated:

- *Enhancement of energy efficiency. This relates to all types of electric thrusters, from smallest μ-pulse systems to projected large booster platform with the total power of hundreds kW; with apparent deficiency of electric power in board, the energy efficiency will always be an issue;*
- *Prolongation of active service life and enhancement of operational reliability. Apparently, these are of ultimate importance for long manned flights to Mars and possible other planets;*
- *Development of compact, efficient, and safe electric power supply systems. While this is not a direct task for the micropropulsion community, it still should be in focus due to extremely important role of power unit in the whole electric thrust system.*

With the consolidated effort of many international teams involved, and in a view of rapid progress in material and semiconductor techniques, these tasks appear to be quite solvable, and we could expect the next-generation electric

power systems in five to ten years. Ultra-compact, very efficient and robust, they will ensure a true Renaissance of space exploration and finally, great benefit to the Mankind.

VII. CONCLUDING REMARKS

In this review, we have briefly outlined the state-of-the-art of micropropulsion technology, as it was presented at the inaugural International Workshop on Micropropulsion and Cubesats (MPCS2017), a joint effort between Plasma Sources and Application Centre/Space Propulsion Centre (Singapore) and the Micropropulsion and Nanotechnology Lab, the G. Washington University (USA), hosted by CNR-Nanotec–P.Las.M.I. lab in Bari, Italy. This focused review has highlighted the most promising developments reported at MPCS-2017 by a number of leading world-reputed experts in miniaturized space propulsion systems. Recent advances in many major types of small thrusters including Hall, ion, helicon, and pulsed vacuum arc devices were presented, and trends and perspectives were outlined.

ACKNOWLEDGMENTS

This work was supported in part by the following funds and organizations: OSTIn-SRP/EDB through National Research Foundation and in part by MoE AcRF (Rp6/16 Xs), Singapore; National Natural Science Foundation of China (Grant Nos. 51777045 and 51477035); National Technical Basic Scientific Research of China, Grant No. JSZL2016203c006; NASA DC Space Grant Consortium; Grant-in-Aid for Scientific Research under Grant S: 21226019 and Grant B: 17H02295 through the Japan Society for the Promotion of Science, and by NIFS budget code NIFS17KLER063, and KAKENHI grant: Grant-in-Aid for Scientific Research (S), No. JP16H06370; S.S. thanks late Professor K. Toki, late Dr. K. P. Shamrai, Dr. Kuwahara, and the HEAT project members for their contribution Y.R. acknowledges the support from the US DOE under Contract No. DE-AC02-09CH11466; I.L. acknowledges the support from the School of Chemistry, Physics and Mechanical Engineering, Science and Engineering Faculty, Queensland University of Technology; special thanks to L. Xu, M. Lim, S. Huang, and the entire PSAC/SPCS for their help.

[1]K. F. LoKeidarng, *Deep Space Propulsion. A Roadmap to Interstellar Flight* (Springer, New York, 2012). DOI: http://dx.doi.org/10.1007/978-1-4614-0607-5
[2]I. Levchenko, S. Xu, G. Teel, D. Mariotti, M. L. R. Walker, and M. Keidar, "Recent progress and perspectives of space electric propulsion systems based on smart nanomaterials," Nat. Commun. (in press).
[3]See http://www.sei.aero/eng/papers/uploads/archive/SpaceWorks_Nano_Microsatellite_Market_Assessment_January_2014.pdf for 2014 Nano/Microsatellite Market Assessment, SpaceWorks Enterprises, Inc.
[4]J. W. Dankanich, B. Vondra, and A. V. Ilin, "Fast transits to Mars using electric propulsion," AIAA Paper 2010-6771.
[5]See https://www.nasa.gov/content/what-are-smallsats-and-cubesats for "What are SmallSats and CubeSats?" (2015).
[6]S. Hurley, G. Teel, J. Lukas, S. Haque, M. Keidar, C. Dinelli, and J. Kang, "Thruster subsystem for the United States Naval Academy's (USNA) Ballistically Reinforced Communication Satellite (BRICSat-P)," Trans. JSASS, Aerosp. Technol. Jpn. **14**, Pb_157–Pb_163 (2016).
[7]See https://www.nasa.gov/sites/default/files/atoms/files/2015_nasa_technology_roadmaps_ta_10_nanotechnology_final.pdf for "NASA Technology Roadmaps. TA10: Nanotechnology" (2015).
[8]G. P. Sutton and O. Biblarz, *Rocket Propulsion Elements* (John Wiley and Sons, New York, 2001), ISBN 0-471-32642-9.
[9]See http://www.airbus.com/newsroom/press-releases/en/2017/06/one-web-satellites-serial-production-line-inauguration.html for OneWeb Satellites inaugurates serial production line for the Assembly, Integration, and Test of OneWeb's first satellites, 27 June 2017.
[10]F. Darnon, D. Arrat, E. Chesta, S. d'Escrivan, and N. Pillet, "Overview of electric propulsion activities in France," paper presented at the 29th International Electric Propulsion Conference, Princeton University, 31 October 2005, Paper IEPC-2005-162.
[11]J. J. Delgado, J. A. Baldwin, and R. L. Corey, "Space systems Loral electric propulsion subsystem: 10 years of on-orbit operation," paper presented at Joint 30th ISTS/34th IEPC/6th NSAT Conference, Kobe-Hyogo, Japan, 4-10 July 2015, Paper IEPC-2015-004/ISTS-2015-b-04.
[12]D. Estublier, G. Saccoccia, and J. G. Amo, "Electric propulsion on SMART-1," ESA Bull. **129**, 41 (2007).
[13]K. Sankaran, L. Cassady, A. D. Kodys, and E. Y. Choueiri, "A survey of propulsion options for cargo and piloted missions to Mars," Ann. NY Acad. Sci. **1017**, 450 (2004).
[14]Y. Takahata, T. Ikeda, M. Nishida, T. Kagota, T. Kakuma, and H. Tahara, "Research and development of high-power, high-specific-impulse magnetic-layer-type Hall thrusters for manned Mars exploration," paper presented at Joint 30th ISTS/34th IEPC/6th NSAT Conference, Kobe-Hyogo, Japan, 4-10 July 2015, Paper IEPC-2015-151/ISTS-2015-b-151.
[15]H. Kuninaka, K. Nishiyama, Y. Shimizu, I. Funaki, H. Koizumi, S. Hosoda, and D. Hayabusa, "ASTEROID explorer powered by ion engines on the way to Earth," paper presented at the 31st International Electric Propulsion Conference (2009), Paper IEPC 2009-267.
[16]H. Kuninaka and J. Kawaguchi, "Lessons learned from round trip of Hayabusa asteroid explorer in deep space," paper presented at IEEE Aerospace Conference, Big Sky, MT, 5 March 2011, http://dx.doi.org/10.1109/AERO.2011.57475999
[17]S. Mazouffre, Plasma Sources Sci. Technol. **25**, 033002 (2016).
[18]C. Charles, J. Phys. D: Appl. Phys. **42**, 163001 (2009).
[19]A. V. Ilin, D. A. Gilman, M. D. Carter, and J. E. Farrias, "VASIMR Solar powered missions for NEA retrieval and NEA deflection," paper presented at the 33rd International Electric Propulsion Conference, Washington D.C., USA, 6-10 October 2013, Paper IEPC-2013-336.
[20]J. Lukas, G. Teel, J. Kolbeck, and M. Keidar, AIP Adv. **6**, 025311 (2016).
[21]I. Levchenko, M. Keidar, and K. Ostrikov, Phys. Lett. A **373**, 1140 (2009).
[22]M. Keidar and I. I. Beilis, IEEE Trans. Plasma Sci. **34**, 804–814 (2006).
[23]I. Levchenko and M. Keidar, "Kinetic model of the electron and ion transport in Hall thrusters," paper presented at the 28th International Electric Propulsion Conference, Toulouse, France, 17-21 March 2003, Paper 0162-0303.
[24]I. Levchenko and M. Keidar, IEEE Trans. Plasma Sci. **33**, 526–527 (2005).
[25]A. Héron and J. C. Adam, Phys. Plasmas **20**, 082313 (2013).
[26]J. L. Ferreira, A. A. Martins, R. Miranda, A. Schelling, L. S. Alves, E. G. Costa, H. O. Coelho, A. C. Branco, and F. N. O. Lopes, J. Phys.: Conf. Ser. **641**, 012016 (2015).
[27]Y. Ding, W. Peng, H. Sun, L. Wei, M. Zeng, F. Wang, and D. Yu, "Performance characteristics of no-wall-losses Hall thruster," Eur. Phys. J. Spec. Top. **226**, 2945 (2017).
[28]Y. Ding, H. Sun, W. Peng, Y. Xu, L. Wei, H. Li, P. Li, H. Su, and D. Yu, Jpn. J. Appl. Phys. **56**, 050312 (2017).
[29]M. Walker, "Electric propulsion," Aerosp. Am. **12**, 54–55 (2005).
[30]Y. Ding, W. Peng, L. Wei, G. Sun, H. Li, and D. Yu, J. Phys. D: Appl. Phys. **49**, 465001 (2016).
[31]Y. Ding, W. Peng, H. Sun, L. Wei, M. Zeng, F. Wang, and D. Yu, Jpn. J. Appl. Phys., Part 1 **56**, 038001 (2017).
[32]Y. Ding, W. Peng, H. Sun, Y. Xu, L. Wei, H. Li, M. Zeng, F. Wang, and D. Yu, Phys. Plasmas. **24**, 023507 (2017).
[33]Y. Ding, H. Sun, P. Li, L. Wei, H. Su, W. Peng, H. Li, and D. Yu, J. Phys. D: Appl. Phys. **50**, 335201 (2017).
[34]Y. Ding, H. Sun, P. Li, L. Wei, Y. Xu, W. Peng, H. Su, and D. Yu, Vacuum **143**, 251–261 (2017).
[35]Y. Ding, H. Sun, L. Wei, P. Li, H. Su, W. Peng, and D. Yu, Acta Astronaut. **139**, 521 (2017).
[36]Y. Raitses and N. J. Fisch, Phys. Plasmas **8**, 2579 (2001).
[37]A. Smirnov, Y. Raitses, and N. J. Fisch, J. Appl. Phys. **92**, 5673 (2002).
[38]A. Smirnov, Y. Raitses, and N. J. Fisch, Phys. Plasmas **14**, 057106 (2007).
[39]Y. Raitses, A. Smirnov, and N. J. Fisch, Phys. Plasmas **16**, 057106 (2009).

[40]A. I. Morozov and V. V. Savelyev, in *Review of Plasma Physics*, edited by B. B. Kadomtsev and V. D. Shafranov (Consultants Bureau, New York, 2000), Vol. 21, p. 203.
[41]Y. Raitses, A. Smirnov, and N. J. Fisch, J. Appl. Phys. **104**, 066102 (2008).
[42]A. Smirnov, Y. Raitses, and N. J. Fisch, IEEE Trans. Plasma Sci. **34**, 132 (2006).
[43]M. Granstedt, Y. Raitses, and N. J. Fisch, J. Appl. Phys. **104**, 103302 (2008).
[44]J. B. Parker, Y. Raitses, and N. J. Fisch, Appl. Phys. Lett. **97**, 091501 (2010).
[45]A. Smirnov, Y. Raitses, and N. J. Fisch, Phys. Plasmas **11**, 4922 (2004).
[46]Y. Raitses, J. C. Gayoso, and N. J. Fisch, "Effect of magnetic shielding on plasma plume of the cylindrical Hall thrusters," paper presented at the 32nd International Electric Propulsion Conference, Wiesbaden, Germany, 11-15 September 2011, Paper IEPC-2011-175.
[47]Y. Raitses, E. Merino, J. B. Parker, and N. J. Fisch, J. Appl. Phys. **108**, 093307 (2010).
[48]N. Koch, H. P. Harmann, and G. Kornfeld, "Development and test status of the THALES high efficiency multistage plasma (HEMP) thruster family," in *Proceedings of the 29th International Electric Propulsion Conference*, Princeton, NJ, October 2005, Paper IEPC-2005-297.
[49]G. Courtney, P. Lozanoy, and M. Martinez-Sanchez, "Continued investigation of diverging cusped field thruster," AIAA Paper 2008-4631.
[50]N. A. MacDonald, M. A. Cappelli, S. R. Gildea, M. Martınez-Sanchez, and W. A. Hargus, Jr., J. Phys. D: Appl. Phys. **44**, 295203 (2011).
[51]R. Spektor, K. D. Diamant, E. J. Beiting, K. A. Swenson, D. T. Goddard, Y. Raitses, and N. J. Fisch, "Characterization of a cylindrical Hall thruster with permanent magnets," paper presented at the 32nd International Electric Propulsion Conference, Wiesbaden, Germany, 11-15 September 2011, Paper IEPC-2011-264.
[52]K. A. Polzin, Y. Raitses, J. C. Gayoso, and N. J. Fisch, "Comparisons in performance of electromagnet and permanent-magnet cylindrical hall-effect thrusters," AIAA Paper 2010-6695.
[53]Y. Ding, Y. Xu, W. Peng, L. Wei, H. Su, H. Sun, P. Li, H. Li, and D. Yu, J. Phys. D: Appl. Phys. **50**, 145203 (2017).
[54]Y. Ding, B. Jia, Y. Xu, L. Wei, H. Su, P. Li, H. Sun, W. Peng, C. Yong, and D. Yu, Phys. Plasmas. **24**, 080703 (2017).
[55]N. Gascon, M. Dudeck, and S. Barral, Phys. Plasmas **10**, 4123 (2003).
[56]S. Mazouffre, K. Dannenmayer, and C. Blank, Phys. Plasmas **18**, 064501 (2011).
[57]S. Mazouffre, R. Perez Luna, and K. Dannenmayer, J. Appl. Phys. **102**, 023304 (2007).
[58]T. Burton, A. M. Schinder, G. Capuano, J. J. Rimoli, M. L. R. Walker, and G. B. Thompson, J. Propul. Power **30**, 690–695 (2014).
[59]I. G. Mikellides, I. Katz, R. R. Hofer, and D. M. Goebel, J. Appl. Phys. **115**, 043303 (2014).
[60]R. R. Hofer, D. M. Goebel, I. G. Mikellides, and I. Katz, J. Appl. Phys. **115**, 043304 (2014).
[61]L. Garrigues, S. Mazouffre, G. Bourgeois, J. Vaudolon, C. Hénaux, R. Vilamot, A. Rossi, D. Harribey, and S. Zurbach, "Design and first test campaign results with a new flexible magnetic circuit for a Hall thruster," paper presented at the 33rd International Electric Propulsion Conference, 2610 Washington D.C., USA, 6–10 October 2013, Paper IEPC-2013-250.
[62]S. Mazouffre, T. Vaudolon, S. Tsikata, C. Henaux, D. Harribey, and A. Rossi, "Optimization of the design of a wall-less Hall thruster," paper presented at the Joint 30th ISTS, 34th IEPC and 6th 2703 NSAT Conference, Kobe-Hyogo, Japan, 4 July 2015, Paper IEPC-2015-182/ISTS-2015-b-182.
[63]R. W. Conversano, D. M. Goebel, R. R. Hofer, I. G. Mikellides, I. Katz, and R. E. Wirz, paper presented at The Joint 30th ISTS, 34th IEPC and 6th NSAT Conference, Kobe-Hyogo, Japan, 4 July (2015), Paper IEPC-2015-100/ISTS-2015-b-100 (2015); paper presented at the 34th International Electric Propulsion Conference, Kobe, 4-10 July (2015).
[64]L. Grimaud and S. Mazouffre, Plasma Sources Sci. Technol. **26**, 055020 (2017).
[65]R. W. Conversano, D. M. Goebel, R. R. Hofer, I. G. Mikellides, and R. E. Wirz, J. Propul. Power **33**, 992–1001 (2017).
[66]L. Grimaud and S. Mazouffre, J. Appl. Phys. **122**, 033305 (2017).
[67]S. Mazouffre, S. Tsikata, and J. Vaudolon, J. Appl. Phys. **116**, 243302 (2014).
[68]J. Vaudolon, S. Mazouffre, C. Hénaux, D. Harribey, and A. Rossi, Appl. Phys. Lett. **107**, 174103 (2015).
[69]B. Karadag, S. Cho, Y. Oshio, Y. Hamada, I. Funaki, and K. Komurasaki, AIAA Paper 2016-4951.
[70]L. Grimaud and S. Mazouffre, J. Appl. Phys. **122**, 033305 (2017).
[71]T. Zhuang, A. Shashurin, T. Denz, P. Vail, A. Pancotti, and M. Keidar, J. Propul. Power **30**, 29–34 (2014).
[72]T. Zhuang, A. Shashurin, I. I. Beilis, and M. Keidar, Phys. Plasmas **19**, 063501 (2012).
[73]M. Keidar, T. Zuang, A. Shashurin, G. Teel, D. Chiu, J. Lucas, S. Haque, and L. Brieda, Plasma Phys. Controlled Fusion **57**, 014005 (2015).
[74]M. Keidar and I. I. Beilis, *Plasma Engineering: Application in Aerospace, Nanotechnology and Bionanotechnology* (Elsevier, Oxford, UK, 2013).
[75]T. Zhuang, A. Shashurin, M. Keidar, and I. I. Beilis, Plasma Sources Sci. Technol. **20**, 015009 (2011).
[76]I. I. Beilis, Contrib. Plasma Phys. **43**, 224 (2003).
[77]K. Lemmer, "Propulsion for CubeSats," Acta Astronaut. **134**, 231 (2017).
[78]See http://busek.com/technologies__espray.htm for Electrospray thrusters available from Busek.
[79]G. Lenguito, J. Fernandez de la Mora, and A. Gomez, J. Micromech. Microeng. **24**, 055003 (2014).
[80]M. Tajmar, I. Vasiljevich, and W. Grienauer, Ultramicroscopy **111**, 1 (2010).
[81]C. Scharlemann, N. Buldrini, R. Killinger, M. Jentsch, A. Polli, L. Ceruti, L. Serafini, D. DiCara, and D. Nicolini, Acta Astronaut. **69**, 822 (2011).
[82]J. Gonzalez del Amo, "European Space Agency (ESA) electric propulsion activities," paper presented at the 34th International Electric Propulsion Conference, Kobe, 4-10 July 2015, Paper IEPC-2015-02.
[83]K. E. Petersen, Proc. IEEE **70**, 420 (1982).
[84]S. Dandavino, C. Ataman, C. N. Ryan, S. Chakraborty, D. Courtney, J. P. W. Stark, and H. Shea, J. Micromech. Microeng. **24**, 075011 (2014).
[85]K. Nakagawa, T. Tsuchiya, and Y. Takao, Jpn. J. Appl. Phys., Part 1 **56**, 06GN18 (2017).
[86]E. Gustan-Gutierrez and M. Gamero-Castaño, J. Propul. Power **33**, 984 (2017).
[87]R. Krpoun and H. R. Shea, J. Micromech. Microeng. **19**, 045019 (2009).
[88]D. G. Courtney, S. Dandavino, and H. Shea, J. Propul. Power **32**, 392 (2016).
[89]F. Mier-Hicks and P. C. Lozano, J. Guid. Control Dynam. **40**, 642 (2017).
[90]C. Guerra-Garcia, D. Krejci, and P. Lozano, J. Phys. D: Appl. Phys. **49**, 115503 (2016).
[91]D. Krejci, F. Mier-Hicks, R. Thomas, T. Haag, and P. Lozano, J. Spacecraft Rockets **54**, 447 (2017).
[92]S. Dandavino, C. Ataman, S. Chakraborty, H. Shea, C. Ryan, and J. Stark, "Design and fabrication of the thruster heads for the MicroThrust MEMS electrospray propulsion system," paper presented at the 33rd International Electric Propulsion Conference, Washington D.C., USA, 6-10 October 2013, Paper IEPC-2013-127 (2013).
[93]M. Piechotka, K. Huhn, T. Henning, D. Feili, and P. J. Klar, "Microfabrication of colloid emitters based on the photo resist SU-8 and electro plating," paper presented at the 32nd International Electric Propulsion Conference, Wiesbaden, Germany, 11-15 September 2011, Paper IEPC-2011-276.
[94]K. Huhn, T. Henning, P. J. Klar, and S. Hengsbach, "Colloid emitters in photostructurable polymer technology: Fabrication and characterization progress report," paper presented at the 34th International Electric Propulsion Conference, Kobe, 4-10 July 2015, Paper IEPC-2015-120.
[95]T. Henning, K. Huhn, S. Feng, Z. Xie, S. Hengsbach, K. Bade, and P. J. Klar, "*Three-dimensional lithography for the microfabrication of colloid emitters*," paper presented at the 5th Space Propulsion Conference, Rome, 2-6 May 2016, Paper SP2016_3124766.
[96]See http://www.nanoscribe.de for Nanoscribe series of instruments.
[97]L. F. Velásquez-García, J. Microelectromech. Syst. **24**, 2117 (2015).
[98]J. A. Nabity, G. Mason, J. E. Engel, J. W. Daily, R. S. Lagumbay, and D. Kassoy, "Studies of MEMS colloid thrusters," AIAA Paper 2006-5007.
[99]R. W. Boswell, Phys. Lett. A **33**, 457 (1970).
[100]S. Shinohara, T. Hada, T. Motomura, K. Tanaka, T. Tanikawa, K. Toki, Y. Tanaka, and K. P. Shamrai, Phys. Plasmas **16**, 057104 (2009).
[101]S. Shinohara, H. Nishida, T. Tanikawa, T. Hada, I. Funaki, and K. P. Shamrai, IEEE Trans. Plasma Sci. **42**, 1245 (2014).
[102]K. Toki, S. Shinohara, T. Tanikawa, and K. P. Shamrai, Thin Solid Films **506-507**, 597 (2006).
[103]O. V. Batishchev, IEEE Trans. Plasma Sci. **37**, 1563 (2009).
[104]D. Kuwahara, A. Mishio, T. Nakagawa, and S. Shinohara, Rev. Sci. Instrum. **84**, 103502 (2013).

[105]T. Nakagawa, S. Shinohara, D. Kuwahara, A. Mishio, and H. Fujitsuka, "Characteristics of RF-produced, high-density plasma with very small diameter," Jpn. Phys. Soc. Conf. Proc. **1**, 015022 (2014).
[106]T. Nakagawa, Y. Sato, H. Iwaya, D. Kuwahara, and S. Shinohara, Plasma Fusion Res. **10**, 3401037 (2015).
[107]T. Ishii, H. Ishii, S. Otsuka, N. Teshigahara, H. Fujitsuka, S. Waseda, D. Kuwahara, and S. Shinohara, "Study on electrodeless electric propulsion in high-density helicon plasma with permanent magnets," Jpn. Phys. Soc. Conf. Proc. **1**, 015047 (2014).
[108]N. Teshigahara, S. Shinohara, Y. Yamagata, D. Kuwahara, and M. Watanabe, Plasma Fusion Res. **9**, 3406055 (2014).
[109]Y. Tanida, D. Kuwahara, and S. Shinohara, "Spatial profile of ion velocity distribution function in helicon high-density plasma by laser induced fluorescence method," Trans. Jpn. Soc. Aeronaut. Space Sci. (JSASS), Aerosp. Tech. Jpn. **14**, Pb_7 (2016).
[110]J. Vlček, J. Phys. D: Appl. Phys. **22**, 623 (1989).
[111]S. Waseda, H. Fujitsuka, S. Shinohara, D. Kuwahara, M. Sakata, and H. Akatsuka, Plasma Fusion Res. **9**, 3406125 (2014).
[112]T. Tanikawa and S. Shinohara, "Large-volume, helicon-plasma source for simulation experiments of space plasmas," in *Proceedings of 12th International Congress on Plasma Physics*, Nice, France, 25-29 October 2004, Paper hal-00002013.
[113]S. Shinohara, T. Tanikawa, T. Hada, I. Funaki, H. Nishida, T. Matsuoka, F. Otsuka, K. P. Shamrai, T. S. Rudenko, T. Nakamura, A. Mishio, H. Ishii, N. Teshigahara, H. Fujitsuoka, and S. Waseda, Trans. Fusion Sci. Technol. **63**, 164 (2013).
[114]G. A. Mesayats, *Cathode Phenomena in a Vacuum Discharge* (Nauka Publishers, Moscow, 2000).
[115]M. Keidar, J. Schein, K. Wilson, A. Gerhan, M. Au, B. Tang, L. Idzkowki, M. Krishnan, and I. I. Beilis, Plasma Sources Sci. Technol. **14**, 661 (2005).
[116]H. Koizumi, A. Kakami, Y. Furuta, K. Komurasaki, and Y. Arakawa, "Liquid propellant pulsed plasma thruster," paper presented at the 28th International Electric Propulsion Conference, Toulouse, France, 17-21 March 2003, Paper IEPC 03-087.
[117]J. Schein, A. Anders, R. Binder, M. Krishnan, J. E. Polk, N. Qi, and J. Ziemer, Rev. Sci. Instrum. **73**, 925 (2002).
[118]A. Anders, J. Schein, and N. Qi, Rev. Sci. Instrum. **71**, 827 (2000).
[119]J. Schein, N. Qi, R. Binder, M. Krishnan, J. K. Ziemer, J. E. Polk, and A. Anders, "Low mass vacuum arc thruster system for station keeping missions," paper presented at the 27th International Electric Propulsion Conference, Pasadena, CA, USA, 15-19 October 2001, Paper IEPC-01-228.
[120]S. Hurley and M. Keidar, "Linear actuated micro-cathode arc thruster system," paper presented at the 52nd AIAA/SAE/ASEE Joint Propulsion Conference, AIAA Propulsion and Energy Forum (AIAA 2016-5043).
[121]I. Kronhaus, M. Laterza, and Y. Manor, Rev. Sci. Instrum. **88**, 043505 (2017).
[122]W. J. Hyun, E. B. Secor, M. C. Hersam, C. D. Frisbie, and L. F. Francis, Adv. Mater. **27**, 109–115 (2015).
[123]S. Mazouffre, Plasma Sources Sci. Technol. **25**, 033002 (2016).
[124]D. M. Goebel and I. Katz, *Fundamentals of Electric Propulsion: Ion and Hall Thrusters* (Wiley, Oxford, 2008).
[125]D. Goebel, K. K. Jameson, and R. R. Hofer, J. Propul. Power **28**, 355 (2012).
[126]D. G. Fearn and C. M. Philip, "An investigation of physical processes in a hollow cathode discharge," AIAA J. **11**, 131 (1973).
[127]J. Polk, D. Goebel, R. Watkins, K. Jameson, and L. Yoneshige, "Characterization of hollow cathode performance and thermal behavior," AIAA Paper 2006-5150.
[128]S. Jahanbakhsh, M. Satir, and M. Celik, Rev. Sci. Instrum. **87**, 02B922 (2016).
[129]R. E. Wirz, "Miniature ion thrusters: A review of modern technologies and mission capabilities," paper presented at the 34th International Electric Propulsion Conference, Kobe, 4-10 July 2015, Paper IEPC-2015-275/ISTS-2015-b-275.
[130]T. Hatakeyama, M. Irie, H. Watanabe, A. Okutsu, J. Aoyagi, and H. Takegahara, "Preliminary study on radio frequency neutralizer for ion engine," paper presented at the 30th International Electric Propulsion Conference, Florence, Italy, 17-20 September 2007, Paper IEPC-2007-226.
[131]Y. Saito and S. Uemura, Carbon **38**, 169 (2000).
[132]L. A. Singh, M. L. R. Walker, G. P. Sanborn, S. P. Turano, and W. J. Ready, "Operation of spindt-type, carbon nanotube cold cathodes in a Hall effect thruster environment," paper presented at the 33rd International Electric Propulsion Conference, Washington D.C., USA, 6-10 October 2013, Paper IEPC-2013-348.
[133]D. Pagnon, S. Pellerin, M. Dudeck, A. V. Loyan, T. A. Maksymenko, and N. N. Koshelev, "Ukrainian SPT-20 Hall effect thruster: Analysis of the plume by optical emission spectroscopy," paper presented at the 30th International Electric Propulsion Conference, Florence, Italy, 17-20 September 2007, Paper IEPC-2007- 361.
[134]D. Manzella, S. Oleson, J. Sankovic, T. Haag, A. Semenkin, and V. Kim, "Evaluation of low power Hall thruster propulsion," AIAA Paper 96-2736.
[135]See www.Busek.com for BHT-200 Datasheet. Product Catalogue: Busek Co. Inc., 2015.
[136]N. Z. Warner, "Theoretical and experimental investigation of Hall thruster miniaturization," Dissertation (Massachusetts Institute of Technology, Department of Aeronautics and Astronautics, 2007).
[137]T. Ito, N. Gascon, W. S. Crawford, and M. A. Cappelli, J. Propul. Power **23**, 1068 (2007).
[138]K. D. Diamant, J. E. Pollard, Y. Raitses, and N. J. Fisch, IEEE Trans. Plasma Sci. **38**, 1052 (2010).
[139]R. Wirz, R. Sullivan, J. Przybylowski, and M. E. Silva, Int. J. Plasma Sci. Eng. **2008**, 693825.
[140]D. Bock, C. Drobny, P. Laufer, M. Kössling, and M. Tajmar, "Development and testing of electric propulsion systems at TU Dresden," AIAA Paper 2016-4848.
[141]G. A. Parakhin, R. S. Pobbubniy, A. N. Nesterenko, and A. P. Sinitsin, Procedia Eng. **185**, 80 (2017).
[142]D. Pedrini, T. Misuri, F. Paganucci, and M. Andrenucci, Aerospace **4**, 26 (2017).
[143]N. N. Koshelev and A. Loyan, "Investigation of hollow cathode for low power Hall effect thruster," paper presented at the 30th International Electric Propulsion Conference, Florence, Italy, 17-20 Septenber 2007, Paper IEPC-2007-103.
[144]D. Lev, G. Alon, D. Mykytchuk, and L. Appel, "Development of a low current heaterless hollow cathode for Hall thrusters," paper presented at the 34th International Electric Propulsion Conference, Hyogo-Kobe, Japan, 4-10 July 2015, Paper IEPC-2015-163.
[145]D. Lev, G. Alon, D. Mykytchuk, and L. Appel, "Heaterless hollow cathode characterization and 1,500 hr wear test," AIAA Paper 2016-4732.
[146]D. Lev and L. Appel, "Heaterless hollow cathode technology—A critical review," paper presented at the 5th Space Propulsion Conference, Rome, Italy, 2-6 May 2016, Paper SP2016_3125366.
[147]D. Lev, G. Alon, A. Warshavsky, and L. Appel, "Low current heaterless hollow cathode RandD at Rafael," paper presented at the 18th Israeli Conference on Plasma Science and its Applications (IPSTA), Beer-Sheva, Israel, 3 March 2016.
[148]D. Lev, R. Eytan, G. Alon, A. Warshavsky, L. Appel, A. Kapulkin, and M. Rubanovych, "The development of CAM200—Low power Hall thruster," Trans. Jpn. Soc. Aeronaut. Space Sci., Aerosp. Technol. Jpn. **14**, Pb_217-Pb_223 (2016).
[149]D. Lev, G. Alon, S. Fisher, and L. Appel, "Cathode test facility at Rafael," paper presented at the 5th Space Propulsion Conference, Rome, Italy, 2-6 May 2016, Paper SP2016_3125365.
[150]D. Goebel, K. K. Jameson, and R. R. Hofer, "Hall thruster cathode flow impact on coupling voltage and cathode life," J. Propul. Power **28**, 355 (2012).
[151]J. P. Sheehan, Y. Raitses, N. Hershkowitz, and M. Mcdonald, J. Propul. Power **33**, 614 (2017).
[152]I. Katz, I. G. Mikellides, D. M. Goebel, and J. E. Polk, IEEE Trans. Plasma Sci. **36**, 2199 (2008).
[153]L. Garrigues, G. J. M. Hagelaar, J. P. Boeuf, Y. Raitses, A. Smirnov, and N. J. Fisch, paper presented at the 30th International Electric Propulsion Conference, Florence, Italy, September 17–20 (2007), Paper IEPC-2007-157, available at (http://erps.spacegrant.org/uploads/images/images/iepc_articledownload_1988-2007/2007index/IEPC-2007-157.pdf).
[154]R. W. Conversano, D. M. Goebel, R. R. Hofer, T. S. Matlock, and R. E. Wirz, paper presented at the 33rd International Electric Propulsion Conference, The George Washington University, Washington, D.C., USA, October 6–10 (2013), Paper IEPC-2013-201; available at (http://erps.spacegrant.org/uploads/images/images/iepc_articledownload_1988-2007/2013index/h8gqm62v.pdf)
[155]F. Taccogna, S. Longo, M. Capitelli, and R. Schneider, Phys. Plasmas **12**, 053502 (2005).
[156]P. Coche and L. Garrigues, Phys. Plasmas **21**, 023503 (2014).
[157]J. C. Adam, A. Heron, and G. Laval, Phys. Plasmas **11**, 295 (2004).

[158]D. Tskhakaya, K. Matyash, R. Schneider, and F. Taccogna, Controlled Plasma Phys. **47**, 563 (2007).
[159]F. Taccogna, J. Plasma Phys. **81**, 305810102 (2015).
[160]K. Nanbu and Y. Kitatani, J. Phys. D: Appl. Phys. **28**, 324 (1995).
[161]K. Nanbu, Phys. Rev. E **55**, 4642 (1997).
[162]M. A. Furman and M. T. F. Pivi, Phys. Rev. Spec. Top. Accel. Beams **5**, 124404 (2002).
[163]Y. Garnier, V. Viel, J.-F. Roussel, and J. Bernard, J. Vac. Sci. Technol. A **17**, 3246 (1999).
[164]See http://crd-legacy.lbl.gov/~xiaoye/SuperLU for description of SuperLU (Supernodal LU, 2015) by X. S. Li, J. Demmel, J. Gilbert, L. Grigori, P. Sao, M. Shao, and I. Yamazaki.
[165]See http://www.mcs.anl.gov/petsc for PETSc/Tao—Portable, Extensible Toolkit for Scientific Computation (2015).
[166]See http://www.research.ibm.com/projects/wsmp for Watson Sparse Matrix Package (WSMP) (2015).
[167]J. P. Boeuf, Front. Phys. **2**, 74 (2014).
[168]D. Sydorenko, I. Kaganovitch, Y. Raitses, and A. Smolyakov, Phys. Rev. Lett. **103**, 145004 (2009).
[169]F. Taccogna, S. Longo, M. Capitelli, and R. Schneider, Controlled Plasma Phys. **48**, 375 (2008).
[170]T. Lafleur, S. D. Baalrud, and P. Chabert, Phys. Plasmas **23**, 053502 (2016).
[171]F. Taccogna, S. Longo, M. Capitelli, and R. Schneider, Phys. Plasmas **12**, 043502 (2005).
[172]F. Taccogna, R. Schneider, S. Longo, and M. Capitelli, Plasma Sources Sci. Technol. **17**, 024003 (2008).
[173]F. Taccogna, S. Longo, M. Capitelli, and R. Schneider, Appl. Phys. Lett. **94**, 251502 (2009).
[174]See http://phys4entrydb.ba.imip.cnr.it/Phys4EntryDB; https://fr.lxcat.net/home; https://www-amdis.iaea.org/ALADDIN; http://srdata.nist.gov/gateway/gateway?keyword=cross+section; http://www-29.eirene.de for various programs and databases.
[175]G. Guerrini, A. N. Vesselovzorov, M. Bacal, and I. B. Pokrovsky, Rev. Sci. Instrum. **67**, 990 (1996).
[176]I. Levchenko, M. Korobov, M. Romanov, and M. Keidar, J. Phys. D.: Appl. Phys. **37**, 1690 (2004).
[177]K. Bazaka, M. V. Jacob, and K. Ostrikov, Chem. Rev. **116**, 163 (2016).
[178]I. Levchenko, K. Ostrikov, A. E. Rider, E. Tam, S. V. Vladimirov, and S. Xu, Phys. Plasmas **14**, 063502 (2007).
[179]M. V. Jacob, R. S. Rawat, B. Ouyang, K. Bazaka, D. S. Kumar, D. Taguchi, M. Iwamoto, R. Neupane, and O. K. Varghese, Nano Lett. **15**, 5702 (2015).
[180]O. Baranov, K. Bazaka, H. Kersten, M. Keidar, U. Cvelbar, S. Xu, and I. Levchenko, Appl. Phys. Rev. **4**, 041302 (2017).
[181]I. Levchenko, K. K. Ostrikov, J. Zheng, X. Li, M. Keidar, and K. B. K. Teo, Nanoscale **8**, 10511 (2016).
[182]I. Levchenko, K. Bazaka, M. Keidar, S. Xu, and J. Fang, "Hierarchical multi-component inorganic metamaterials: Intrinsically driven self-assembly at nanoscale," Adv. Mater. **30**, 1702226 (2018).
[183]J. Fang, I. Aharonovich, I. Levchenko, K. Ostrikov, P. Spizzirri, and S. Rubanov, Cryst. Growth Des. **12**, 2917 (2012).
[184]See www.qb50.eu for QB50—An international network of CubeSats.
[185]See http://sydney.edu.au/inspire-cubesat for "INSPIRE-2," a space research satellite.
[186]C. Charles, R. W. Boswell, and K. Takahashi, Plasma Phys. Control. Fusion **54**, 124021 (2012).
[187]A. Stuchbery, "Development, integration and testing of the pocket plasma thruster," Honours thesis (The Australian National University, 2017).
[188]C. Charles and R. Boswell, Plasma Sources Sci. Technol. **21**, 022002 (2012).
[189]W. Liang, L. Raymond, J. Rivas, C. Charles, and R. Boswell, "Structurally supportive RF power inverter for a CubeSat electrothermal plasma micro-thruster with PCB inductors," paper presented at the 32nd Annual IEEE Applied Power Electronics Conference and Exposition (APEC), Tampa, FL, USA, 26–30 March 2017, pp. 2141–2145.
[190]C. Charles, W. Liang, L. Raymond, J. Rivas-Davilla, and R. W. Boswell, Front. Phys. **5**, 36 (2017).
[191]A. Pascale, "Design and construction of a propellant sub-system for SP3s CubeSat plasma thruster," Honours thesis (The Australian National University, 2016).
[192]C. Charles, T. S. Ho, A. Ellis, and T. Charoy, "The pocket rocket electrothermal plasma thruster for 'CubeSat' nano-satellites," in *Proceeding of the 68th International Astronautical Congress*, Adelaide, Australia, 25-29 September 2017, Paper IAC-17, x38547.
[193]C. Charles, R. W. Boswell, A. Bish, V. Khayms, and E. F. Scholz, Front. Phys. **4**, 19 (2016).
[194]T. S. Ho, C. Charles, and R. W. Boswell, Front. Phys. **4**, 55 (2017).
[195]S. Hurley, G. Teel, J. Lukas, S. Haque, M. Keidar, C. Dinelli, and J. Kang, "Thruster subsystem for the United States Naval Academy's (USNA) Ballistically Reinforced Communication Satellite (BRICSat-P)," paper presented at the Joint Conference of 30th International Symposium on Space Technology and Science, 34th International Electric Propulsion Conference and 6th Nano-satellite Symposium, Hyogo-Kobe, Japan, July 4–10 (2015), Paper IEPC-2015-37 /ISTS-2015-b.
[196]See https://svs.gsfc.nasa.gov/12025 for NASA's CANYVAL-X booklet describing these satellites.
[197]B. Seifert, A. Reissner, N. Buldrini, D. Krejci, F. Plesescu, T. Hörbe, and C. Scharlemann, "Integrated electric propulsion systems for small satellites," paper presented at the 4th Space Propulsion Conference, Cologne, Germany, 19-22 May 2014.
[198]See www.enpulsion.at for IMF Nanothruster—Product overview (January 2017).
[199]J. R. C. Alarcon, N. Örger, S. Kim, T. Vinh, L. W. Seng, B. T. Duy Vu, and M. Cho, "Moon mission lifetime analysis of a 2U CubeSat equipped with pulsed plasma thrusters: The Aoba-VELOX IV mission case," paper presented at the 31st International Symposium on Space Technology and Science (ISTS), Matsuyama, Japan, 3-9 June 2017.
[200]S. J. Pottinger, D. Krejci, and C. A. Scharlemann, Acta Astronaut. **68**, 1996 (2011).
[201]M. Tajmar, "Overview of indium LMIS for the NASA-MMS mission and its suitability for an In-FEEP thruster on LISA," paper presented at the 32nd International Electric Propulsion Conference, Wiesbaden, Germany, 11-15 September 2011, Paper IEPC-2011-009.
[202]See https://lisa.nasa.gov.
[203]B. Seifert, A. Reissner, D. Jelem, and T. Hörbe, "Development of a low cost PPU for FEEP electric propulsion using cots components," E3S Web Conf. **16**, 15003 (2017).
[204]A. Reissner, "Lifetime testing of the mN-FEEP thruster," AIAA Paper 2016-5045. DOI:doi.org/10.2514/6.2016-5045.
[205]D. Jelem, A. Reissner, C. Scharlemann, B. Seifert, N. Buldrini, F. Plesescu, and T. Hörbe, "IMF nano thruster," paper presented at the 68th International Astronautical Congress (IAC), Adelaide, Australia, 25-29 September 2017, Paper IAC-17-C4.5.8.
[206]S. Shiraska and S. Nakasuka, "Realization of the concept of reasonably reliable systems engineering in the design of nano-satellites," Trans. JSASS, Aerosp. Technol. Jpn. **10**, Tt_7–Tt_12 (2012).
[207]S. Yoshimoto, S. Nakasuka, Y. Tsuruda, Y. Aoyanagi, T. Tanaka, H. Sahara, T. Ohira, Y. Araki, I. Mase, M. Ito, V. Kainov, A. Karandaev, and O. Silkin, "Cluster launch of Hodoyoshi-3 and -4 satellites from Yasny by Dnepr Launch Vehicle," Trans. JSASS, Aerosp. Technol. Jpn. **14**, Pf_35–Pf_43 (2016).
[208]H. Koizumi, K. Komurasaki, J. Aoyama, and K. Yamaguchi, "Engineering model of the miniature ion propulsion system for the nano-satellite," Trans. JSASS, Aerosp. Technol. Jpn. **12**, Tb_19–Tb_24 (2014).
[209]H. Koizumi, K. Komurasaki, J. Aoyama, and K. Yamaguchi, "Development and flight operation of a miniature ion propulsion system," J. Prop. Power (published online).
[210]R. Funase, T. Inamori, S. Ikari, N. Ozaki, H. Koizumi, A. Tomiki, Y. Kobayashi, and Y. Kawakatsu, "Initial operation results of a 50-kg-class deep space exploration micro-spacecraft PROCYON," paper presented at The AIAA/USU Conference on Small Satellites, AIAA/USU, Logan, UT, 2015, Paper SSC15-V-5, see https://digitalcommons.usu.edu/smallsat/2015/all2015/34.
[211]H. Koizumi, T. Inagaki, Y. Kasagi, T. Naoi, T. Hayashi, R. Funase, and K. Komurasaki, "Unified propulsion system to explore near-earth asteroids by a 50 kg spacecraft," paper presented at The AIAA/USU Conference on Small Satellites, Logan, UT, 2014, Paper SSC14-VI-6, see https://digitalcommons.usu.edu/smallsat/2014/NextPad/6.
[212]H. Koizumi, H. Kawahara, K. Yaginuma, J. Asakawa, Y. Nakagawa, Y. Nakamura, S. Kojima, T. Matsuguma, R. Funase, J. Nakatsuka, and K. Komurasaki, "Initial flight operations of the miniature propulsion system installed on small space probe: PROCYON," Trans. JSASS, Aerosp. Technol. Jpn. **14**, Pb_13–Pb_22 (2016).

[213]See https://www.iceye.com for the details on the microsatellie.
[214]H. Koizumi and H. Kuninaka, J. Propul. Power **26**, 601 (2010).
[215]M. Yoshikawa, S. Watanabe, Y. Tsuda, and H. Kuninaka, "Hayabusa 2—The next asteroid sample return mission of Japan," Trans. JSASS, Aerosp. Technol. Jpn. **12**, Tk_29–Tk_33 (2014).
[216]A. I. Morozov, Plasma Phys. Rep. **29**, 235–250 (2003).
[217]S. Yan, G. Jun, and W. Conglong, "Development and primary in-flight experience of electric propulsion system on satellite," paper presented at the 33rd International Electric Propulsion Conference, Washington D.C., USA, 6-10 October 2013, Paper IEPC-2013-K.
[218]J. G. Amo and D. Estublier, "Spacecraft/thrusters interaction analysis for Smart-1," paper presented at the 29th International Electric Propulsion Conference, Princeton University, 31 October 2005, Paper IEPC-2005-003.
[219]M. Capacci, G. Matticari, M. Materassi, E. Artina, and V. Vetorello, "Electrical propulsion diagnostic package for the FEEP thruster on Lisa path finder: Review of status of achievements at TAS-1," paper presented at the 30th International Electric Propulsion Conference, Florence, 17-20 September 2007, Paper IEPC-2007-103.
[220]I. Levchenko, I. I. Beilis, and M. Keidar, Adv. Mater. Technol. **1**, 1600008 (2016).